A REVISED PARALLEL-SEQUENCE MORPHOLOGICAL CLASSIFICATION OF GALAXIES: STRUCTURE AND FORMATION OF S0 AND SPHEROIDAL GALAXIES

John Kormendy[1,2,3] and Ralf Bender[2,3]
[1] Department of Astronomy, University of Texas, Austin, TX 78712, USA; kormendy@astro.as.utexas.edu
[2] Universitäts-Sternwarte, Ludwig-Maximilians-Universität, Scheinerstrasse 1, D-81679 München, Germany
[3] Max-Planck-Institut für Extraterrestrische Physik, Giessenbachstrasse, D-85748 Garching-bei-München, Germany; bender@mpe.mpg.de

ABSTRACT

We update van den Bergh's parallel-sequence galaxy classification in which S0 galaxies form a sequence S0a–S0b–S0c that parallels the sequence Sa–Sb–Sc of spiral galaxies. The ratio B/T of bulge-to-total light defines the position of a galaxy in this tuning-fork diagram. Our classification makes one major improvement. We extend the S0a–S0b–S0c sequence to spheroidal ("Sph") galaxies that are positioned in parallel to irregular galaxies in a similarly extended Sa–Sb–Sc–Im sequence. This provides a natural "home" for spheroidals, which previously were omitted from galaxy classification schemes or inappropriately combined with ellipticals. To motivate our juxtaposition of Sph and Im galaxies, we present photometry and bulge–disk decompositions of four rare, late-type S0s that bridge the gap between the more common S0b and Sph galaxies. NGC 4762 is an edge-on SB0bc galaxy with a very small classical-bulge-to-total ratio of $B/T = 0.13 \pm 0.02$. NGC 4452 is an edge-on SB0 galaxy with an even tinier pseudobulge-to-total ratio of $PB/T = 0.017 \pm 0.004$. It is therefore an SB0c. VCC 2048, whose published classification is S0, contains an edge-on disk, but its "bulge" plots in the structural parameter sequence of spheroidals. It is therefore a disky Sph. And NGC 4638 is similarly a "missing link" between S0s and Sphs—it has a tiny bulge and an edge-on disk embedded in an Sph halo. In the Appendix, we present photometry and bulge–disk decompositions of all *Hubble Space Telescope* Advanced Camera for Surveys Virgo Cluster Survey S0s that do not have published decompositions. We use these data to update the structural parameter correlations of Sph, S + Im, and E galaxies. We show that Sph galaxies of increasing luminosity form a continuous sequence with the disks (but not bulges) of S0c–S0b–S0a galaxies. Remarkably, the Sph–S0–disk sequence is almost identical to that of Im galaxies and spiral galaxy disks. We review published observations for galaxy transformation processes, particularly ram-pressure stripping of cold gas. We suggest that Sph galaxies are transformed, "red and dead" Scd–Im galaxies in the same way that many S0 galaxies are transformed, red and dead Sa–Sc spiral galaxies.

Key words: galaxies: elliptical and lenticular, cD – galaxies: evolution – galaxies: formation – galaxies: photometry – galaxies: structure

1. INTRODUCTION

Sidney van den Bergh's (1976) alternative to Hubble types puts S0s in a sequence S0a–S0b–S0c that parallels the sequence Sa–Sb–Sc of spiral galaxies. Only the ratio B/T of bulge-to-total light and not (e.g.) spiral arm pitch angle defines the position of a galaxy in the classification. The motivation was the observation that many S0s have small B/T values that are not consistent with the traditional interpretation that they are a transition class between E and Sa galaxies. Rather, they are structurally similar to Sa–Sc galaxies. Their lack of spiral structure, of substantial H I gas, and of obvious star formation was attributed to S $\rightarrow$ S0 conversion processes such as ram-pressure stripping of cold gas by hot gas in galaxy clusters.

Van den Bergh's classification encodes important aspects of galaxy evolution and therefore is a valuable complement to Hubble types. It has had substantial impact. Still, we believe that it has been underappreciated because the importance of galaxy transformation has been unclear. Now, new observations and theoretical developments on a variety of evolution processes make galaxy transformation "an idea whose time has come." With small revisions, re-introduction of parallel-sequence classification is timely.

Figure 1 shows our proposed classification scheme. The most important revision is the addition of spheroidal ("Sph") galaxies in parallel to irregulars. The rest of this paper explains and justifies this change.

To motivate our juxtaposition of Sph and Im galaxies at the late end of the Hubble sequence, we update in Sections 3 and 4 the observational evidence that Sphs are not dwarf examples of elliptical galaxies. With much larger samples of published parameters, we confirm the results of Kormendy (1985, 1987, 2009) and Kormendy et al. (2009) that the correlations of half-light radius r_e and surface brightness μ_e with each other and with absolute magnitude M_V show that spheroidal and elliptical galaxies form disjoint sequences. We show for the first time that the sequence of Sphs is continuous with that of S0 disks (Section 5). And in Section 6, we confirm the results of the above papers that the sequence of S0 disks+Sphs is essentially indistinguishable from the sequence of spiral galaxy disks. As in the above papers, we conclude that spheroidal galaxies are "red and dead," dwarf S+Im galaxies that have been transformed by a variety of internal and external evolution processes. Thus they are closely similar to S0a–S0c galaxies. We summarize the evidence that these are transformed spiral galaxies.

Adding Sphs resolves a puzzle with van den Bergh's classification that has become more acute since 1976. If S0s are defunct spirals, where are the defunct Scs? Van den Bergh (1976) classifies only the Hubble Atlas galaxies (Sandage 1961). They are few. But he lists 13 ellipticals (omitting 2 spheroidals), 11 E/S0a and S0a galaxies, 5 S0a/b and S0b galaxies, and no S0c galaxies. Among anemics, there are 4 Aa galaxies, 22 Aab and Ab galaxies, 5 Ab/c galaxies, and 2 Ac galaxies,
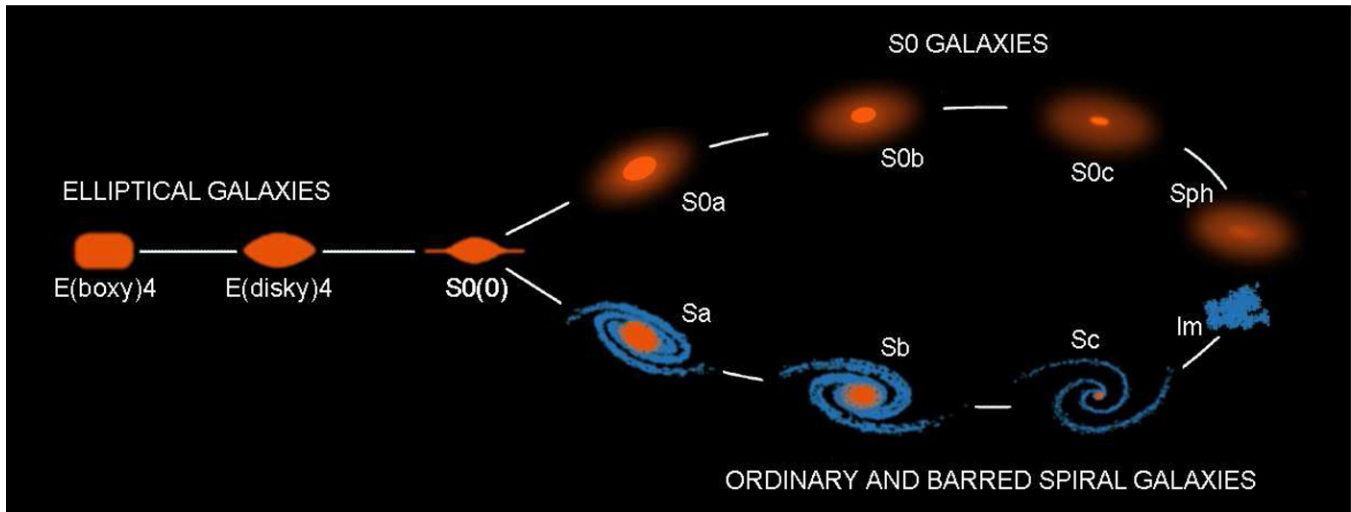
Figure 1. Revised parallel-sequence morphological classification of galaxies. E types are from Kormendy & Bender (1996). Transition objects between spirals and S0s (van den Bergh's anemic galaxies) exist but are not illustrated. Bulge-to-total ratios decrease toward the right; Sc and S0c galaxies have tiny or no pseudobulges. Sph and Im galaxies are bulgeless.

both uncertain. These statistics invite the interpretation that partial transformation from spiral to anemic galaxies is easier than complete transformation from spiral to S0 galaxies and that it is easier to transform earlier-type galaxies. Nevertheless, the complete lack of S0cs is remarkable considering that bulgeless progenitors are common and (in many cases) low in total mass. Specifically, in terms of the finer-binned de Vaucouleurs (1959) classification, one could reasonably expect to find defunct Sd, Sm, and Im galaxies. These are progressively fainter objects with progressively shallower gravitational potential wells. Moreover, Sc galaxies do not contain classical bulges, and later-type galaxies scarcely even contain pseudobulges (Kormendy & Kennicutt 2004; Kormendy et al. 2010). If spirals can turn into S0s, then should it not be easier to transform the latest-type galaxies into "bulgeless S0s"? Where are they?

We suggest that they are the spheroidal galaxies.

In Section 3, we present new photometry and bulge–disk decompositions of rare, late-type S0 galaxies that bridge the gap between the more common S0b galaxies and the exceedingly common Sph galaxies. NGC 4762 is an edge-on SB(lens)0bc galaxy with a very small classical-bulge-to-total ratio of $B/T = 0.13 \pm 0.02$. NGC 4452 is an edge-on SB(lens)0 galaxy with an even tinier pseudobulge-to-total ratio of $PB/T = 0.017 \pm 0.004$. It is the first known true SB0c. VCC 2048, whose published classification also is S0, proves to contain an edge-on disk, but its "bulge" parameters lie in the structural parameter sequence of Sph galaxies. It is therefore an edge-on Sph that still contains a disk. Finally, NGC 4638 is an edge-on S0 with a spectacularly boxy Sph halo. In all respects, galaxy structural parameters are continuous between Sph galaxies and the disks (but not the bulges) of S0c–S0b–S0a galaxies. This is consistent with S → Sph transformation.

After this research was finished but before this paper was written, we became aware that the ATLAS3D group independently propose a parallel-sequence classification motivated by their kinematic results (Cappellari et al. 2011b; Krajnović 2011). Also, after this paper was refereed and resubmitted, a paper by Laurikainen et al. (2011) was posted; it includes additional examples of S0c galaxies and discusses the connection with van den Bergh's (1976) classification. We kept our paper separate

from the above to emphasize how three groups independently reach similar conclusions. This is a sign that the ideas that we all discuss are robust.

2. E–S0c GALAXIES

Before we focus on spheroidal galaxies, we update the motivation that underlies the E–S0(0) part of Figure 1.

2.1. Elliptical Galaxies

The classification of elliptical galaxies is from Kormendy & Bender (1996). The physically important distinction is not among galaxies with different apparent flattenings, which mostly reflect our viewing geometry. Rather, it is between the two varieties of ellipticals, as reviewed in Kormendy & Bender (1996), Kormendy et al. (2009), and Kormendy (2009). From this last paper, "giant ellipticals ($M_V \lesssim -21.5$; $H_0 = 72$ km s^{-1} Mpc^{-1})

1. have cores, i.e., central missing light with respect to an inward extrapolation of the outer Sérsic profile;
2. rotate slowly, so rotation is unimportant dynamically;
3. therefore are moderately anisotropic and triaxial;
4. are less flattened (ellipticity ~ 0.15) than smaller Es;
5. have boxy-distorted isophotes;
6. have Sérsic (1968) function outer profiles with $n > 4$;
7. are mostly made up of very old stars that are enhanced in α elements;
8. often contain strong radio sources; and
9. contain X-ray-emitting gas, more of it in bigger Es.

Normal and dwarf true ellipticals ($M_V \gtrsim -21.5$) generally

1. are coreless and have central extra light with respect to an inward extrapolation of the outer Sérsic profile;
2. rotate rapidly, so rotation is dynamically important to their structure;
3. are nearly isotropic and oblate spheroidal, with axial dispersions σ_z that are somewhat smaller than the dispersions σ_r, σ_ϕ in the equatorial plane;
4. are flatter than giant ellipticals (ellipticity ~ 0.3);
5. have disky-distorted isophotes;
6. have Sérsic function outer profiles with $n \lesssim 4$;

7. are made of (still old but) younger stars with only modest or no α-element enhancement;
8. rarely contain strong radio sources; and
9. rarely contain X-ray-emitting gas."

Here, "dwarf true elliptical" means compact ellipticals like M 32 that extend the fundamental plane correlations of bigger elliptical galaxies to the lowest luminosities (Section 3).

We do not repeat here the many references to the papers that derived the above results. They are listed in the above reviews. However, it is important to note the generally good agreement between the above dichotomy and the results of the SAURON and ATLAS^{3D} surveys (e.g., de Zeeuw et al. 2002; Emsellem et al. 2004, 2007, 2011; Cappellari et al. 2007, 2011a, 2011b; Krajnović et al. 2008, 2011; McDermid et al. 2006).

1. The important difference between our analysis and that of the SAURON group is that we decompose S0s into (pseudo)bulge and disk parts and then treat each component separately. In contrast, the SAURON team treats S0s as single-component systems and derives one set of parameters (e.g., anisotropy measure β) for each galaxy. Point 3, below, results from this difference in analysis.
2. The SAURON division of ellipticals into slow and fast rotators is almost identical to ours. Instead of just choosing a value of their rotation parameter λ at which to divide slow and fast rotators, we find the value that is most consistent with the core–no-core division. This value is $\lambda = 0.13$ instead of $\lambda = 0.10$. If we divide the Emsellem et al. (2007) sample of ellipticals at $\lambda = 0.13$, then the only exception to the core–rotation correlation (points 1 and 2 above) is that NGC 4458 is an extra light galaxy that rotates slowly. However, it is almost exactly circular, so it can be a rapid rotator that is viewed face-on.
3. The SAURON group concludes that extra light ellipticals are very anisotropic, with $\sigma_z \ll \sigma_r$ and σ_ϕ. We agree that σ_z is in general smaller than the other two dispersion components, but we suspect that the large difference found by the SAURON team results from the inclusion of disk light in S0s, which are all coreless.
4. The SAURON group concludes that core galaxies are nearly isotropic. They find moderate triaxiality in some galaxies, but they omit the most anisotropic galaxies from their statistics, because they cannot be fitted with three-integral models. In fact, they have analyzed their most anisotropic galaxies with triaxial models (e.g., NGC 4365; van den Bosch et al. 2008), and these reveal the triaxiality.

We believe that the agreements in our pictures of the two varieties of ellipticals far outweigh the differences. We also emphasize that many kinds of physical properties other than kinematics combine to create the dichotomy listed above. We therefore believe that the difference between the two kinds of ellipticals is robust.

The formation physics that underlies the E–E dichotomy is suggested in Kormendy et al. (2009). The "smoking gun" differences are 1 (cores versus extra light) and 9 (X-ray gas is or is not present). In coreless galaxies, the distinct, extra light component above the inward extrapolation of the outer Sérsic profile first seen by Kormendy (1999) strongly resembles the distinct central components predicted in numerical simulations of mergers of galaxies that contain gas. In the simulations, the gas dissipates, falls toward the center, undergoes a starburst, and builds a compact stellar component that is distinct from the Sérsic-function main body of the elliptical (e.g., Mihos &

Hernquist 1994; Hopkins et al. 2009a). This led Kormendy (1999, see also Côté et al. 2007; Kormendy et al. 2009) to suggest how the E–E dichotomy arose: the most recent major merger that made extra light ellipticals involved cold gas dissipation and a central starburst (it was "wet"), whereas the most recent major merger that made core ellipticals was dissipationless ("dry"). Central to this picture is our understanding that cores (i.e., missing light with respect to the inward extrapolation of the outer Sérsic function) were scoured by black hole binaries that were made in mergers and that flung stars away from the center as they sunk toward their own eventual merger (Begelman et al. 1980; Ebisuzaki et al. 1991; Makino & Ebisuzaki 1996; Quinlan & Hernquist 1997; Faber et al. 1997; Milosavljević & Merritt 2001; Milosavljević et al. 2002; Merritt 2006). This is important because it underscores the need for *major* mergers: only they and not minor mergers with progenitor mass ratios of (say) $\lesssim 1/10$—and therefore black hole mass ratios of $\lesssim 1/10$—can scour the large amounts of light (not) observed in cores (Kormendy & Bender 2009). Observation 9 led Kormendy et al. (2009) to suggest why the E–E dichotomy arose. If energy feedback from (for example) active galactic nuclei (AGNs) requires a working surface of hot gas (Kauffmann et al. 2008), then this is present in core galaxies but absent in extra light galaxies. This suggests that effects of energy feedback are a strong function of galaxy mass: they are weak enough in small Es not to prevent merger starbursts but strong enough in giant Es and their progenitors to make dry mergers dry.

An additional aspect of the formation puzzle has become clearer since Kormendy et al. (2009): it may explain the difference between the small Sérsic indices $n \sim 3 \pm 1$ of extra light ellipticals and the much larger Sérsic indices $n \sim 5$–12 of core galaxies. The Sérsic indices of extra light Es are consistent with those found in simulations of single major merger events (Hopkins et al. 2009a). The large Sérsic indices of core galaxies are not explained in Kormendy et al. (2009). The extra light in these galaxies that converts $n \simeq 3 \pm 1$ into $n \gg 4$ may be the debris accumulated in many minor mergers (e.g., Naab et al. 2009; Hopkins et al. 2010; van Dokkum et al. 2010; Oser et al. 2010, 2011).

2.2. S0(0) Galaxies

We retain class S0(0) for the largest-B/T S0s that are transition galaxies between ellipticals and spirals (e.g., van den Bergh 1994a). It has long been clear that there is a complete continuity between ellipticals and large-B/T S0s. However, we do not suggest a B/T value at which to divide S0(0) and S0a galaxies. To determine a physically meaningful value requires bulge–disk decompositions of large numbers of Sa galaxies. These are not available. On the other hand, we know of no physics that depends on the exact definition of S0(0) galaxies or on their distinction from disky-distorted ellipticals (Bender 1987; Bender et al. 1987, 1988, 1989).

Note that S0(0) galaxies are—to our knowledge—never barred. Their disk-to-total luminosity ratios D/T are so small that their disks are not self-gravitating. Under these circumstances, a bar instability is impossible. It is similarly impossible to have a bar in an elliptical galaxy.

2.3. Comments about the Parallel S and S0 Sequences

Unbarred and barred galaxies are not distinguished in Figure 1. This difference is important in many contexts; it is

embodied in Hubble–Sandage–de Vaucouleurs classes. We do not suggest that Figure 1 should replace Hubble classes. Each classification is designed for the astrophysical context in which it is useful. We focus on the difference between gas-rich, star-forming galaxies and gas-poor, mostly non-star-forming galaxies. The tines of the tuning-fork diagram correspond roughly to the red sequence and blue cloud in the Sloan Digital Sky Survey (SDSS) color–magnitude diagram (Strateva et al. 2001; Bernardi et al. 2003; Hogg et al. 2002, 2004; Blanton et al. 2003, 2005; Baldry et al. 2004).

We choose in Figure 1 to emphasize simplicity by not adopting de Vaucouleurs' (1959) fine morphological divisions Sc–Sd–Sm–Im. This results in an important caveat. We want to ensure that the caveat not lead to a misunderstanding. Most bright Sphs contain nuclear star clusters ("nuclei"), whereas most faint Sphs do not (Sandage et al. 1985b; van den Bergh 1986; Côté et al. 2007). Among possible progenitors, many Sd and Sm galaxies contain nuclei (Böker et al. 2002, 2004), but most Im galaxies do not (van den Bergh 1995). *Our juxtaposition of Sph and Im galaxies should not be taken to imply that all progenitors of Sphs are irregulars.* This would conflict with the evidence from nuclei. Although it is possible that nuclei can be manufactured as part of the galaxy transformation process, it is more likely that nucleated spheroidals have Sd–Sm progenitors whereas non-nucleated spheroidals mostly have Im progenitors. This distinction is "hidden" when Sc, Sd, and Sm galaxies are all shown as Scs in Figure 1. More generally, we do not mean to imply that transformation processes move galaxies exactly vertically in Figure 1.

Minor comments are as follows.

In Figure 1, E–S0(0) galaxies are illustrated edge-on but S0a–Sph and Sa–Im galaxies are illustrated at viewing angles intermediate between edge-on and face-on. This is consistent with past versions of the tuning-fork diagram.

Figure 1 shows all galaxies similar in size. In reality, Sph and Sd–Im galaxies are smaller than earlier types.

The stage-dependent separation of the tuning-fork tines in Figure 1 is deliberate. Sph galaxies and irregulars are more similar than (say) Sc and S0c galaxies. *Unlike* spirals, some Im galaxies look like Sphs at 3.6 μm; i.e., the underlying old galaxy is Sph-like (Buta et al. 2010b). The increasing similarity of all morphologies at the lowest luminosities has been emphasized by van den Bergh (1977, 2007).

The relative numbers of galaxies depend importantly on stage along each sequence. This is discussed in Section 8.

3. FAMILIES OF STELLAR SYSTEMS: THE E–Sph DICHOTOMY

3.1. From Classical Morphology to Physical Morphology: Reasons for the Name "Spheroidal Galaxy"

At the start of research on a new kind of object—fish, rocks, planets, stars, or galaxies—it is useful to classify the objects under study into "natural groups" (Morgan 1951) that isolate common features. Sandage & Bedke (1994) and Sandage (2004) emphasize that, at this stage, no attempt must be made to attach physical interpretation to the classification. Nevertheless, the morphologist must make choices about which features to use in constructing the classification. *A classification scheme remains useful as the subject matures only if the natural groups succeed in ordering objects in a physically interpretable way.* Hubble knew this. He chose to use parameters that later became central

to our understanding when he set up his galaxy classification (Hubble 1936; Sandage 1961, 1975; Sandage & Bedke 1994; see de Vaucouleurs 1959 for refinements). Sandage recognizes Hubble's genius in the *Carnegie Atlas of Galaxies*: "Hubble correctly guessed that the presence or absence of a disk, the openness of the spiral-arm pattern, and the degree of resolution of the arms into stars, would be highly relevant. It was an indefinable genius of Hubble that enabled him to understand in an unknown way... that this start to galaxy classification had relevance to nature itself." That is, in setting up his classification, Hubble made choices with future interpretation in mind. The result is successful precisely because it orders galaxies by properties that reflect essential physics.

Nevertheless, it is no surprise that a purely descriptive classification can miss essential physics. One reason is that convergent evolution happens. In the animal kingdom on Earth, dolphins look like fish but instead are mammals. We understand how convergent evolution has engineered this similarity. In the same way, we argue that convergent evolution has engineered two kinds of galaxies—ellipticals and spheroidals—that look similar but that have different origins. The difference is the main subject of this paper.

The similarity between E and Sph galaxies that gets classical morphology into trouble is that both lack cold gas and (by and large) stellar disks. Gas dissipation cannot make lumpy structure or young stars. Phase mixing and relaxation quickly smooth isophotes into near-ellipses. Then both kinds of galaxies satisfy the definition (no disk; smooth, nearly elliptical isophotes; and no young stars; Sandage 1961) of an elliptical galaxy. In most papers, spheroidals are called "dwarf elliptical" or "dE" galaxies. However, beginning in Section 3.2, we argue that ellipticals are made via major mergers whereas "dE galaxies" are defunct late-type galaxies that lost their gas by transformation processes that do not involve mergers. And we show that "dE galaxies" are recognizably different from ellipticals when we look beyond descriptive morphology and measure structural parameters. Because "dE galaxies" are not dwarf examples of ellipticals—as, e.g., dwarf elephants should be dwarf examples of elephants—we do not call them "dwarf ellipticals." However, it is impractical and unnecessary to drastically change established names. The term "dwarf spheroidal" has long been used for the smallest "dEs" that are companions of our Galaxy (e.g., Draco). We therefore call all "dE galaxies" spheroidals. Tiny objects like Draco are dwarf spheroidals. Large ones like NGC 205 in the Local Group and the many similar objects in the Virgo Cluster are just called spheroidals. This terminology follows Kormendy (1985, 1987, 2009), Kormendy & Bender (1994), and Kormendy et al. (2009). Recognizing that E and Sph galaxies are different is the first step in understanding why we place Sphs at the late end of the parallel-sequence classification.

We emphasize that the name "spheroidal" is not meant to imply anything about the intrinsic shapes of these galaxies.

Readers will note—perhaps with concern—that we appear to be injecting interpretation into our classification. However, *we use interpretation mainly to guide our choice of which observations to use in constructing our classification. The main difference from classical morphology is that we use quantitative measurements of structural parameters and not just visual impressions to define the classification.* Hubble, Sandage, and de Vaucouleurs also made (slightly different) choices about which observations to embody in their classifications.

At the same time, we do not try to fix what is not broken. Our aim is not to replace Hubble classification. Rather, we try

to improve a conceptual tool that is useful in parallel (no pun intended) with other tools. We propose a step in the development of a "physical morphology" (Kormendy 1979a, 1979b, 1981, 1982; Kormendy & Bender 1996) whose aim is to construct a classification that is based on our physical understanding of galaxies. Quoting Kormendy (2004), "I believe that we are now approaching the end of what we can accomplish by separating morphology and physics. I would like to argue that we must break down the wall between morphology and interpretation. Doing this successfully has always been a sign of the maturity of a subject. For example, it has happened in stellar astronomy. I cannot imagine that people who observe and classify phenomena without interpretation would ever discover solar oscillations. Without guidance from a theory, how would one ever conceive of the complicated measurements required to see solar oscillations or to use them to study the interior structure of the Sun? In the same way, we need the guidance of a theory to make sense of the bewildering variety of phenomena associated with galaxies and to recognize what is fundamental and what is not. Sandage (2004)... opened the door to such a phase when he wrote... that morphology and interpretation must be kept separate 'at least until the tension between induction and deduction' gets mature enough. [Our aim here is to develop] physical morphology,... not as a replacement for classical morphology—which remains vitally important—but as a step beyond it. Physical morphology is an iteration in detail that is analogous to de Vaucouleurs' iteration beyond the Hubble tuning-fork diagram."

If we are successful, then parallel-sequence classification will turn out to embody essential physics in ways that Hubble types do not.

3.2. The Elliptical–Spheroidal Dichotomy

3.2.1. Discovery

Wirth & Gallagher (1984) were the first to suggest that compact dwarfs like M 32 and not diffuse dwarfs like NGC 205 are the low-luminosity versions of giant ellipticals. The existence of free-flying analogs of M 32 implied to them that the compactness of better known dwarfs such as M 32, NGC 4486B, and NGC 5846A (Faber 1973) is not due only to tidal truncation by giant galaxy neighbors. Wirth and Gallagher suggested that E and Sph galaxies form disjoint luminosity sequences that overlap for $-15 \gtrsim M_B \gtrsim -18$ but that differ in mean surface brightness at $M_B = -15$ "by nearly two orders of magnitude." An implication is that the luminosity function of true ellipticals is bounded and that M 32 is one of the faintest examples. Sandage et al. (1985a, 1985b) and Binggeli et al. (1988) confirmed this result for Virgo Cluster galaxies (Section 3.2.3 here).

Kormendy (1985, 1987) used high-spatial-resolution photometry from the Canada–France–Hawaii Telescope to demonstrate that elliptical and spheroidal galaxies show a clear-cut dichotomy in parameter space. Ellipticals form a well-defined sequence from cD galaxies to dwarfs like M 32. Lower-luminosity ellipticals have higher central surface brightnesses, whereas lower-luminosity spheroidals have lower central surface brightnesses. Far from extending the E parameter correlations to low luminosities, spheroidals show almost the same correlations as spiral-galaxy disks and Magellanic irregulars. The above results are based on near-central galaxy properties, but they are also seen in global properties (Kormendy 1987; Binggeli & Cameron 1991; Bender et al. 1992, 1993). They are also confirmed with larger galaxy samples (Kormendy & Bender 1994).

Kormendy (1985, 1987) concluded that E and Sph galaxies are distinct types of stellar systems that formed differently. Spheroidals are not dwarf ellipticals; they are physically related to S+Im galaxies. They may be late-type galaxies that lost their gas or processed it all into stars. Relevant evolution processes already known at that time included supernova-driven gas ejection (Saito 1979; Dekel & Silk 1986), ram-pressure gas stripping (Gunn & Gott 1972; Lin & Faber 1983; Kormendy 1985, 1987), and stochastic starbursts (Gerola et al. 1980, 1983). Section 8 discusses these processes.

Kormendy et al. (2009, hereafter KFCB) update and confirm the above results with a sample that includes all known elliptical galaxy members of the Virgo Cluster and a large number of spheroidal galaxies. They carry out photometry on a variety of images with different spatial scales, fields of view, and point-spread function (PSF) resolutions. This provides more robust composite profiles over larger radius ranges than were available before. The resulting correlations between effective radius r_e, surface brightness μ_e at r_e, and absolute magnitude M_{VT} confirm the above conclusions. KFCB refute criticisms of the dichotomy as summarized here in Section 3.2.2. And they provide a detailed review of formation processes—major mergers for ellipticals and gas-removal transformation processes for spheroidals. This paper enlarges on that work.

Figure 2 shows the r_e–μ_e–M_{VT} correlations from Kormendy (2009). Ellipticals from Bender et al. (1992) and classical bulges from Fisher & Drory (2008) are added to increase the sample size further. Figure 2 is the starting point for the present study.

3.2.2. Published Criticisms and Our Responses

The E–Sph dichotomy has been challenged by many papers in the past decade. The main arguments and our responses to them are as follows.

1. Sph and E galaxies have surface brightness profiles that are well described by Sérsic functions; together, they show a continuous correlation of Sérsic index n with galaxy luminosity (Jerjen & Binggeli 1997).
   We agree with this observation (Figure 33 of KFCB). However, conclusions about which objects are or are not physically related should not be based on just one measured parameter.
2. "The striking dichotomy observed by Kormendy (1985) could be due to the lack, in Kormendy's sample, of galaxies in the -20 mag $< M_B < -18$ mag range, corresponding precisely to the transition region between the two families." This quote is from Ferrarese et al. (2006, hereafter F2006), but the same criticism was also made by Binggeli (1994) and by Graham & Guzmán (2003, 2004).
   There was a 2 mag range in M_B in which Kormendy (1985, 1987) had no bulges and only one spheroidal, but the two sequences were clearly diverging outside this magnitude range. In any case, sample size and M_{VT} gaps are not an issue in Kormendy et al. (2009) or in Figure 2 here.
3. Spheroidal galaxies and coreless ("power-law") Es form a single sequence in fundamental plane parameter space from which core ellipticals deviate because of the light missing in cores (Graham & Guzmán 2003, 2004; Gavazzi et al. 2005).
   This is wrong. The fraction of the galaxy light that is missing in cores ranges from almost 0% to just over 2% (Table 1 and Figure 41 in KFCB). The effects of the missing light on global parameters is negligible. In any case, bulges and
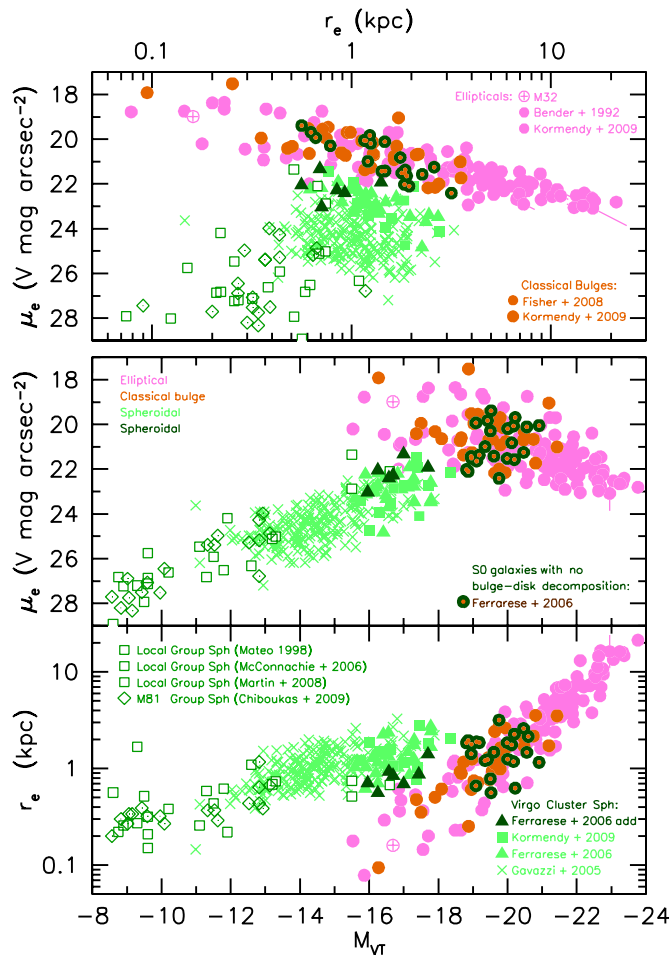
Figure 2. Global parameter correlations for ellipticals (pink), classical bulges (light brown), and spheroidals (light green) from Kormendy et al. (2009, KFCB) and from Kormendy (2009). Local Group Sphs have been updated and M 81 Group Sphs have been added. The bottom panels show effective radius r_e and surface brightness μ_e at the effective radius vs. galaxy absolute magnitude. The top panel is the μ_e–r_e or Kormendy (1977b) relation that shows the fundamental plane almost edge-on. Data sources are given in the keys. Light green filled squares show the Sph galaxies whose brightness profiles were measured in KFCB. Green triangles show all galaxies from Ferrarese et al. (2006, F2006) that were classified as dE there and that were not remeasured in KFCB. Crosses show all spheroidals from Gavazzi et al. (2005, "dE" there) that are not in KFCB or in F2006. Dark green triangles show the seven galaxies from F2006 that were omitted from KFCB because they were typed E, S0, or dS0 but that turn out to be spheroidals. Dark green filled circles with brown centers show the 23 remaining galaxies from F2006 that were omitted in KFCB because they were typed S0 by F2006 but did not have bulge–disk decompositions published there. They are plotted here using the F2006 parameters measured for the whole galaxy, i.e., for the bulge and disk together. To properly study bulge and disk scaling relations, bulge–disk decompositions are required; these are carried out in Section 4 and in the Appendix. However, even the whole-galaxy parameters do not conflict with the KFCB conclusion that spheroidals define a parameter sequence that is very different from the fundamental plane of classical bulges and ellipticals. This point was emphasized in Appendix B of KFCB. Section 4 uses these correlations to illustrate results of bulge–disk decompositions, to demonstrate that Sphs are continuous in parameter space with the disks (but not the bulges) of S0 galaxies, and to show that the disks of S0 and S + Im galaxies have similar correlations. This provides justification for juxtaposing Sph and Im galaxies in the parallel-sequence classification.

coreless ellipticals together define a sequence that extends toward more compact objects than any spheroidals (to the left of the Sphs in Figure 2). That sequence also is extended seamlessly toward more fluffy objects by other coreless ellipticals and by ellipticals with cores. The E

and Sph sequences do not quite join up in Figure 2, and they are more disjoint when more central parameters are measured.

4. The ellipticals that are more compact than (in Figure 2, to the left of) the continuous Sph–coreless–E sequence are pathological: they all have close, giant-galaxy companions, and they are all tidally stripped remnants of much bigger ellipticals (Ferrarese et al. 2006; Chen et al. 2010).

There are many reasons why we believe that tidal truncation cannot be the reason why the E sequence extends to more compact objects than Sphs. (1) Not all compact ellipticals are companions of bright galaxies. Some are fairly isolated (e.g., VCC 1871, which is $\sim 12 r_{e,\mathrm{NGC\,4621}}$ from the giant elliptical NGC 4621; IC 767 = VCC 32). (2) Compact ellipticals do not systematically have small Sérsic indices indicative of outer truncation; instead, they have the same range of Sérsic indices $n \sim 2$ to 3.5 as isolated coreless ellipticals. In particular, M 32 has $n \simeq 2.9$, larger than the median value for isolated coreless ellipticals. These Sérsic indices are exactly as found in n-body simulations of major galaxy mergers (Hopkins et al. 2009a; see also van Albada 1982). (3) Many Sph galaxies also are companions of bright galaxies, but we do not argue that they have been truncated into compact objects. An example is NGC 205. (4) The compact end of the E sequence is also defined by tiny bulges (Figure 2). Classical bulges and ellipticals have closely similar fundamental plane correlations. The classical bulges that appear in our correlation diagrams do not have bright companion galaxies. (5) Our intuition about tidal truncation comes from globular clusters. They have no "protective" dark matter halos, and the truncator is overwhelmingly more massive than the victim. Elliptical galaxies certainly can be tidally distorted, but the dark matter tends to be more distorted, so the galaxies merge relatively quickly once tidal effects start. We conclude that some compact Es may have been pruned slightly but that tidal truncation is not the reason why the E sequence extends to the left of where it is approached by the Sph sequence in Figure 2.

5. Côté et al. (2007), Chen et al. (2010), and Glass et al. (2011) argue that KFCB included only a biased subsample of the Advanced Camera for Surveys (ACS) Virgo Cluster Survey (VCS) galaxies. Quoting Glass et al. (2011): "K09 excluded 60% of the ACS VCS sample—in particular, the vast majority of the galaxies in the $-21.5 \lesssim M_B \lesssim -18.5$ range."

This statement is wrong. KFCB did surface photometry of 40 of the 100 ACS VCS galaxies, i.e., all ellipticals known to be cluster members when their survey was begun plus five S0s and 10 Sphs. The latter were included because, absent detailed photometry, it was not known whether they are Es. *In addition, correlation diagrams such as Figure 2 here included 26 ACS VCS Sph galaxies with parameters from Ferrarese et al. (2006, green triangles in KFCB and in this paper).* Two more galaxies did not have parameters in Ferrarese et al. (2006) because of dust. Therefore, KFCB omitted 32—not 60—viable ACS VCS galaxies. Most are S0s. KFCB studied ellipticals and objects that get confused with ellipticals. The study of S0s—including the necessary bulge–disk decomposition—was postponed until future papers. This is the first of those papers. Adding ACS VCS S0s is the subject of Section 4 and the Appendix of this paper.
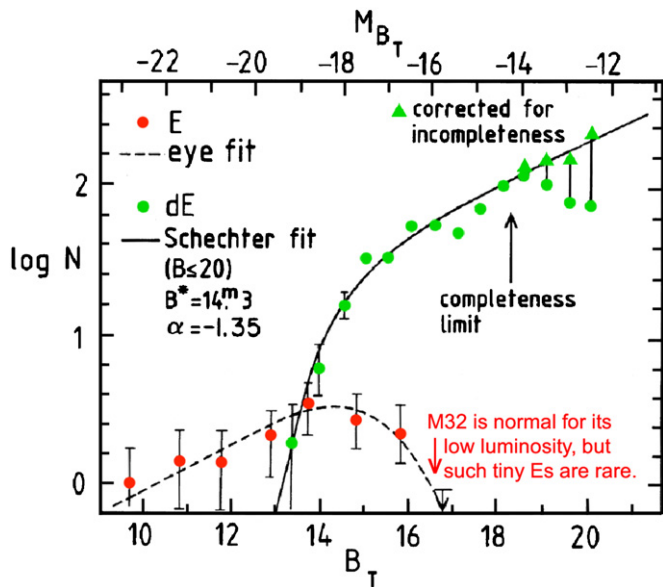
Figure 3. Luminosity functions of elliptical and spheroidal galaxies in the Virgo Cluster. This figure is adapted from Sandage et al. (1985b), who used the traditional name "dE" for spheroidals. We have updated the Hubble constant from $H_0 = 50$ to 70 km s^{-1} Mpc^{-1}. Note that magnitudes are in B band here but in V band in the rest of this paper.

3.2.3. The Luminosity Functions of Elliptical and Spheroidal Galaxies are Different

Figure 3 shows the luminosity functions of Virgo Cluster elliptical and spheroidal galaxies as determined by Sandage et al. (1985b). As these authors emphasize, the luminosity functions are remarkably different. And as these authors recognize, this is additional evidence that ellipticals and spheroidals are different kinds of galaxies. Particularly remarkable is the fact that the E and Sph luminosity functions overlap. This means that *Sandage and collaborators can distinguish between E and Sph galaxies even when they have the same brightness.* Consider how remarkable this statement is.

A dwarf version of a creature is one that, when mature, is smaller than the normal sizes of non-dwarf versions of that creature. "Shetland ponies are the *dwarfs* of the horse world." is a quote from the online Webster dictionary, http://www.merriam-webster.com/dictionary/. Their definition of "dwarf" recognizes that "bodily proportions [may be] abnormal," too, but the main defining feature is small stature. And yet, Figure 3 invites us to imagine that the smallest non-dwarf ellipticals are 20 times less luminous than the brightest "dwarf ellipticals."

In fact, Sandage and collaborators distinguish between elliptical and dwarf elliptical galaxies of the same luminosity with remarkable accuracy. Quoting Sandage & Binggeli (1984): "The distinction between E and dE is made on morphological grounds alone, using surface brightness as the criterion. Normal E galaxies have a steep radial profile (generally following an $r^{1/4}$ law) with high central brightness. The typical dE has a *nearly flat* radial profile, following either a King [1966] model with a small concentration index or equally well an exponential law.... The morphological transition from E to dE is roughly at $M_B \simeq -18$, but there is overlap." KFCB classify E and Sph $\simeq$ dE galaxies using a more quantitative version of the above criteria, i.e., the fundamental plane correlations updated here in Figures 2, 7, 9, 12, 16–18, and 20. In difficult cases, they use

parameters measured at the radius that contains 10% of the total light of the galaxy (Figure 34 in KFCB).

At first, the Sandage group was ambivalent about whether or not the E–dE distinction has a physical basis. This is evident in Figure 7 of Sandage et al. (1985a), where they argue for both opposing points of view in the same sentence. Similarly, Sandage et al. (1985b) admit that "We are not certain if this [dichotomy] is totally a tautology due merely to the arbitrary classification criteria that separate E from dE types... or if the faint cutoff in the [E luminosity function] has physical meaning related to the properties of E and dE types. In the first case, the problem would be only one of definition. In the second, the fundamental difference in the forms of the luminosity functions of E and dE types ... would suggest that two separate physical families may, in fact, exist with *no* continuity between them (cf. Kormendy 1985 for a similar conclusion)." Revising a long-held picture can be uncomfortable.

Later, Binggeli et al. (1988) came to recognize that "The distinction [between] Es and dEs must almost certainly mean that the two classes are of different origin (Kormendy 1985; Dekel & Silk 1986). This is also supported by the fact that the luminosity functions of Virgo Es and dEs [are different]."

3.2.4. The E–Sph Dichotomy: Perspective

Finally, we emphasize that the criticisms of the E–Sph dichotomy in Section 3.2.2 treat the issue as nothing more than an exercise in the analysis of surface photometry. It is much more than this, as the difference in luminosity functions illustrates. In addition, the E and Sph parameter sequences in Figure 2 are consistent with what we know about galaxy formation. The E sequence constitutes the classical "fundamental plane" parameter correlations (Djorgovski & Davis 1987; Faber et al. 1987; Djorgovski et al. 1988; Bender et al. 1992, 1993). Its interpretation is well known: galaxy structure is controlled by the Virial theorem, $r_e \propto \sigma^2 I_e^{-1}$, modified by small non-homologies. The scatter in the E fundamental plane is small (Saglia et al. 1993; Jørgensen et al. 1996). And simulations of major galaxy mergers reproduce the elliptical-galaxy fundamental plane, not a parameter correlation that is almost perpendicular to it (e.g., Robertson et al. 2006; Hopkins et al. 2008, 2009b). Equating spheroidals with low-luminosity ellipticals would imply that they formed similarly, but we are confident that ellipticals formed via major galaxy mergers, and we believe that dwarf spheroidals cannot have formed by mergers (Tremaine 1981). The E sequence is well understood. Dekel & Silk (1986) suggest that spheroidal and S + Im galaxies together form a sequence of decreasing baryon retention at lower galaxy luminosities. We agree (Section 8).

4. THE LARGE RANGE IN S0 BULGE-TO-TOTAL RATIOS

A study of S0s that is as thorough as the KFCB study of ellipticals requires photometry of a large sample of galaxies, each observed with multiple telescopes to provide redundancy and large dynamic range. That study is in progress. Here, explanation and justification of the proposed parallel-sequence classification requires only a proof-of-concept study that explores the observed range of bulge-to-total ratios and bulge and disk parameters. We do this with photometry and bulge–disk decomposition of Virgo Cluster S0s. This also serves the need of Section 3 by adding all ACS VCS galaxies to our parameter correlations.

Figure 2 includes all omitted ACS VCS galaxies with parameters taken from F2006. KFCB omitted 3 peculiar Es, 26 S0s,
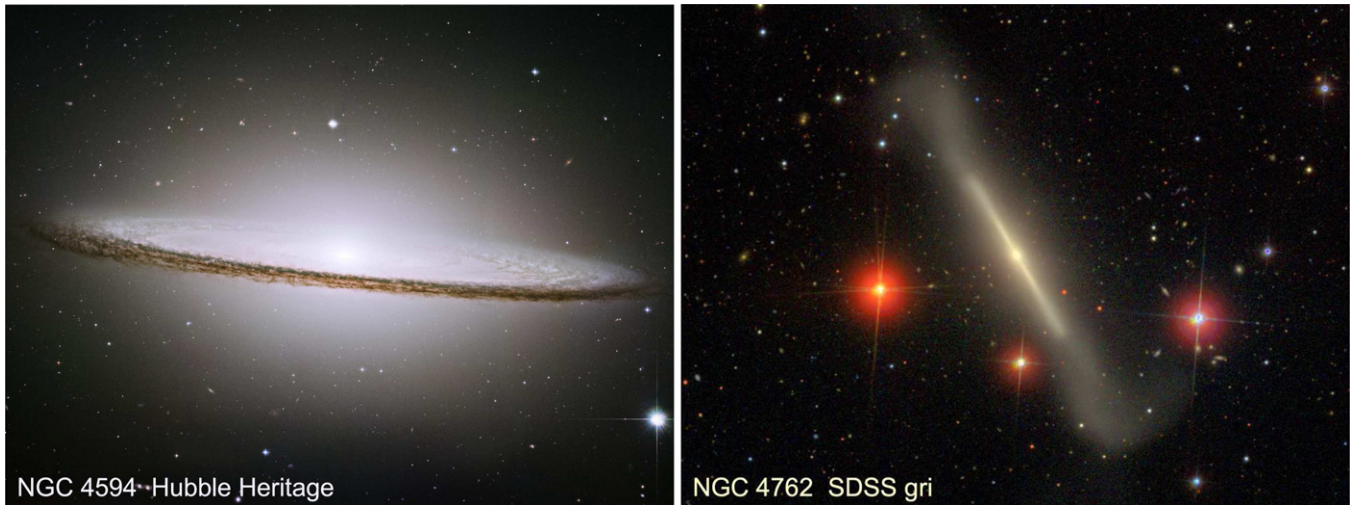
Figure 4. Left: Hubble Heritage image (http://hubblesite.org/newscenter/archive/releases/2003/28/image/a/) of the Sombrero Galaxy, NGC 4594. Right: SDSS *gri* color image of NGC 4762, the second-brightest S0 galaxy in the Virgo Cluster. These galaxies illustrate why bulge–disk decomposition is necessary. NGC 4594 is an Sa galaxy with $B/T = 0.93 \pm 0.02$ (Kormendy 2011b). Without photometric decomposition, we measure essentially only the bulge. We learn nothing about the disk. If an S0 version of this galaxy—e.g., NGC 3115—were viewed face-on, it would be difficult even to see the disk (Hamabe 1982), and whole-galaxy parameters would not measure it at all. In contrast, NGC 4762 is one of the "missing" late-type S0s: we find in this section that $B/T = 0.13 \pm 0.02$. Without photometric decomposition, we measure essentially only the disk. We learn nothing about the bulge. Moreover, the azimuthally averaged parameters used in F2006 are particularly difficult to interpret.

and 2 dS0s. All three peculiar Es, both dS0s, and three of the S0s turn out to be one-component systems that plot as Sphs. They are shown as dark green triangles in Figure 2. They have slightly bright μ_e and small r_e; this is not surprising, given that they were classified E, S0, and dS0. But they lie within the scatter of Sph points and affect no conclusions. They appear in all further parameter plots.

The green circles with brown centers show the remaining ACS VCS S0s that KFCB omitted. Adding these points does not invalidate the E–Sph dichotomy. However, they also do not give a realistic view of bulge and disk scaling relations for S0 galaxies. In particular, since whole-galaxy parameters lump tiny bulges with large disks, they make it harder to see that the E correlation extends leftward of the Sph sequence in Figure 2. This section provides the results of bulge–disk decompositions.

4.1. The "Missing" Latest-type S0 Galaxies

Our aim in this section is to solve the puzzle of the "missing" S0c galaxies. Recall from Section 1 that van den Bergh (1976) list 13 Hubble Atlas ellipticals, 11 E/S0a and S0a galaxies, 5 S0a/b and S0b galaxies, and no S0c galaxies. In contrast, along the spiral sequence, Sc galaxies are more common than Sas. If spiral and S0 galaxies are proposed to form parallel sequences with stage along the sequence defined by B/T ratios, then this is already enough to make us wonder how small the B/T ratios of S0s can be. If in addition we inject interpretation and suspect that S0s are transformed spirals, then where are the defunct Scs? Especially when we have already identified Sph galaxies as defunct versions of later-type, bulgeless Sd–Im galaxies.

#### 4.1.1. NGC 4762 (SB0bc): The Need for Bulge–Disk Decomposition

We begin with the well known, edge-on SB0 NGC 4762 (Sandage 1961; Kormendy & Kennicutt 2004). It was recognized as a small-bulge S0 by van den Bergh (1976) and classified as S0b. We will tweak the classification slightly to (R)SB0(lens)bc.

Figure 4 contrasts the tiny bulge in NGC 4762 with the dominant bulge in NGC 4594. It illustrates why bulge–disk

Figure 5. (R)SB(lens)0 galaxy NGC 3945, a more face-on analog of NGC 4762. The bar fills the lens component in one dimension. The lens is the elliptical "shelf" in the brightness distribution interior to the outer ring. Note that it has a sharp outer edge. Such profiles are well described by Sérsic functions with $n < 0.5$; that is, ones that cut off at large radii faster than a Gaussian. If NGC 3945 were rotated clockwise slightly and then rotated about a horizontal axis until it is seen edge-on, the bar would look shorter than the major-axis radius of the lens. Then the major-axis brightness profile would show three shelves as in NGC 4762—the bar, the lens, and the outer ring.

decomposition is necessary. Whole-galaxy parameters measure only the dominant component. At all B/T, they measure each separate component incorrectly. S0 galaxies prove to exist with all B/T values from 0 to $\sim$1, so *using whole-disk parameters for S0s is guaranteed to imply continuity between pure-bulge and pure-disk galaxies.* We regret the need to belabor this point, because bulge–disk decomposition was developed long ago (Kormendy 1977a) and has been standard analysis machinery ever since (e.g., Burstein 1979; Kent 1985; Byun & Freeman 1995; Scorza & Bender 1995; Baggett et al. 1998; GIM2D: Simard et al. 2002; GALFIT: Peng et al. 2002; BUDA: de Souza et al. 2004; Laurikainen et al. 2005, 2007; Courteau et al. 2007; GASP2D: Méndez-Abreu et al. 2008; Fisher & Drory 2008; Weinzirl et al. 2009). Nevertheless, several groups now
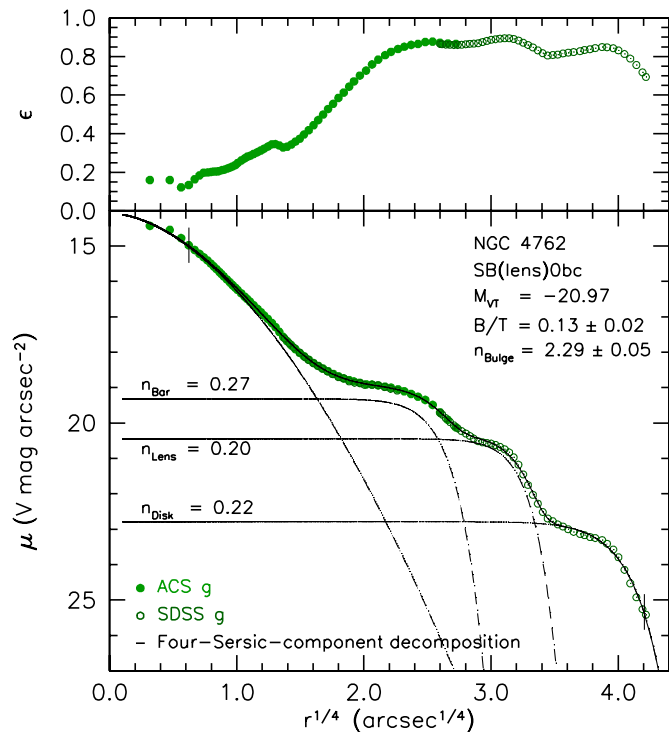
Figure 6. Ellipticity ϵ and surface brightness μ_V along the major axis of NGC 4762 measured by fitting ellipses to the isophotes in the ACS and SDSS g-band images. We used the transformation $V = g + 0.320 - 0.399(g - z)$ from KFCB and the galaxy color $g - z = 2.076$ from F2006. All magnitudes and colors are VEGAmag. The dashed curves show a decomposition of the profile inside the fit range (vertical dashes across the profile). The bulge, bar, lens, and disk are represented by Sérsic functions with indices n given in the figure. Their intensity sum (solid curve) fits the data with an rms of 0.033 V mag arcsec^{-2}.

Figure 7. Parameter correlations from Figure 2 showing the results of the bulge–disk decomposition of NGC 4762. The green filled circles with the brown centers show the total parameters measured by F2006 for the bulge and disk together. These points are connected by straight lines to the bulge parameters (dark brown filled circles) and the disk parameters (dark green crosses).

analyze composite (bulge + disk) galaxies as single-component systems. This mixes up the different formation physics and properties of these very different components.

Before we analyze surface photometry, we need to understand what kind of galaxy NGC 4762 is. This is both easy and well known (Wakamatsu & Hamabe 1984; Kormendy & Kennicutt 2004). Figure 4 shows the essential features that are discussed in the Hubble Atlas and in the above papers: the galaxy has three "shelves" in its major-axis brightness profile outside its central bulge. This means that it is an edge-on (R)SB(lens)0 galaxy, as illustrated by the more face-on, prototypical (R)SB(lens)0 galaxy NGC 3945 (Kormendy 1979b) in Figure 5.

We measure the composite, major-axis brightness profile of NGC 4762 shown in Figure 6. It clearly shows the three shelves in surface brightness discussed above.

Normally, a four-component photometric decomposition would involve ferocious parameter coupling; Appendix A of KFCB shows how serious this problem can be even for one-component fits of the three-parameter Sérsic function. However, parameter coupling is serious when n is large. The more nearly each shelf has constant brightness interior to an infinitely sharp outer cutoff, the less coupling there is between components. Bars, lenses, and outer rings have sharp outer cutoffs (Kormendy 1979b). Four-component decomposition shows that the bar, lens, and outer ring of NGC 4762 are best fitted with Sérsic functions that have extraordinarily small $n \sim 0.2$ to 0.3 (a Gaussian profile has $n = 0.5$). That is, each component looks to all components interior to it as being almost constant in surface brightness. The decomposition is therefore robust. In particular, the bulge parameters are well determined. Table 1 in
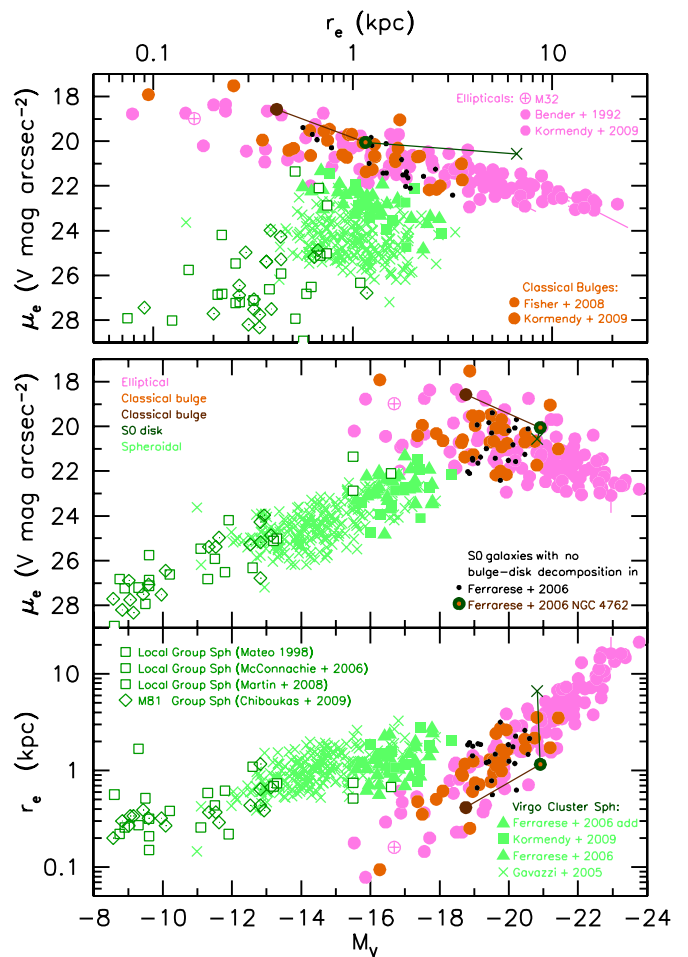
Section 4.2 lists the bulge and disk parameters for the 13 ACS VCS S0 galaxies for which we do photometry in this paper. Gavazzi et al. (2000) provide decompositions of the remaining S0s.

We measure a bulge Sérsic index of $n = 2.29 \pm 0.05$. Also, the bulge ellipticity $\epsilon \simeq 0.3$ is like that of a typical elliptical. All this suggests that the bulge is classical (Kormendy & Kennicutt 2004; Fisher & Drory 2008).

Figure 7 shows the bulge and disk of NGC 4762 in the parameter correlations of Figure 2. The disk parameters are determined by integrating the total disk model out to half of the disk luminosity taking component flattening into account. They refer to all disk components together. They look counterintuitive: r_e is seven times larger than for the galaxy as a whole. This is explained in the Appendix.

The bulge parameters illustrate how the decomposition results strengthen our understanding of the parameter correlations. In the top panel, the bulge of NGC 4762 contributes to the compact extension of the E + bulge correlations leftward of the Sph sequence. Taking the different flattenings of the bulge and disk into account, the bulge absolute magnitude is $M_{V,\text{bulge}} = -18.76$. NGC 4762 helps to define the compact end of the correlations in the bottom panels.

The bulge-to-total ratio is $B/T = 0.13 \pm 0.02$, similar to $B/T = 0.12 \pm 0.02$ in the SABbc galaxy NGC 4258
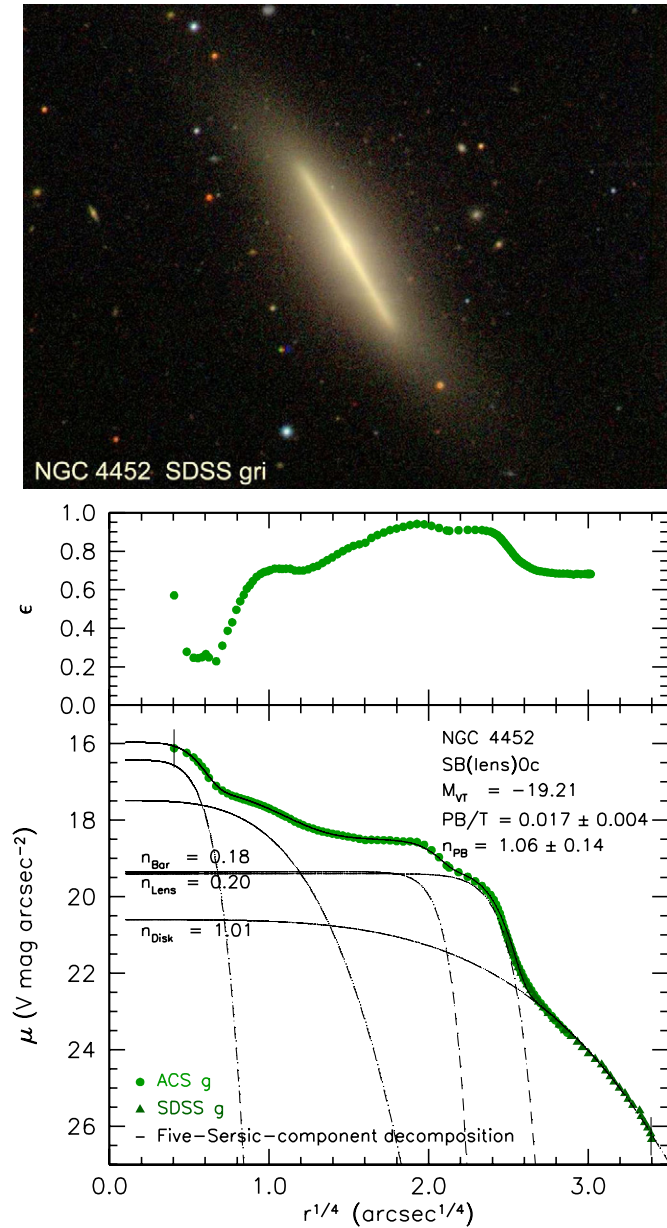
Figure 8. Top: color image of SB(lens)0 galaxy NGC 4452 from the SDSS *g,r,i* images via http://www.wikisky.org. The bulge—which proves to be pseudo—is so tiny that it is almost invisible. The inner disk is edge-on and very flat; it again consists of two shelves in surface brightness. Including the outer, thicker disk, these three shelves are signatures of a bar, lens, and disk. Bottom: ellipticity ϵ and surface brightness μ_V along the major axis of NGC 4452 measured by fitting ellipses to the isophotes in the ACS and SDSS *g*-band images. The five dashed curves show a decomposition of the profile inside the fit range (vertical dashes). The nucleus, bulge, bar, lens, and disk are represented by Sérsic functions with indices *n* as given in the figure. The sum of the components (solid curve) fits the data with an rms of 0.044 *V* mag arcsec^{-2}.

(Kormendy et al. 2010). Given the observation that classical bulges do not occur in Sc galaxies (Kormendy & Kennicutt 2004), the morphological type of NGC 4762 is well constrained to be (R)SB0(lens)bc. It begins to extend the parallel-sequence classification beyond S0b.

4.1.2. NGC 4452 (S0c)

NGC 4452 is closely similar to NGC 4762 but even later in type. Figure 8 shows that it has an edge-on thin disk with a sharp outer cutoff again indicative of a bar or lens. Our
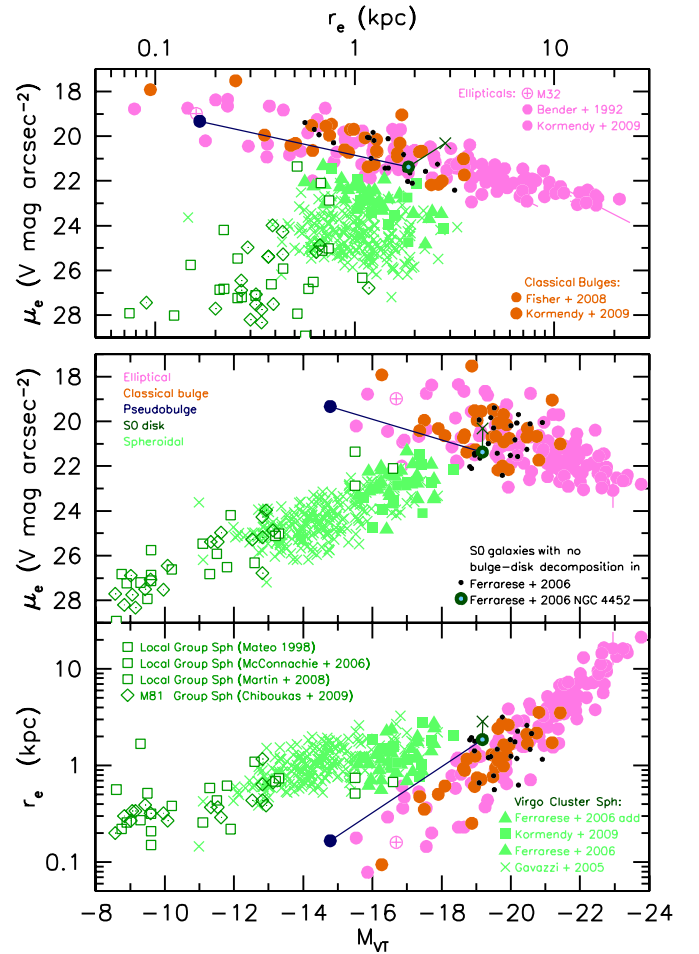
Figure 9. Parameter correlations from Figure 2 showing the results of the bulge–disk decomposition of NGC 4452. The green filled circles with the blue centers show the total parameters measured by F2006 for the bulge and disk together. These points are connected by straight lines to the pseudobulge parameters (dark blue filled circles) and the disk parameters (dark green crosses).

photometry—also illustrated in Figure 8—shows that the thin disk consists of two shelves as in NGC 4762. Together with the (thick and warped) outer disk, this implies that NGC 4452 is an edge-on SB(lens)0 galaxy.

The brightness profile is more complicated than that of NGC 4762 in that NGC 4452 also contains a nuclear star cluster. We derive an AB *g* magnitude of this nucleus of 20.56, in good agreement with the F2006 value of 20.49. Fortunately, the nucleus has a steep outer profile (formally, $n = 0.68 \pm 0.09$, but this is consistent with a Gaussian, and it applies to the PSF-convolved, observed profile). The point is that the nuclear profile does not much influence the photometric decomposition.

The bar and lens also have very cutoff profiles ($n = 0.18$ and $n = 0.20$, respectively); both have essentially constant surface brightness underlying the (pseudo)bulge.

Thus, the five-component decomposition in Figure 8 is surprisingly robust. NGC 4452 contains a pseudobulge with $n = 1.06 \pm 0.14$. Pseudobulges have fundamental plane correlations similar to those of classical bulges but with larger scatter (Fisher & Drory 2008; Kormendy & Fisher 2008). The bulge and disk parameters of NGC 4452 are shown in Figure 9. The pseudobulge provides further support for the compact extension of the E correlations.

NGC 4452 is important for two additional reasons. First, the pseudobulge-to-total luminosity ratio is only $PB/T =$
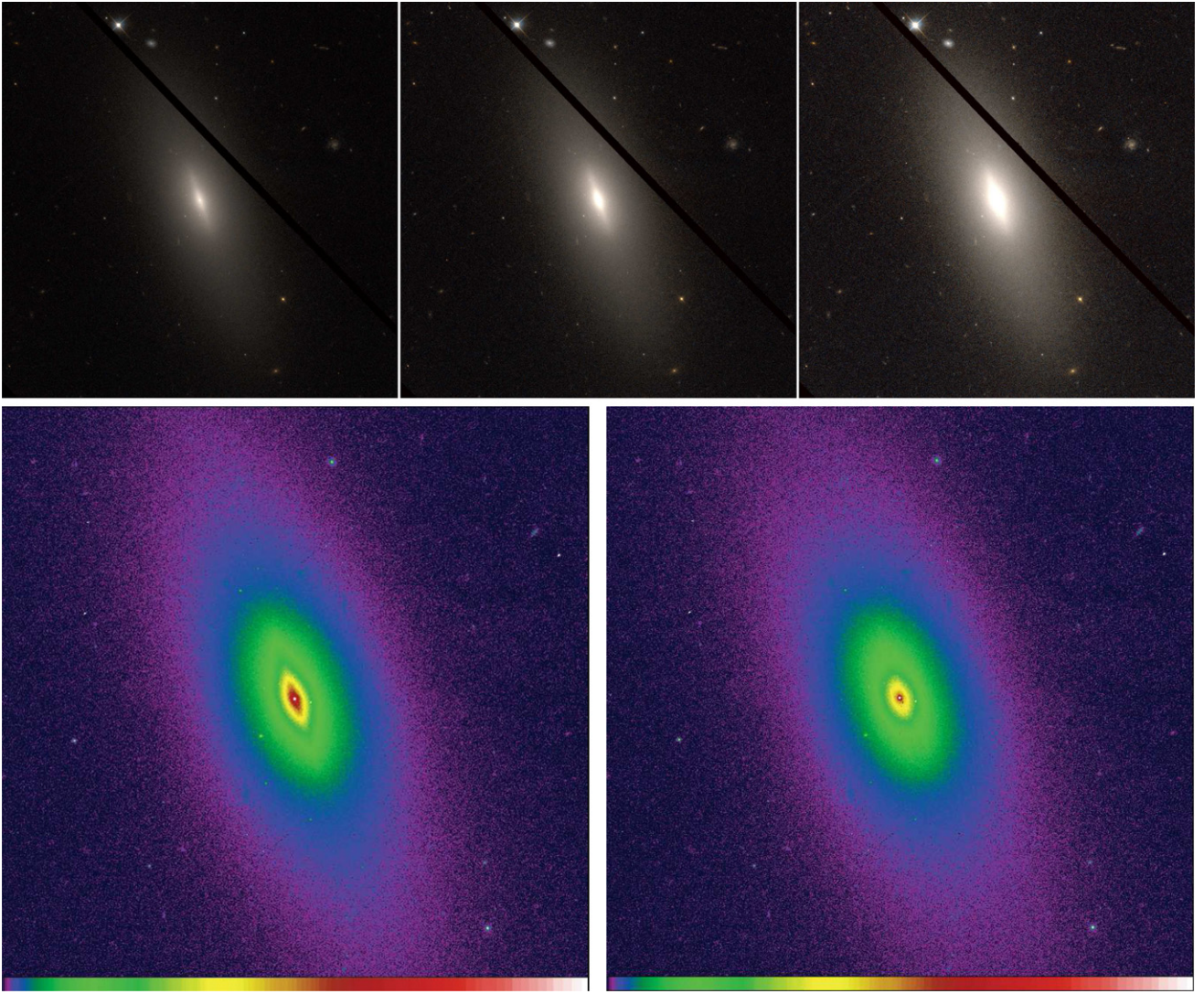
Figure 10. Top: color images of VCC 2048 constructed from the *Hubble Space Telescope* (*HST*) ACS *g* image (blue), the mean of the *g* and *z* images (green), and the *z* image (red). Different brightness "stretches" emphasize the embedded disk and nucleus (left), the disk (center), and the outer envelope (right). VCC 2048 is classified as an edge-on S0 by Binggeli et al. (1985) and Ferrarese et al. (2006). It clearly has an edge-on disk embedded in an ellipsoidal halo. Bottom: false-color images of VCC 2048 as observed (left) and after subtraction of the model, almost-edge-on ($i \simeq 81°$) disk that renders the residual isophotes as nearly elliptical as possible. This remnant envelope proves to have structural parameters characteristic of an Sph galaxy, not a bulge (Figure 12). VCC 2048 is therefore not an S0 galaxy but rather is an Sph,N galaxy with an embedded disk.

0.017 ± 0.004. This is closely similar to PB/T in the Scd galaxies M 101, NGC 6946, and IC 342 (Kormendy et al. 2010). Thus, NGC 4452 is an S0c galaxy. (If we had chosen the finer bins of the de Vaucouleurs classes, then NGC 4452 would be S0cd.) Similarly, with $B/T \simeq 0.08$, NGC 1411 is a more face-on S0c (Laurikainen et al. 2006).

Second, the outer disk of NGC 4452 is warped and thicker than the "superthin" edge-on, late-type galaxies seen in isolated environments (van der Kruit & Freeman 2011). Similarly, NGC 4762's outer disk is thick, warped, and tidally distorted. Gravitational encounters may be at fault (NGC 4762 with NGC 4754; NGC 4452 with IC 3381). We suggest that these are signs of environmental heating that helps to convert flat disks into less flat spheroidals.

4.1.3. The "Rosetta Stone" Galaxy VCC 2048: An Edge-on Sph Galaxy that "Still" Contains a Disk

VCC 2048 is—we suggest—just such a galaxy. It is usually classified E, but it contains an edge-on disk, suggesting that it

is a dS0 (F2006). The disk is illustrated in Figure 10. However, we will show that the rounder component of VCC 2048 is not a bulge. Rather, it is a more extreme version of the fat outer disks of NGC 4452 and NGC 4762. In fact, the outer component of VCC 2048 plots within the Sph sequence in the fundamental plane parameter correlations. This is therefore an Sph galaxy that "still" contains a small edge-on disk. It provides a compelling connection between Sphs and S0 disks, showing properties of both. VCC 2048 is a "Rosetta Stone galaxy" that supports the results of this paper especially clearly.
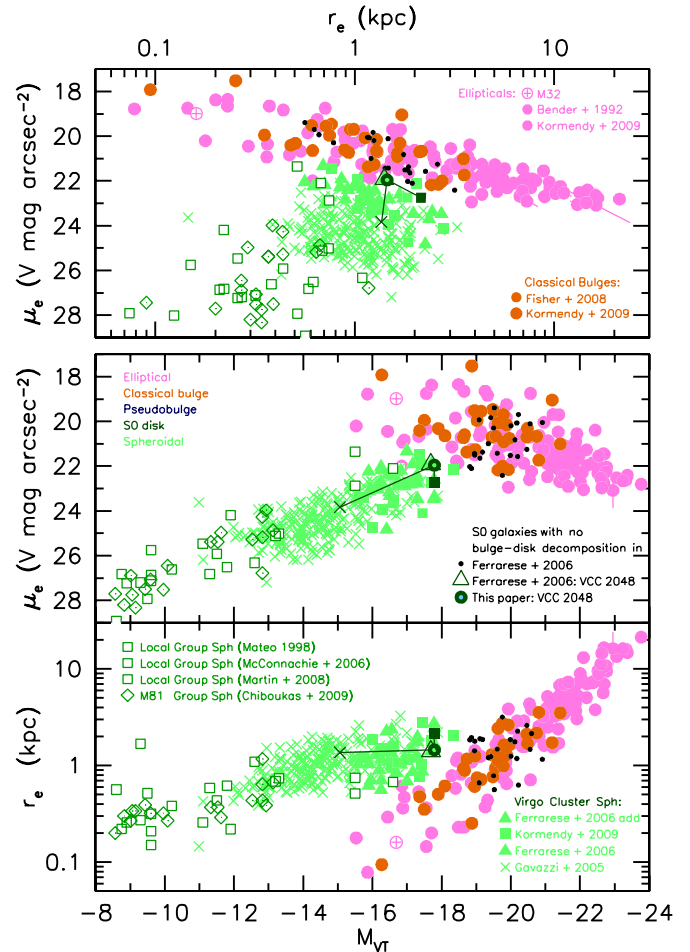
Figures 10 and 11 show our photometry and photometric decomposition of VCC 2048. The photometry uses the algorithm of Bender (1987), Bender & Möllenhoff (1987), and Bender et al. (1987, 1988) to fit the two-dimensional isophotes with ellipses plus deviations from ellipses that are expanded in a Fourier series in $a_k \cos k\theta$ and $b_k \sin k\theta$, where θ is the eccentric anomaly of the ellipse (Appendix A.1). The a_4 and a_6 terms measure disky ($a_4 > 0$) and boxy ($a_4 < 0$) distortions from exactly elliptical isophotes. The strong and weaker signatures
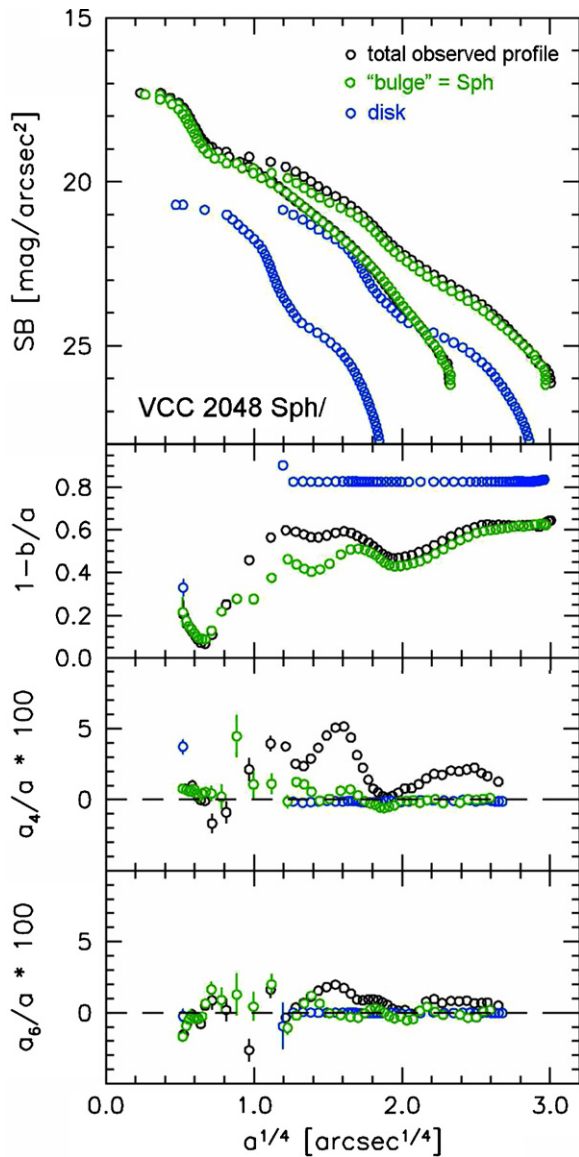
Figure 11. Profiles in VCC 2048 of (top–bottom) *V*-band surface brightness, ellipticity, and the isophote shape parameters a_4/a and a_6/a as functions of the major-axis radius *a*. Both major- and minor-axis profiles are shown. The observed profiles are shown by the black circles. The green and blue circles show the results of a photometric decomposition following the procedure of Scorza & Bender (1995) and illustrated here in Figure 10. A thin disk profile (blue points) is constructed non-parametrically such that, when inclined at the optimum inclination $i = 81°$ and subtracted from the two-dimensional light distribution, it renders the residual isophotes as nearly elliptical as possible. This is shown by the bottom two panels here: disk subtraction removes the large a_4 and a_6 disky signature in the original isophotes (black points) and leaves residual a_4 and a_6 profiles (green circles) that are consistent with zero, i.e., elliptical isophotes.

Figure 12. Parameter correlations from Figure 2 showing the results of the photometric decomposition of VCC 2048. Large green triangles show the total parameters measured by F2006 for the disk and envelope together. Our corresponding measurement for the whole galaxy agrees with F2006; it is shown by the green filled circle with the light green center. Our points are connected by straight lines to the envelope parameters (dark green filled squares) and the disk parameters (dark green crosses).

of an inner and an outer part of the embedded disk are clear in the raw a_4 and a_6 profiles (black points) in Figure 11.

Photometric decomposition was carried out using the procedure of Scorza & Bender (1995) and Scorza et al. (1998). A non-parametric profile is calculated for an infinitely thin disk with inclination $i = 81°$ such that subtraction of the disk from the two-dimensional image leaves behind residual isophotes that are as nearly elliptical as possible (Figure 10). Figure 11 (green points) shows that we succeed in removing the $a_4 > 0$ and $a_6 > 0$ disk signatures. The disk profile is shown blue in Figure 11. The effective parameters of the disk and main body

of the galaxy are calculated by integrating each profile. Results are shown in Figure 12. *We conclude that the main body of VCC 2048 is not a bulge. It is a spheroidal, and we classify the galaxy as Sph,N. Taking component flattening into account,* Sph/$T = 0.92 \pm 0.02$.

We emphasize that the difference between VCC 2048 and NGC 4452 is mainly quantitative and fairly subtle. NGC 4452 has a disk-to-total ratio of $D/T \simeq 0.43$, typical of S0 galaxies (e.g., Simien & de Vaucouleurs 1986). The inner parts of NGC 4452 contain a bar and a lens, these are common and characteristic components in SB0 galaxies (Kormendy 1979b, 1981, 1982; Buta & Crocker 1991; Sellwood & Wilkinson 1993; Buta 1995, 2011; Buta & Combes 1996; Buta et al. 2007, 2010a, 2010b). VCC 2048 has Sph/$T = 0.90$, $D/T \simeq 0.10$, and $B/T = 0$. Most of the light is in a component that is indistinguishable from spheroidal galaxies. Absent the embedded disk and given its effective parameters, the galaxy would certainly be classified as Sph,N. On the other hand, the similarities to NGC 4452 and NGC 4762 are compelling, too. The thick, main component of VCC 2048 does not look very different from the thick outer disks of the above S0 galaxies. We see signs that those outer S0 disks are even now being heated and thickened by tidal encounters with neighbors. We will find
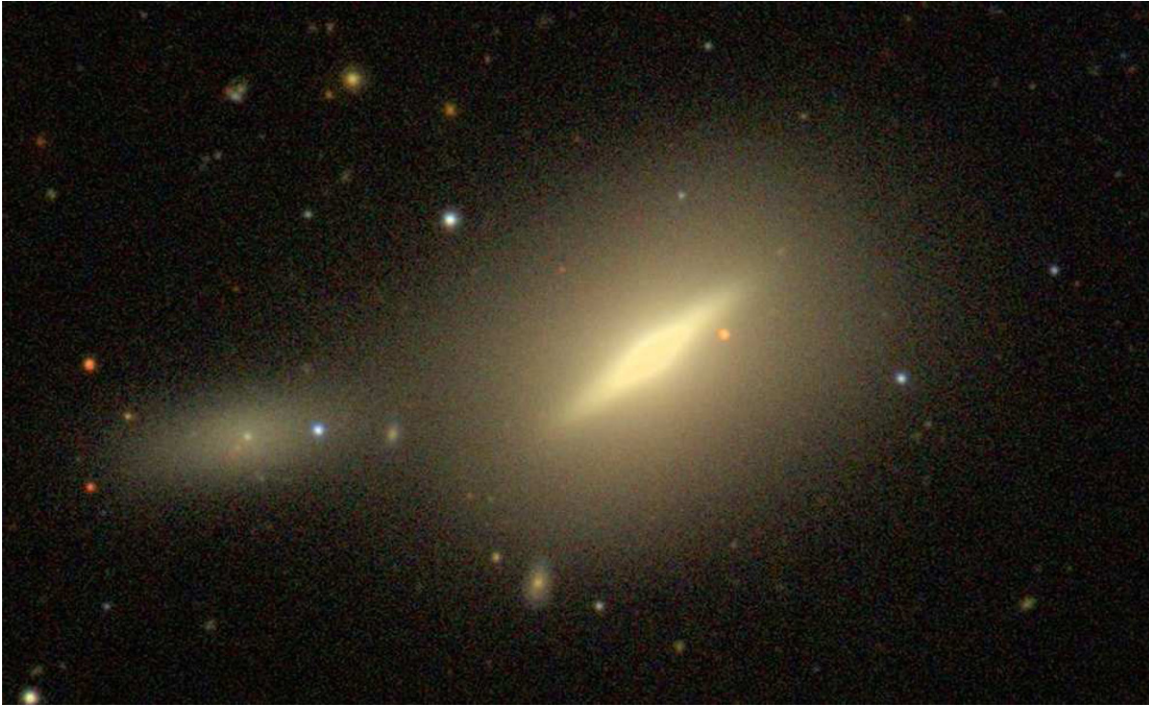
Figure 13. Color image of NGC 4638 = VCC 1938 from WIKISKY. The brightness "stretch" here emphasizes faint features, i.e., the extremely boxy, low-surface-brightness halo in which the S0 disk and bulge are embedded. The latter are illustrated using the *HST* ACS images in Figure 14. The elongated dwarf to the west of NGC 4638 is the Sph,N galaxy NGC 4637.

in the next section that S0 disks are continuous with spheroidals in their parameter correlations. This is an early sign of that result (see Appendix A.12 for further discussion).

We conclude that VCC 2048 is a "missing link" between S0 galaxies and spheroidals. We interpret the main body of the galaxy as a dynamically heated and therefore thick version of an S0 disk. We interpret the embedded disk as the inner, most robust remnant of the former S0 disk (although it is also possible that a small disk grew after the formation of the Sph by late infall of cold gas).

We note that similar edge-on disks have been detected in Fornax cluster Sph galaxies by De Rijcke et al. (2003).

The galaxies NGC 4762 (S0bc), NGC 4452 (S0c), and VCC 2048 (disky Sph,N) provide a continuous link between earlier-type S0 galaxies and Sphs. They include examples of the formerly missing, latest-type S0 galaxies. They are part of our motivation in placing Sph galaxies at the late-type end of the S0a–S0b–S0c sequence in Figure 1.

4.1.4. Another Missing Link between S0 and Sph Galaxies: NGC 4638 = VCC 1938

With the experience of the previous section, we are better prepared to interpret NGC 4638 = VCC 1938. It is illustrated in Figures 13 and 14. At first sight, it appears to be yet another ACS VCS S0 galaxy, that is, an edge-on S0 with a bulge that dominates at both small and large radii. However, the photometry reveals something much more remarkable. At the center, there is a normal, small, classical bulge (it is overexposed in Figure 13 but evident in Figure 14). The edge-on disk is essentially normal, too; it has a higher-than-normal apparent surface brightness only because of the long path length resulting from the fact that we see it edge-on. The remarkable thing about NGC 4638 is the diffuse, boxy halo. It proves to be a separate component from the disk and bulge. And its shallow surface brightness gradient is characteristic of a large spheroidal

Figure 14. Color image of NGC 4638 = VCC 1938 made from the *HST* ACS *g*, mean of *g* and *z*, and *z* images. This image shows the edge-on disk and central bulge. Brightness is proportional to the square root of intensity, so the brightness gradient in the bulge is much steeper than that in the boxy halo. The very red foreground star near the northeast side of the disk is also evident in Figure 13.

galaxy, not a bulge. NGC 4638 therefore has both S0 and Sph characteristics.

Figure 15 shows our photometry of NGC 4638. The bulge has the flattening and the large Sérsic index (albeit with large uncertainties) of a classical bulge. The disk is Gaussian, as are all lenses and many outer S0 disks discussed in the previous sections and in the Appendix.

The boxy halo is clearly distinct from the disk and bulge. Its profile is robustly concave-downward in Figure 15, indicating a small Sérsic index $n \simeq 1$. In contrast, if the bulge and halo formed a single component with a large Sérsic index, the halo profile would look concave-up in Figure 15. The small Sérsic
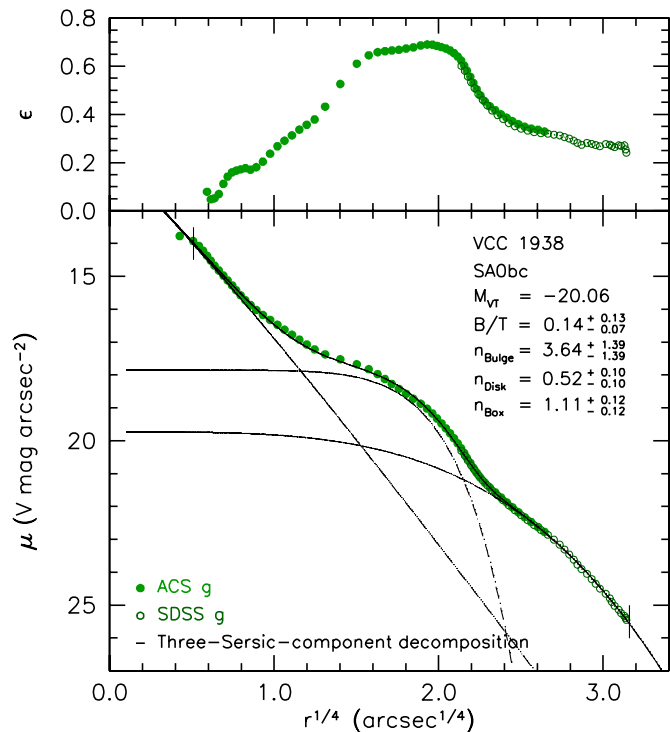
Figure 15. Ellipticity ϵ and surface brightness μ_V along the major axis of NGC 4638 as measured on the *HST* ACS and SDSS *g* images. Dashed curves show a three-Sérsic-function decomposition of the profile inside the fit range (vertical dashes). The bulge is small, but it is (at least) mainly classical. The disk has a Gaussian profile, as do many other S0s discussed in the Appendix. Remarkably, the outer, boxy halo is clearly distinct from the bulge and disk and has a Sérsic index $n = 1.11 \pm 0.12$ characteristic of an Sph galaxy. The sum of the components (solid curve) fits the data with an rms of 0.054 *V* mag arcsec^{-2}.

index is characteristic of an Sph galaxy or disk. Figure 16 shows how the F2006 whole-galaxy parameters are decomposed into bulge, disk, and halo parts. The halo plots within the bulge sequence, but it will prove to be consistent with S0 disks (Figure 18).

So NGC 4638 has properties of both S0 and Sph galaxies. We suggest that it was produced from a relatively normal SB(lens)0 or similar spiral galaxy by dynamical heating (i.e., harassment: Section 8.3) in a dense part of the Virgo Cluster (in projection, near NGC 4649 and surrounded on three sides by other galaxies: Figure 40). Its remaining disk may be the (robust) remnant of the lens, and the boxy halo may be the heavily heated remnant of a (much less robust) disk. Variants of this interpretation are possible (e.g., the disk may have formed after the Sph by late infall of cold gas).

4.2. Photometric Parameters of Virgo Cluster S0 Galaxies

Table 1 lists the photometric parameters of Virgo Cluster S0 galaxies measured in this paper. All ACS VCS S0s that are not measured in this paper have bulge–disk decompositions in Gavazzi et al. (2000), Laurikainen et al. (2010, VCC 1030 = NGC 4435; this *K*-band measurement is insensitive to dust), or Baggett et al. (1998, VCC 1535 = NGC 4526). Thus, all 100 galaxies from Ferrarese et al. (2006) appear in all of our parameter correlation diagrams.

Galaxies in Table 1 are listed in order of (pseudo)bulge-to-total luminosity ratio $(P)B/T$ (Column 5). Recall that all of these objects except the E galaxy NGC 4551 were classified S0 in F2006 and in standard catalogs. We base our conclusions on Table 1 and on the Virgo Cluster S0s discussed in KFCB.
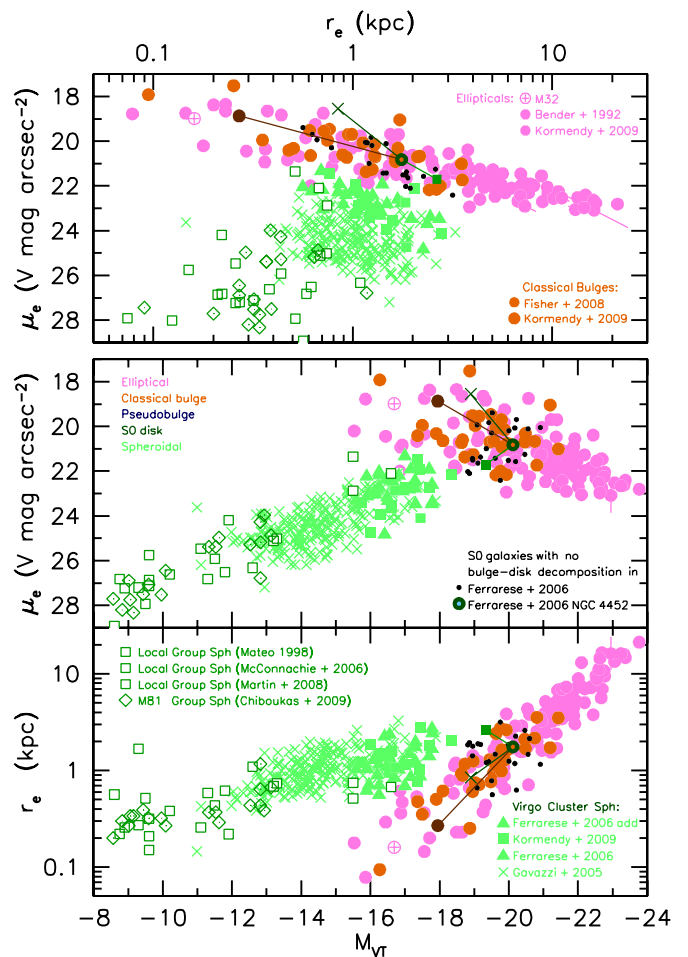
Figure 16. Parameter correlations showing the results of the photometric decomposition of NGC 4638. The green filled circles with the brown centers show the whole-galaxy parameters measured by F2006. Lines connect them to our measurements of the bulge (brown filled circles), disk (green crosses), and boxy halo (dark green filled squares).

Additional B/T values for S0 galaxies analyzed in KFCB are 0.77 ± 0.02 in NGC 4660 (S0a), 0.67 ± 0.04 in NGC 4564 (S0a), 0.52 in NGC 4570 (S0ab), 0.33 in NGC 4489 (S0b), and 0.13 in NGC 4318 (S0bc). *We conclude that S0 galaxies span the complete range of $(P)B/T$ ratios from 1 to 0. This provides quantitative justification for the parallel-sequence classification and for the addition of Sph galaxies, which have $(P)B/T \simeq 0$, at the end of the sequence.*

A provisional correspondence between $(P)B/T$ and stage along the Hubble sequence is proposed in Column 3. It was constructed by comparing these S0 galaxies to prototypical spiral galaxies with known $(P)B/T$ ratios. In addition, we choose to convert an *observational conclusion* about spiral galaxies into a *classification criterion* for S0s. Kormendy & Kennicutt (2004) conclude that no Sc galaxy known to them contains a classical bulge. Consequently, we choose here to classify any galaxy that contains even a small classical bulge as S0bc or earlier. In fact, the smallest $B/T = 0.13 \pm 0.02$ in NGC 4762 that we associate with type S0bc here corresponds well to $B/T = 0.12 \pm 0.02$ in the Sbc galaxy NGC 4258 (Kormendy 2011b). A detailed study of bulge classifications and $(P)B/T$ ratios in larger samples of spiral and S0 galaxies will be required to suggest more accurate Hubble stage classifications for S0s. Such studies are in progress.

Table 1
Structural Parameters of Virgo Cluster S0 and Sph Galaxies

Galaxy NGC (1)	Galaxy VCC (2)	Type (3)	D (Mpc) (4)	$(P)B/T$ (5)	$M_{V,\text{bulge}}$ (6)	n_{bulge} (7)	$\mu_{eV,\text{bulge}}$ (mag arcsec^{-2}) (8)	$\log r_{e,\text{bulge}}$ (kpc) (9)	$M_{V,\text{disk}}$ (10)	n_{disk} (11)	$\mu_{eV,\text{disk}}$ (mag arcsec^{-2}) (12)	$\log r_{e,\text{disk}}$ (kpc) (13)
N4551	V1630	E	16.14	$1.00^{+0.00}_{-0.00}$	-19.11	$1.968^{+0.056}_{-0.056}$	$20.715^{+0.032}_{-0.032}$	$0.080^{+0.005}_{-0.005}$	...	...	...	...
N4417	V944	SA0a	16.00	$0.88^{+0.06}_{-0.11}$	-19.89	$3.80^{+0.07}_{-0.11}$	$20.51^{+0.07}_{-0.07}$	$0.186^{+0.012}_{-0.012}$	-17.73	$0.52^{+0.06}_{-0.06}$	$21.70^{+0.12}_{-0.12}$	$0.495^{+0.014}_{-0.015}$
N4442	V1062	SB0a	15.28	$0.78^{+0.09}_{-0.11}$	-20.44	$3.20^{+0.31}_{-0.31}$	$20.06^{+0.38}_{-0.38}$	$0.193^{+0.095}_{-0.121}$	-19.07	$0.48^{+0.15}_{-0.15}$	$22.47^{+0.32}_{-0.32}$	$0.718^{+0.021}_{-0.022}$
N4352	V698	SA0a	18.7	$0.71^{+0.13}_{-0.05}$	-18.49	$3.70^{+0.5}_{-0.9}$	$21.89^{+0.05}_{-0.50}$	$0.191^{+0.053}_{-0.107}$	-17.52	$0.50^{+0.05}_{-0.12}$	$22.23^{+0.15}_{-0.02}$	$0.388^{+0.027}_{-0.015}$
N4578	V1720	SA0ab	16.29	$0.56^{+0.12}_{-0.12}$	-19.09	$3.13^{+0.44}_{-0.44}$	$20.70^{+0.47}_{-0.47}$	$0.035^{+0.110}_{-0.147}$	-18.83	$0.56^{+0.11}_{-0.11}$	$22.99^{+0.25}_{-0.25}$	$0.628^{+0.016}_{-0.017}$
N4483	V1303	SB0ab	16.75	$0.47^{+0.09}_{-0.09}$	-18.20	$4.5^{+0.5}_{-0.5}$	$21.34^{+0.35}_{-0.35}$	$-0.066^{+0.120}_{-0.167}$	-18.33	$1.1^{+0.2}_{-0.2}$	$21.89^{+0.29}_{-0.29}$	$0.266^{+0.032}_{-0.035}$
N4528	V1537	SB0ab	15.8	$0.38^{+0.13}_{-0.13}$	-18.04	$2.55^{+0.61}_{-0.20}$	$18.83^{+0.66}_{-0.26}$	$-0.533^{+0.169}_{-0.076}$	-18.43	$1.00^{+0.05}_{-0.05}$	$20.69^{+0.09}_{-0.14}$	$0.089^{+0.012}_{-0.012}$
N4623	V1913	SA0b	17.38	$0.26^{+0.12}_{-0.09}$	-17.47	$3.34^{+0.76}_{-0.76}$	$21.18^{+0.85}_{-0.85}$	$-0.166^{+0.188}_{-0.339}$	-18.61	1.00	$21.41^{+0.08}_{-0.08}$	$0.387^{+0.008}_{-0.008}$
N4638	V1938	SA0bc	17.46	$0.14^{+0.13}_{-0.07}$	-17.94	$3.64^{+1.39}_{-1.39}$	$18.87^{+1.54}_{-1.54}$	$-0.570^{+0.224}_{-0.490}$	-18.90	$0.52^{+0.10}_{-0.10}$	$18.55^{+0.14}_{-0.14}$	$-0.074^{+0.014}_{-0.014}$
N4638	V1938	SA0bc	17.46	$0.14^{+0.13}_{-0.07}$	...	...	...	...	-19.34	$1.11^{+0.12}_{-0.12}$	$21.70^{+0.16}_{-0.16}$	$0.422^{+0.025}_{-0.027}$
N4762	V2095	SB0bc	16.53	$0.13^{+0.02}_{-0.02}$	-18.76	$2.29^{+0.05}_{-0.05}$	$18.58^{+0.05}_{-0.05}$	$-0.382^{+0.014}_{-0.015}$	-20.82	...	$20.57^{+0.09}_{-0.09}$	$0.822^{+0.043}_{-0.048}$
N4550	V1619	SA0c	15.49	$0.018^{+0.003}_{-0.005}$	-15.04	$1.54^{+0.20}_{-0.38}$	$17.16^{+0.25}_{-0.45}$	$-1.382^{+0.065}_{-0.160}$	-19.38	$1.69^{+0.13}_{-0.08}$	$20.21^{+0.33}_{-0.33}$	$0.240^{+0.006}_{-0.005}$
N4452	V1125	SB0c	16.53	$0.017^{+0.004}_{-0.004}$	-14.78	$1.06^{+0.14}_{-0.14}$	$19.33^{+0.17}_{-0.17}$	$-0.778^{+0.046}_{-0.051}$	-19.19	...	$20.31^{+0.05}_{-0.05}$	$0.454^{+0.005}_{-0.005}$
...	V2048	Sph, N	16.53	$0.000^{+0.00}_{-0.00}$	...	...	...	...	-15.06	...	$23.83^{+0.20}_{-0.15}$	$0.134^{+0.057}_{-0.013}$
...	V2048	Sph, N	16.53	$0.000^{+0.00}_{-0.00}$	...	...	...	...	-17.78	...	$22.75^{+0.20}_{-0.09}$	$0.332^{+0.052}_{-0.025}$

Notes. We adopt individual distances D (Column 4) from Mei et al. (2007) when available. Otherwise, we use the mean distance $D = 16.53$ Mpc for "all [79] galaxies (no W′ cloud)" given in Table 3 of Mei's paper. Colors encode structural component types to match colors used for symbols in correlation plots: red for elliptical galaxies, brown for classical bulges, blue for pseudobulges and disks, and green for spheroidals. Column 5 gives the classical-bulge-to-total luminosity ratio B/T or the pseudobulge-to-total luminosity ration PB/T. Columns 6–9 list the (pseudo)bulge parameters bulge absolute magnitude $M_{V,\text{bulge}}$, Sérsic index n, effective brightness $\mu_{eV,\text{bulge}}$ at the effective radius, and the base-10 logarithm of the major-axis effective radius $r_{e,\text{bulge}}$ that contains half of the light of the bulge. Columns 10–13 similarly list the disk parameters. Two galaxies contain a component that looks indistinguishable from spheroidal galaxies, it is listed in the disk columns in green. Both of these galaxies also have disks and so appear in two lines. Parameter errors are the internal errors given by the Sérsic–Sérsic decomposition program combined with errors given by comparing decompositions made with different assumptions (e.g., disk fixed as exponential, or different fitting ranges). Parameter errors for photometric decompositions are uncertain because of strong (e.g., bulge–disk) parameter coupling and because they depend on the fitting functions that are assumed to describe the components.

4.3. Parameter Correlations Including Virgo Cluster S0 Galaxies

Figure 17 shows the $\mu_e - r_e - M_V$ correlations with the bulges of Virgo Cluster S0s added. All ACS VCS galaxies are included here and in all further figures. Also added are S0 bulges from the bulge–disk decompositions of Baggett et al. (1998). Bulge results are discussed here; S0 + S galaxy disks are added in the next section.

Figure 17 shows that classical bulges and elliptical galaxies have indistinguishable parameter correlations. The few pseudobulges that happen to be in our S0 sample deviate only a little from the above correlations, but larger samples of pseudobulges in later-type galaxies show larger scatter than classical bulges toward both high and low surface brightnesses. These results confirm the conclusions of many previous studies (e.g., Kormendy & Fisher 2008; Fisher & Drory 2008). The important new result is that adding the ACS VCS and Baggett S0s strengthens our derivation of the E + bulge correlations, especially at the compact end of the luminosity sequence. The conclusion that Sph galaxies are not dwarf ≡ low-luminosity ellipticals is correspondingly strengthened also.

5. THE PARAMETER CORRELATIONS OF Sph GALAXIES ARE CONTINUOUS WITH THOSE OF S0 DISKS

Section 4 establishes complete continuity between early-type S0 galaxies with large bulges and Sph galaxies with no bulges. It includes examples of the formerly missing, late-type (S0bc–S0c) galaxies with tiny bulges. Also, the Sph VCC 2048 and the S0 NGC 4638 show aspects of both kind of galaxy, i.e., edge-on disks embedded in Sph-like halos. In this section, we make this link more quantitative with a larger sample of galaxies.

Figure 18 shows the $\mu_e - r_e - M_V$ correlations for Es + bulges and Sph galaxies with S0 disks added. The data come from the bulge–disk decomposition papers listed in the key in the middle panel. Extending results from the previous section, Figure 18 shows that the Sph galaxy sequence is continuous with the sequence of S0 galaxy disks. There is a kink where bulges disappear and where (we suggest) the correlations turn into a sequence of decreasing baryon retention at lower galaxy luminosity (Sections 3.2.4, 8, and 9).

Figure 18 includes 127 S0 galaxy disks from five sources:

Five disks are from decompositions in KFCB. This paper provides four from the main text and eight from the Appendix.

Gavazzi et al. (2000) provide H-band photometry and photometric decompositions for 19 Virgo Cluster S0s, 13 of which are also in the ACS VCS. The 19 galaxies that we use here do not include NGC 4489 = VCC 1321 (we use KFCB results), or 3 more galaxies that we remeasure here. One additional galaxy was discarded because it is severely tidally distorted, and one is clearly an Sa.

Baggett et al. (1998) provide 16 S0 disk parameters. These decompositions are somewhat less accurate than the more recent ones, because they use $r^{1/4}$ laws to describe the bulges. We therefore apply somewhat stricter quality cuts: we keep the
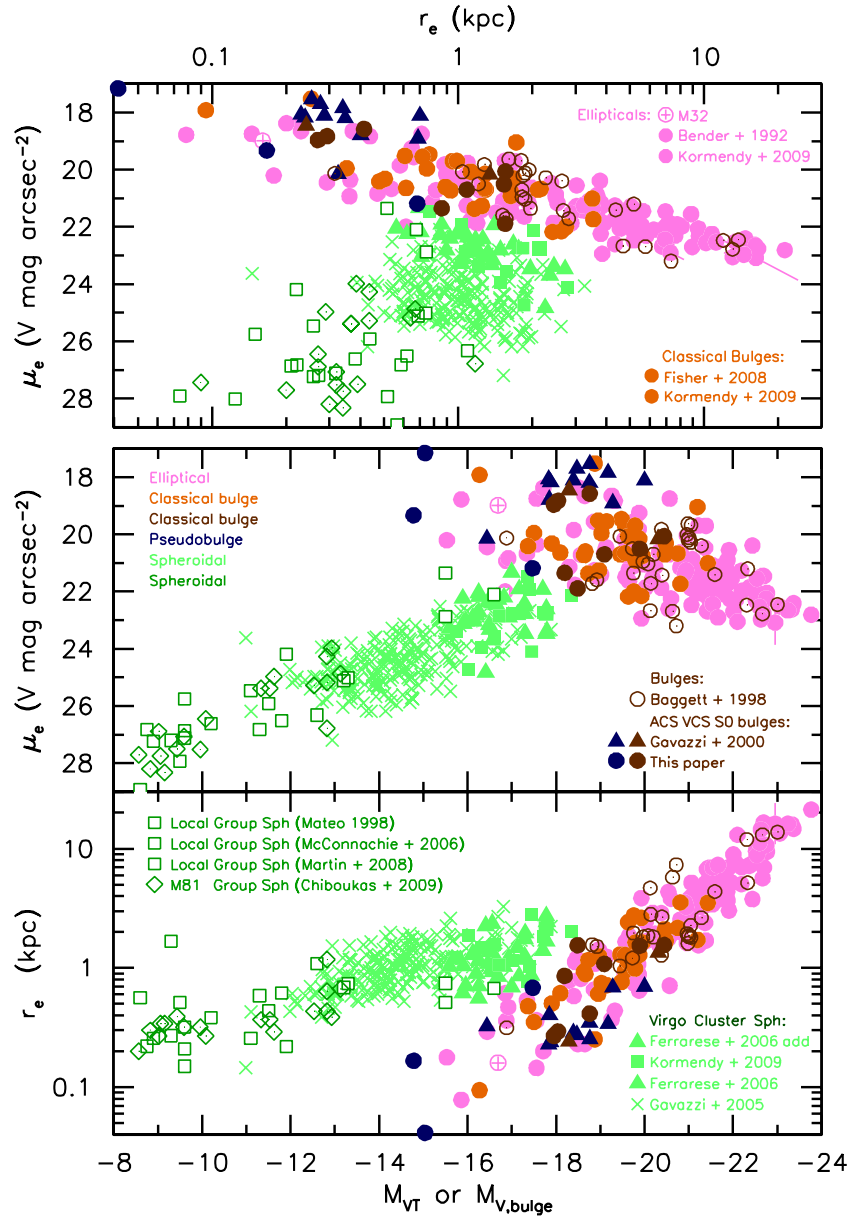
Figure 17. Global parameter correlations from Figure 2 including the augmented sample of bulges from this study. All 26 ACS VCS S0s that were omitted in KFCB are included here, 3 as Sphs and 23 as bulges. Galaxies with profile measurements and photometric decompositions in this paper are shown as dark brown or dark blue filled circles. The remaining ACS VCS S0s have photometric decompositions in Gavazzi et al. (2000) and are similarly shown as filled triangles. In addition, S0 bulges from the photometric decompositions of Baggett et al. (1998) are added as open circles. We do not have bulge–pseudobulge classifications for them, but most are likely to be classical based on their bright $M_{V,bulge}$. This is our final E + bulge sample. For simplicity, points in further figures encode bulge type but not the source of the data.

galaxy only if r_e/seeing > 4.5 and if $T < 0$, where "seeing" is tabulated in Baggett's paper.

Laurikainen et al. (2010) provide 85 S0 galaxies; i.e., de Vaucouleurs type $T \leqslant 0$ and yet not elliptical and not a merger in progress (i.e., a disturbed E with shells and tidal tails). We were conservative in correcting Hubble types. The most common correction is that many of the brightest cataloged "S0s" are really ellipticals. They get misclassified as S0s for two reasons. (1) A prominent dust disk is enough to earn an S0 classification in many papers. An example in the Virgo Cluster is NGC 4459. KFCB show that its main body is well described by a single Sérsic function with, at small radii, extra light over the inward extrapolation of the outer Sérsic fit. (2) The brightest ellipticals have Sérsic profiles with $n \gg 4$. Morphologists sometimes see these as core-halo objects and so classify the galaxies as S0.

NGC 4406 is an example. KFCB discuss these classification problems. In the present sample, some of the brightest "S0s" probably are ellipticals. Figure 18 shows that such objects are consistent with the E correlations even when they are treated as S0s.

Only a limited number of S0s are near enough for detailed component studies. It is inevitable that various authors' samples overlap. We made sure that each galaxy is plotted only once in Figure 18. In cases of duplication, we usually kept the results from our work, Gavazzi, Baggett, and Laurikainen in this order. This is why numbers of galaxies from some sources look surprisingly small.

We conclude from Figure 18 that the main bodies of Sph galaxies (not including nuclei) form a continuous sequence in parameter space with the disks (but not the bulges) of S0
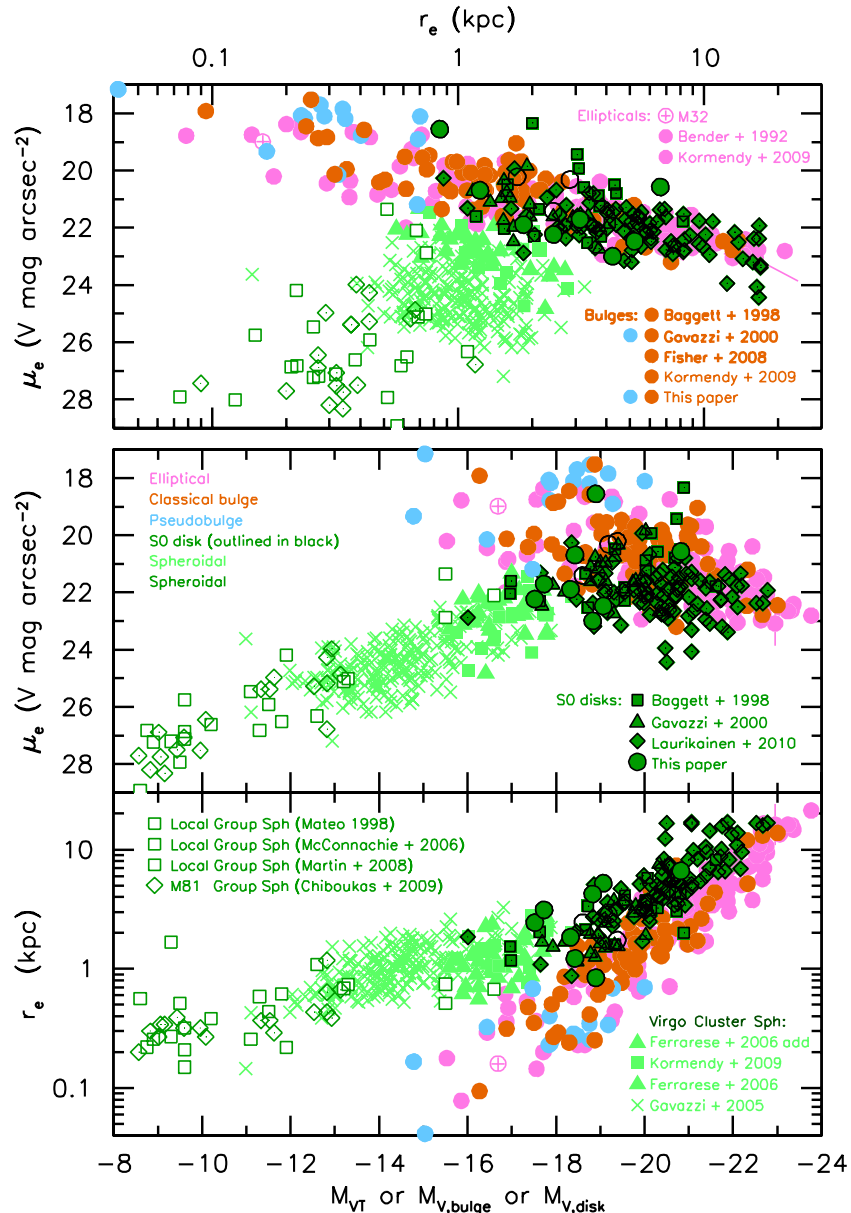
Figure 18. Parameter correlations for ellipticals, bulges, and Sphs with S0 disks added (green points outlined in black). Bulges and disks of S0 galaxies are plotted separately. All S0 galaxies from the ACS VCS survey (Ferrarese et al. 2006) are plotted. The middle panel shows the Freeman (1970) result that disks of high-luminosity galaxies tend to have the same central surface brightness μ_0. Here, $\mu_e \simeq 22.0$ V mag arcsec^{-2} corresponds to $\mu_0 = \mu_e - 1.82 \simeq 20.2$ V mag arcsec^{-2} or about 21.1 B mag arcsec^{-2}. This is slightly brighter than the Freeman value of 21.65 B mag arcsec^{-2}, because many of the disk parameters are not corrected to face-on orientation. Most disks that have higher-than-normal surface brightnesses are edge-on (e.g., our measurements of NGC 4762 and NGC 4452). Most disks that have lower-than-normal surface brightnesses are in galaxies that have outer rings; μ_e is faint because the outer ring is included in the measurements. We conclude from this figure that Sph galaxies are continuous with the disks but not the bulges of S0 galaxies.

galaxies. This is consistent with and one of the motivations for our suggestion that Sph galaxies belong at the late-type end of the Figure 1 tuning-fork diagram next to S0cs.

The Sph and S0 disk sequences overlap a little but not very much. This is partly a selection effect. The faintest true S0s do not make it into most galaxy samples. Objects that are traditionally classified as dS0 almost always turn out to be bulgeless and therefore (by definition) are Sph.

Nevertheless, S0 galaxies with disk absolute magnitudes $M_{V,disk} \gtrsim -18$ are rare. Figure 19 (reproduced from Kormendy & Freeman 2011) shows why. It quantifies the "rotation curve conspiracy" that visible matter and dark matter (DM) are arranged in galaxies so as to produce approximately featureless, flat rotation curves (Bahcall & Casertano 1985; van Albada

& Sancisi 1986; Sancisi & van Albada 1987). The rotation velocities produced by the bulge, disk, and halo are nearly equal ($V_{circ,bulge} \simeq V_{circ,disk} \simeq V_{circ}$) in galaxies with $V_{circ} \sim 200$ km s^{-1}. In smaller galaxies, $V_{circ,disk} \rightarrow 0$ at finite $V_{circ} \simeq 42 \pm 4$ km s^{-1}. This tells us the mass scale below which dark halos generally cannot capture or retain baryons (Kormendy & Freeman 2011). It is in good agreement with the theoretical prediction that the formation of visible dwarfs is suppressed below $V_{circ} \sim 30$–40 km s^{-1} because few such galaxies accrete enough gas before cosmological reionization to become discoverable (Bullock et al. 2000; Cattaneo et al. 2011).

The important point here is that the correlation for bulges is steeper than the one for disks and reaches zero at
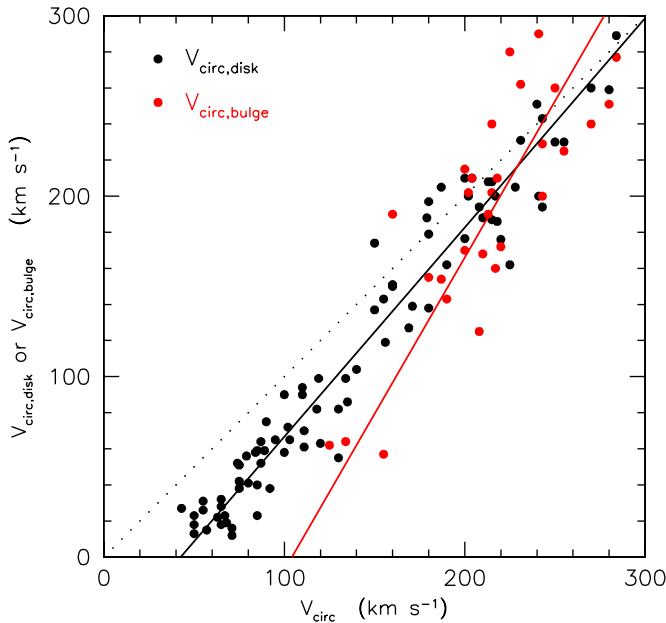
Figure 19. Maximum rotation velocity of the bulge $V_{circ,bulge}$ (red points) and disk $V_{circ,disk}$ (black points) given in bulge–disk–halo decompositions of observed rotation curves $V(r)$ whose outer, DM rotation velocities are V_{circ}. This figure is from Kormendy & Freeman (2011, updated from Figure S2 in Kormendy & Bender 2011); references to the $V(r)$ decomposition papers are given there. The dotted line indicates that the rotation velocities of the visible and dark matter are equal. Every red point has a corresponding black point, but many late-type galaxies are bulgeless, and then the plot shows only a black point. The lines are symmetric least-squares fits; the disk fit is $V_{circ,disk} = (1.16 \pm 0.03)(V_{circ} - 200) + (183 \pm 3)$ km s^{-1}; $V_{circ,bulge} = (1.73 \pm 0.29)(V_{circ} - 200) + (166 \pm 9)$ km s^{-1} is the bulge fit. The correlation for bulges is steeper than that for disks; bulges disappear at $V_{circ} \sim 104 \pm 16$ km s^{-1}.

$V_{circ} \sim 104 \pm 16$ km s^{-1}. Progenitor late-type galaxies like M 33 and fainter do not—by and large—contain bulges.

The Tully & Fisher (1977) relation for S0 galaxies tells us that $V_{circ} = 104$ km s^{-1} at $M_V \simeq -17$ to -18 (Neistein et al. 1999; Hinz et al. 2003; Bedregal et al. 2006; Williams et al. 2010). This is in excellent agreement with Figure 18: it is the disk absolute magnitude where S0s stop and spheroidals take over. When no bulge is visible, morphologists call the galaxy a spheroidal. S0s and Sphs overlap a little in luminosity, because the disappearance of bulges does not happen exactly at some magic disk $M_{V,disk}$.

In summary, the structural parameter correlations of spheroidal galaxies are continuous with the disks of S0 galaxies. The changeover in nomenclature does not reflect some fundamental change in galaxy properties but rather happens at the disk absolute magnitude where rotation curve decompositions tell us that bulges disappear.

6. THE PARAMETER CORRELATIONS OF SPHEROIDAL GALAXIES AND S0 GALAXY DISKS ARE INDISTINGUISHABLE FROM THOSE OF SPIRAL-GALAXY DISKS AND MAGELLANIC IRREGULARS

The result which suggested that Sph galaxies are defunct S + Im galaxies was the observation by Kormendy (1985, 1987) that their parameter correlations are indistinguishable over the absolute magnitude range in which they overlap. However, galaxy samples were small in the 1980s. Also, we now need

to understand a sequence of Sphs + S0 disks that is continuous from S0s with $M_{V,disk} \simeq -22$ to Sphs with $M_{VT} \simeq -8$ and probably much fainter. Figure 20 brings the results of Kormendy (1985, 1987) up to date with a much larger sample of spiral-galaxy disks and Im galaxies. It confirms that early- and late-type galaxies have similar disk parameter correlations from the brightest disks to the faintest spheroidals and irregulars.

Figure 20 includes 407 Sa–Im galaxy disks from 14 sources. We concentrate on Sc–Im galaxies because our purpose is to compare S0 disks with late-type galaxies that may be progenitors. Also, disk parameters of Sc–Im galaxies are relatively well determined because decompositions do not have to deal with large bulges. However, we do include a sample of 28 Sa galaxy disks from Laurikainen et al. (2010) to demonstrate that early-type disks are not very different from late-type disks in their structural parameters. As in Section 5, the number of nearby galaxies is limited, so there is overlap between papers. We ensure that each galaxy is plotted only once and take galaxies from various samples in the following order of preference (highest first).

Parameters for the irregular galaxies in the Local Group were taken from Bothun & Thompson (1988, LMC and SMC), Mateo (1998, 10 objects), Karachentsev et al. (1999, Sag DIG), Irwin et al. (2007, Leo T), and Kirby et al. (2008, DDO 210 and IC 5152).

Chiboukas et al. (2009) measured 19 dwarf Sph and 16 dS + Im galaxies in the M 81 group. The spheroidals were added earlier to all parameter correlation figures; the late-type galaxies are added here. These objects greatly strengthen the derivation of the Sph and disk sequences at the lowest luminosities and show that the sequences remain remarkably similar all the way down to $M_V \simeq -9$.

Turning next to the Virgo Cluster, this paper contributes one object, VCC 1512. It was recognized by F2006 as an Sph/Im transition object. They "deemed... all [their measurements of] integrated quantities for this galaxy [as] unreliable." We classify it as Im, although the difference is small and not important for our interpretation. We remeasured the ACS g image and derive the parameters shown in Figure 20 by the blue filled square.

F2006 recognized four additional galaxies as Sph/Im transition objects, VCC 21, VCC 571, VCC 1499, and VCC 1779. All have some star formation, and several show prominent blue star clusters. These objects were plotted as Sphs in KFCB, but it is more appropriate to plot them as blue filled triangles here.

Gavazzi et al. (2000) published K'-band photometry and photometric decompositions of late-type VCC galaxies. This contributes 29 Sc–Im galaxies to our sample. About 1/3 of the galaxies are giants ($M_{V,disk} < -18$), so this sample provides good overlap between giants and dwarfs.

Courteau et al. (2007) is our primary source of disk parameters. Figure 20 includes 181 Courteau Sc–Im galaxies measured in I band and transformed to V band using $V - I$ colors tabulated in his paper. We kept galaxies with distances $D < 70$ Mpc. Courteau studied mostly giant galaxies, but a few dwarfs overlap the Sph sequence.

Baggett et al. (1998) is the source for 27 Scd–Im disk parameters. As we did for S0 disks, we keep a galaxy only if the $bulge$ r_e/seeing > 4.5, where "seeing" is tabulated in Baggett's paper. This eliminates galaxies that show larger-than-normal scatter, presumably because they are not well enough resolved for reliable bulge–disk decomposition. Our Hubble type selection is $T > 5$. Recall that Baggett's measurements are in V band.
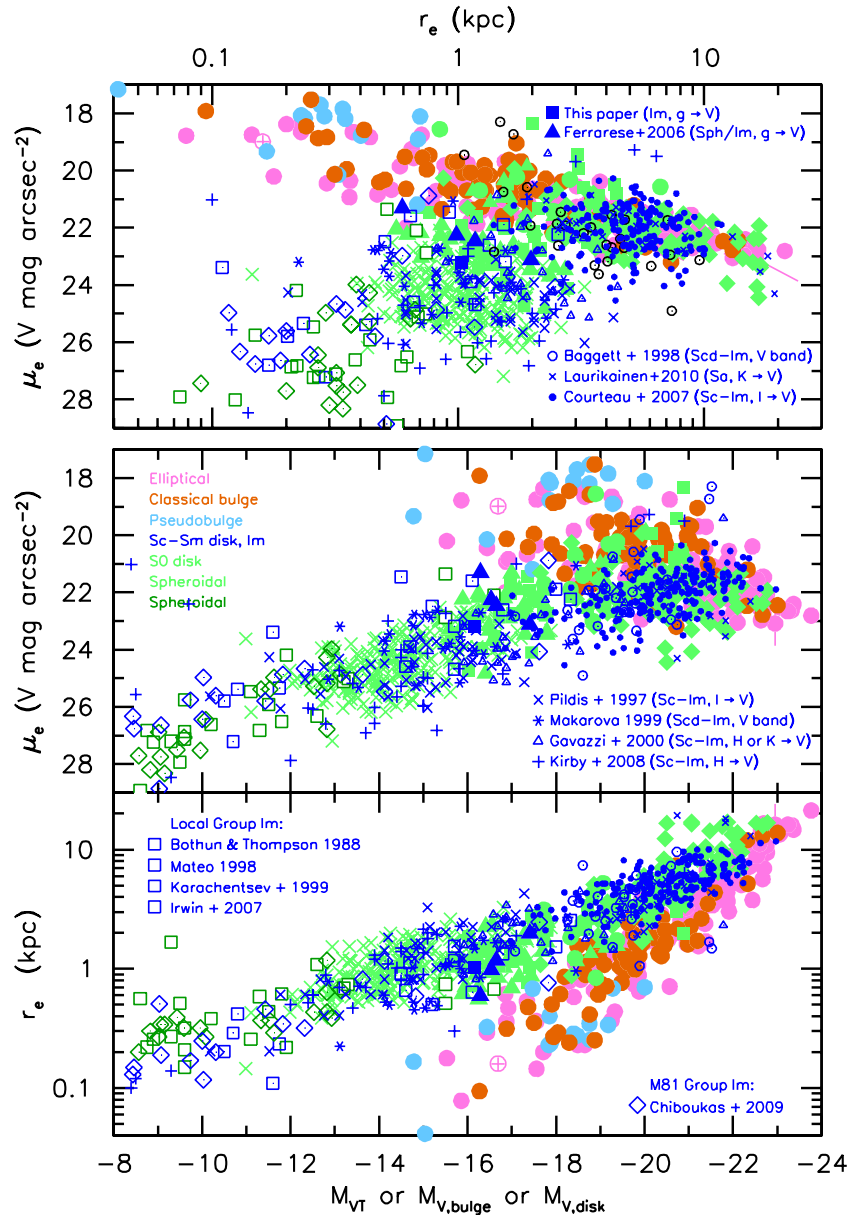
Figure 20. Parameter correlations for ellipticals, bulges, Sphs, and S0 disks, plus disks of Sa–Im galaxies (blue points). When (pseudo)bulge–disk decomposition is necessary, the two components are plotted separately. All S0 galaxies from the ACS VCS survey (Ferrarese et al. 2006) are plotted (light brown and light green points). Also, blue points show four galaxies from Ferrarese et al. (2006) that they note are Sph/Im transition galaxies and one galaxy (VCC 1512) from the above paper that we classify as Im and that we remeasured. Most disks that have lower-than-normal surface brightnesses are in galaxies that have outer rings, and most disks that have higher-than-normal surface brightnesses are either edge-on or starbursting. However, starbursting blue compact dwarf galaxies (BCGs) are omitted; they would add a few galaxies that scatter to higher surface brightnesses. The blue points represent 407 galaxies from 14 sources listed in the keys.

Laurikainen et al. (2010) provide 28 mostly Sa galaxies; i.e., de Vaucouleurs type $T = 1$. Sa galaxies are invariably giants (e.g., Sandage 1975; van den Bergh 2009a), so they help to constrain the S0–Sc comparison, but they do not overlap the spheroidals.

Pildis et al. (1997) measured 46 Sc—(mostly) Im galaxies in I band. Most galaxies are faint and help to define the dwarf part of the disk sequence. We kept galaxies with heliocentric velocities < 3000 km s^{-1}.

Makarova (1999) measured 26 Scd—(mostly) Im galaxies; all except one are at distances $D \leqslant 8.6$ Mpc. This paper helps greatly to define the dwarf part of the disk sequence. The measurements were made in V band.

Kirby et al. (2008) measured 33 Sc—(mostly) Im and mostly dwarf galaxies in H band.

Figure 20 updates parameter correlations of late-type galaxy disks studied previously by many authors beginning with Freeman (1970). As noted also in Figure 18, we confirm yet again the Freeman (1970) result that giant galaxy disks generally have nearly uniform central surface brightnesses that vary little with disk luminosity. In contrast, r_e or equivalently the exponential scale length $h = r_e/1.678$ varies with $L_{V,\mathrm{disk}}$ over the whole luminosity range, accounting in giant galaxies for most of the variation in $L_{V,\mathrm{disk}} \simeq 2\pi I_0 h^2$, where $\mu_0 = -2.5 \log I_0 = \mu_e - 1.822$ is the central surface brightness in magnitude units.

Figure 20 confirms the results of Kormendy (1985, 1987) that the parameter correlations for late-type and spheroidal galaxies are indistinguishable. It extends this result to the brightest S0 and Sc–Scd disks. This is consistent with our suggestion that
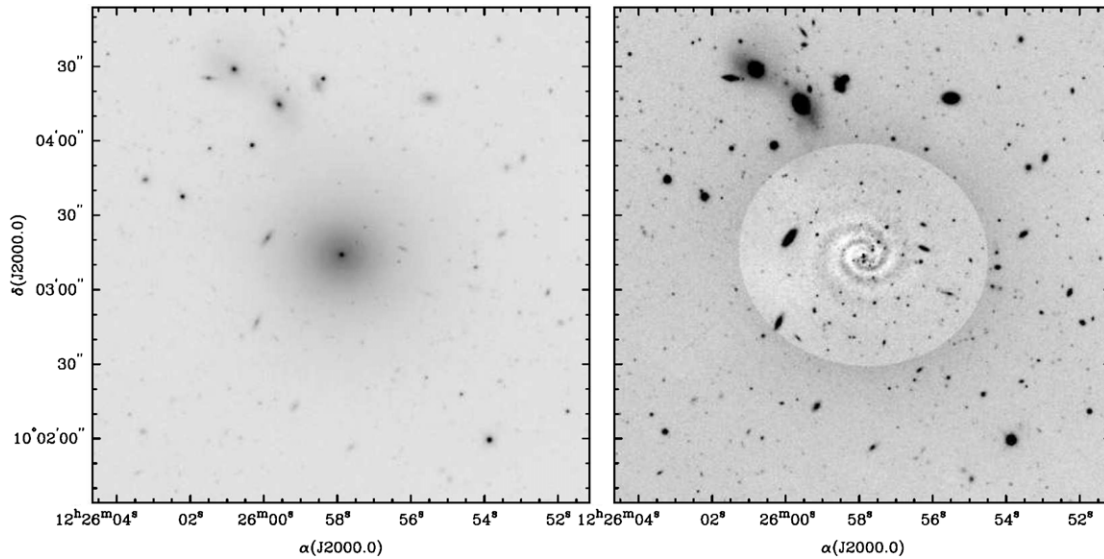
Figure 21. Spiral structure in the Sph,N galaxy IC 3328 = VCC 856. At $M_V \simeq -17.8$, this is one of the brightest spheroidals in the Virgo Cluster. An R-band image (left) shows the low-surface-brightness, shallow-brightness-gradient, but nucleated light distribution that is characteristic of Sph galaxies. After subtraction of the overall, elliptically symmetric light distribution (right), the residual image shows tightly wound, two-armed spiral structure. This means that IC 3328 is—or at least contains—a disk. This figure is taken from and kindly provided by Jerjen et al. (2000).

Sph and late-type galaxies are closely related. The nature of the relationship is complicated: ongoing star formation increases the disk surface brightness whereas dust extinction reduces it, and the quenching of star formation by ram-pressure stripping results in fading of the young stellar population and hence of the disk as a whole. We return to this issue in Section 8. Here, we emphasize that the similarity of the S and S0 disk correlations forms part of our motivation for suggesting parallel S0–Sph and spiral galaxy sequences in Figure 1.

Deriving these results accurately over large ranges in M_V requires detailed photometry and photometric decomposition of nearby, well-resolved galaxies. However, we note that the difference between the E + bulge and Sph + disk sequences is also seen in an SDSS study of 140,000 galaxies by Shen et al. (2003).

Figure 20 has implications for the formation of elliptical galaxies by major mergers. In terms of effective parameters (i.e., those relevant to Virial theorem arguments), making present-day normal-luminosity giant ellipticals out of present-day giant disks requires relatively little dissipation. We observe that such mergers happen, and their remnants are consistent with extra-light Es (see KFCB for a review). This is plausible: present-day disk galaxies contain little enough gas so that rearranging it during a merger cannot have a large effect on effective parameters. However, making the high-density centers of ellipticals requires substantial dissipation and star formation, as reviewed in KFCB. And making present-day small ellipticals out of present-day progenitors requires much more dissipation as galaxy luminosity decreases (Kormendy 1989).

We emphasize that these reassuring consistency checks apply only to the relatively few ellipticals that are made recently enough so that the properties of present-day progenitors are relevant. Most ellipticals formed much longer ago out of progenitors that we are only beginning to observe.

7. ADDITIONAL CONNECTIONS BETWEEN Sph GALAXIES AND S0 AND SPIRAL GALAXY DISKS

In Section 7.1, we review additional observations which show that Sph galaxies are related to S0 galaxy disks, especially at

high luminosities. Then in Section 7.2, we review observations which support the idea that Sph and S0 galaxies are transformed, "red and dead" spiral and irregular galaxies.

7.1. Further Evidence that Higher-Luminosity Sphs are More Disk-Like

The fact that spheroidal galaxies can contain disks was emphasized in Section 4.1.3 using VCC 2048, an edge-on Sph that shows the disk directly. A close relation to S0 disks is also implied by the observation that the main body of VCC 2048 is flatter than any elliptical (E6.2 plus an additional 2% disky distortion—see Figure 11). Two additional observations show more indirectly but for a larger sample of objects that Sphs are related to disks.

First, some of the brighter Sph galaxies in Virgo show low-amplitude spiral structure in their otherwise-smooth light distributions. This was first—and still best—seen by Jerjen et al. (2000) in IC 3328. Their result is reproduced here in Figure 21. No dynamically hot stellar system such as an elliptical galaxy can produce fine-scale spiral structure. Barazza et al. (2002) confirmed Jerjen's result and concluded that "This is unambiguous evidence for the presence of a disk."

Similar but less obvious spiral structure has been seen in other spheroidals (Jerjen et al. 2001; Barazza et al. 2002; De Rijcke et al. 2003; Graham et al. 2003; Ferrarese et al. 2006; Lisker et al. 2006, 2007, 2009). Not all cases are significant. Barazza et al. (2002) caution us that, when the spirals are weak, features in the ellipticity and position angle profiles that are not spiral structure "can indeed produce amazingly spiral-like twisting isophotes and thus mimic genuine spiral structure." The weakest observed spiral signals should be interpreted with caution, but the large number of detections implies that some spirals are real. Again, this is compelling evidence that bright Sph galaxies are related to S0 disks.

The second kind of evidence comes from measurements of rotation velocities and velocity dispersions. At a time when it was already understood that low-luminosity ellipticals rotate roughly like isotropic spheroids (Davies et al. 1983; see

Section 2.1 here), it was a surprise when Bender & Nieto (1990) found that the Sphs Fornax, NGC 205, IC 794, and VCC 351 rotate so little that they must be anisotropic. VCC 351 is particularly interesting: it is flatter than any elliptical (E7), but it has the smallest ratio of rotation velocity to velocity dispersion of any galaxy in their sample. Some spheroidals must be anisotropic. Similar studies followed, with mixed results. The Local Group spheroidals NGC 147, NGC 185, and NGC 205 are moderately (Bender et al. 1991) but not extremely (De Rijcke et al. 2006; Geha et al. 2006) anisotropic. More generally, some Sphs rotate rapidly (de Rijcke et al. 2001; Simien & Prugniel 2002; Pedraz et al. 2002; Tolstoy et al. 2009), while others do not (Geha et al. 2003; Thomas et al. 2006). Most tellingly, van Zee et al. (2004) find that "the rotation amplitudes of the rotating [Sphs] are comparable to those of similar-brightness dwarf irregular galaxies (dIs). Evidence of a relationship between the rotation amplitude and galaxy luminosity is found and, in fact, agrees well with the Tully–Fisher relation.... These observations reaffirm the possibility that some cluster [Sphs] may be formed when the neutral gaseous medium is stripped from dIs in the cluster environment. We hypothesize that several different mechanisms are involved in the creation of the overall population of [Sphs] and that stripping of infalling dIs may be the dominant process in the creation of [Sphs] in clusters like Virgo." We agree with all of these statements.

7.2. Stellar Population Evidence that Sphs are Related to Irregulars

We have known for many years that Local Group dwarf spheroidals have episodically been converted into irregulars (Kormendy & Bender 1994). Their intermediate-age stellar populations (Da Costa 1994) tell us that they had a variety of different, bursty star formation histories ending, in some cases, only a short time ago. For example, Hurley-Keller et al. (1998) concluded that the Carina dSph is made up of three stellar populations: 10%–20% of its stars are ∼12 Gyr old, but at least 50% of the stars are 6–8 Gyr old, and ∼30% formed only 3 Gyr ago. Hernandez et al. (2000) used an *HST* color–magnitude diagram to get qualitatively similar results: bursts happened ∼8, 5, and 3 Gyr ago with some star formation extending to 1 Gyr ago (see also Dolphin 2002). There must have been gas at all of these times in order to make these stars. Gas-rich, star-forming dwarfs are Magellanic irregulars.

Mateo (1998) and Tolstoy et al. (2009) provide thorough reviews of star formation histories. A few Sphs consist almost exclusively of old stars (e.g., Draco and UMi). But in general, the star formation histories of Sph and Im galaxies look similarly bursty over most of cosmic time. Again, the main difference is that the Sphs have essentially no star formation now. That is why we call them Sphs.

Metal abundance distributions also imply heterogeneous star formation and abundance enrichment histories in Sph and (albeit with sparser data) dIm galaxies (see, e.g., Venn & Hill 2008; Tolstoy et al. 2009, and Frebel 2010 for reviews). The α element abundances in dSph galaxies are not much enhanced with respect to solar, also consistent with prolonged star formation histories (Shetrone et al. 1998, 2001, 2003, 2009; Tolstoy et al. 2003; Venn et al. 2004; Geisler et al. 2005). However, *"there are no examples of any dwarf systems that do not contain an 'ancient' population of stars"* (Mateo 2008). Tolstoy et al. (2009) agree: "No genuinely young galaxy (of any type) has ever been found; stars are always found at the oldest lookback

times observed." So these relics from the earliest days of galaxy formation sputtered along, forming stars for billions of years before changing into Sphs.

Measurements of star formation histories have now been extended to larger samples of galaxies outside the Local Group. Figures 22 and 23 show the individual cumulative star formation histories and the mean specific star formation histories of galaxies in the *HST* ACS Nearby Galaxy Survey Treasury (ANGST; Weisz et al. 2011a). The survey covers 60 nearby ($D \lesssim 4$ Mpc) dwarfs of both early and late types. Weisz et al. (2011a) conclude that "the average dwarf formed ≳50% of its stars by $z \sim 2$ and 60% of its stars by $z \sim 1$, regardless of its current morphological type" and that "the mean [star formation histories] of dIs, [dwarf Sph/Im transition galaxies], and dSphs are similar over most of cosmic time, and only begin to diverge a few Gyr ago, with the clearest differences between the three appearing during the most recent 1 Gyr." These results echo the results obtained in the Local Group (Weisz et al. 2011b). The conversion of irregulars to spheroidals happened at different times for different spheroidals; this conversion does not seem to correlate with galaxy parameters, but it correlates strongly with environment (Section 8).

8. OBSERVATIONAL EVIDENCE FOR ENVIRONMENTAL GALAXY TRANSFORMATION PROCESSES

The observations presented so far suggest that S0 + Sph galaxies are red and dead S + Im galaxies, but they mostly do not point to any specific transformation process. This section reviews possible transformation processes and the observations that support them. A comprehensive review is beyond the scope of this paper. However, we discuss the most important results that help to justify and explain the parallel-sequence galaxy classification scheme.

The central observational results presented in this paper are (1) the continuous structural parameter correlations of S0 disks and Sph galaxies and (2) the close similarity between the S0 disk + Sph parameter sequences and those of spiral galaxy disks and Magellanic irregulars. This section focuses on environmental galaxy transformation processes that may explain this similarity. However, at least one internal process is more fundamental than all external processes, because it affects both star-forming and non-star-forming galaxies similarly and independently of environment:

Dekel & Silk (1986) "suggest that *both the dIs and the [dSphs] have lost most of their mass* in winds after the first burst of star formation, and that this process determined their final structural relations. The dIs somehow managed to retain a small fraction of their original gas, while the [dSphs] either have lost all of their gas at the first burst of star formation or passed through a dI stage before they lost the rest of the gas and turned [dSph]." That is, the *Sph + Im sequence of decreasing surface brightness with decreasing galaxy luminosity is a sequence of decreasing baryon retention.* The idea of baryonic mass loss via winds had been suggested earlier by Larson (1974) and Saito (1979). It has become more plausible as evidence has accumulated that smaller dwarfs are more dominated by dark matter and hence that potential wells exist that can retain the miniscule amounts of visible matter that remain in dSphs such as Draco (Kormendy & Freeman 2004, 2011). Otherwise, if more than half of the total mass were expelled, the galaxy would have been unbound.
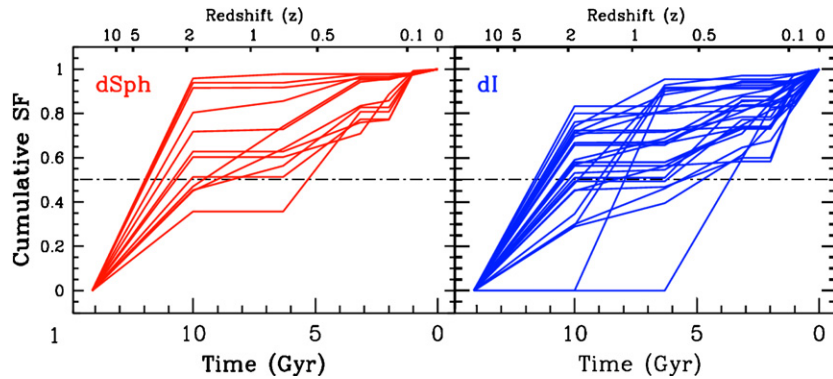
Figure 22. Individual star formation histories, i.e., the cumulative fraction of all current stars that were already formed as functions of lookback time and redshift z for (left) Sph galaxies and (right) Im galaxies. A horizontal line is drawn at 50% of the current stellar mass. The means of these star formation histories of Sph, Im, spiral, and Sph/Im transition galaxies are virtually indistinguishable. This figure is adapted from Figure 5 of Weisz et al. (2011a).
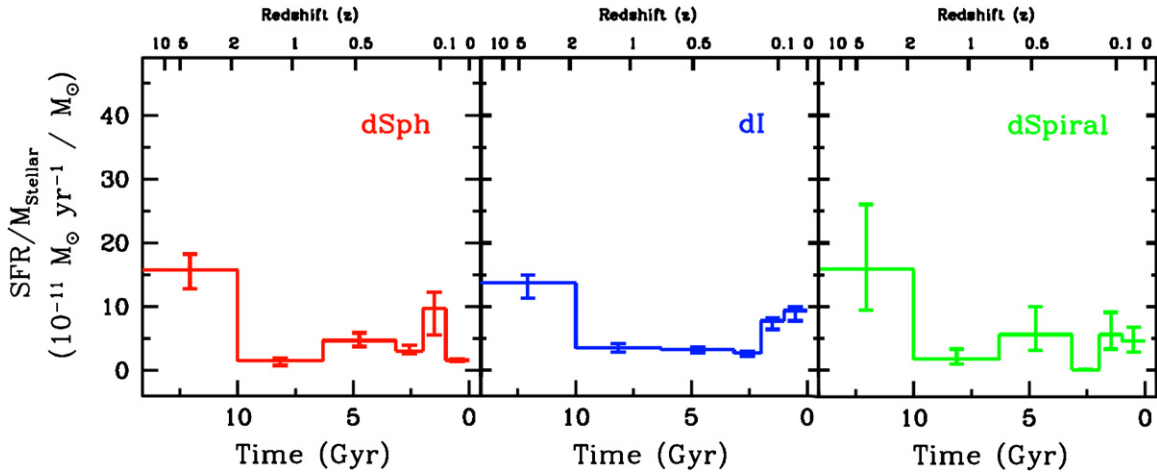
Figure 23. Mean specific star formation histories, i.e., star formation rate divided by the integrated stellar mass, for ANGST dwarf galaxies divided up by morphological type. Different types have essentially indistinguishable star formation histories, except that Sphs do not form stars now. This figure is adapted from Figure 4 in Weisz et al. (2011a).

8.1. Ram-Pressure Stripping.
I. Evidence for Ongoing Stripping

Gunn & Gott (1972) suggested that, given the density of hot gas in the Coma cluster implied by the then-recent detection of X-ray emission (Meekins et al. 1971; Gursky et al. 1971), *"a typical galaxy moving in it will be stripped of its interstellar material.* We expect *no normal spirals* in the central regions of clusters like Coma. The lack of such systems is, of course, observed."

The idea of ram-pressure stripping has fluctuated in popularity, never retreating very far into the background but never enjoying universal acceptance, either. This situation is changing rapidly. Observations of the ongoing stripping of H I and Hα-emitting gas are turning ram-pressure stripping into An Idea Whose Time Has Come. Van Gorkom & Kenney (2011) provide a comprehensive review of these developments. Here, we concentrate on some of the most direct evidence for ram-pressure stripping in action. We tie these results together with observations of the morphology–density relation that contribute to a more compelling picture of the importance of stripping. These ideas underlay the parallel-sequence classification from the beginning (van den Bergh 1976). They still do so here. In later subsections, we argue that the situation is only a little more complicated, i.e., that ram-pressure stripping is the principal S + Im → S0 + Sph transformation process but that other, mostly

heating processes also help to engineer the galaxy structure that we observe.

Figure 24 shows some of the best evidence for ongoing ram-pressure stripping in the Virgo Cluster (adapted from Chung et al. 2007; Kenney et al. 2004, 2008). Many spiral galaxies near the center of the cluster show H I tails; the above authors interpret them as gas that is being stripped by the hot, X-ray-emitting gas that pervades the cluster (see Chung et al. 2009 for an update and van Gorkom & Kenney 2011 for a review). If tails trail behind their galaxies, then they imply that most of these spirals are falling into the cluster. A spectacular example (Kenney et al. 2008; see Kotanyi et al. 1983; Combes et al. 1988; Veilleux et al. 1999; Vollmer et al. 2005 for progressive improvements in the data) is the tidally disturbed spiral NGC 4438, which shows Hα filaments extending all the way (we assume:) back to the giant elliptical NGC 4406. These galaxies have recession velocities of −1000 and −1300 km s^{-1} with respect to the Virgo Cluster core; it is usually assumed that they form part of a subgroup that is falling into the Virgo Cluster from behind. In addition, NGC 4438 has likely just had an encounter with NGC 4406 and is still both tidally distorted and shedding cold gas into the combined hot gas of NGC 4406 and the Virgo Cluster.

A related result is the observation that spiral galaxies near the center of Virgo are smaller and more depleted in H I gas than galaxies in the cluster outskirts (e.g., Cayette et al. 1990, 1994; Chung et al. 2009). Chung and collaborators add that
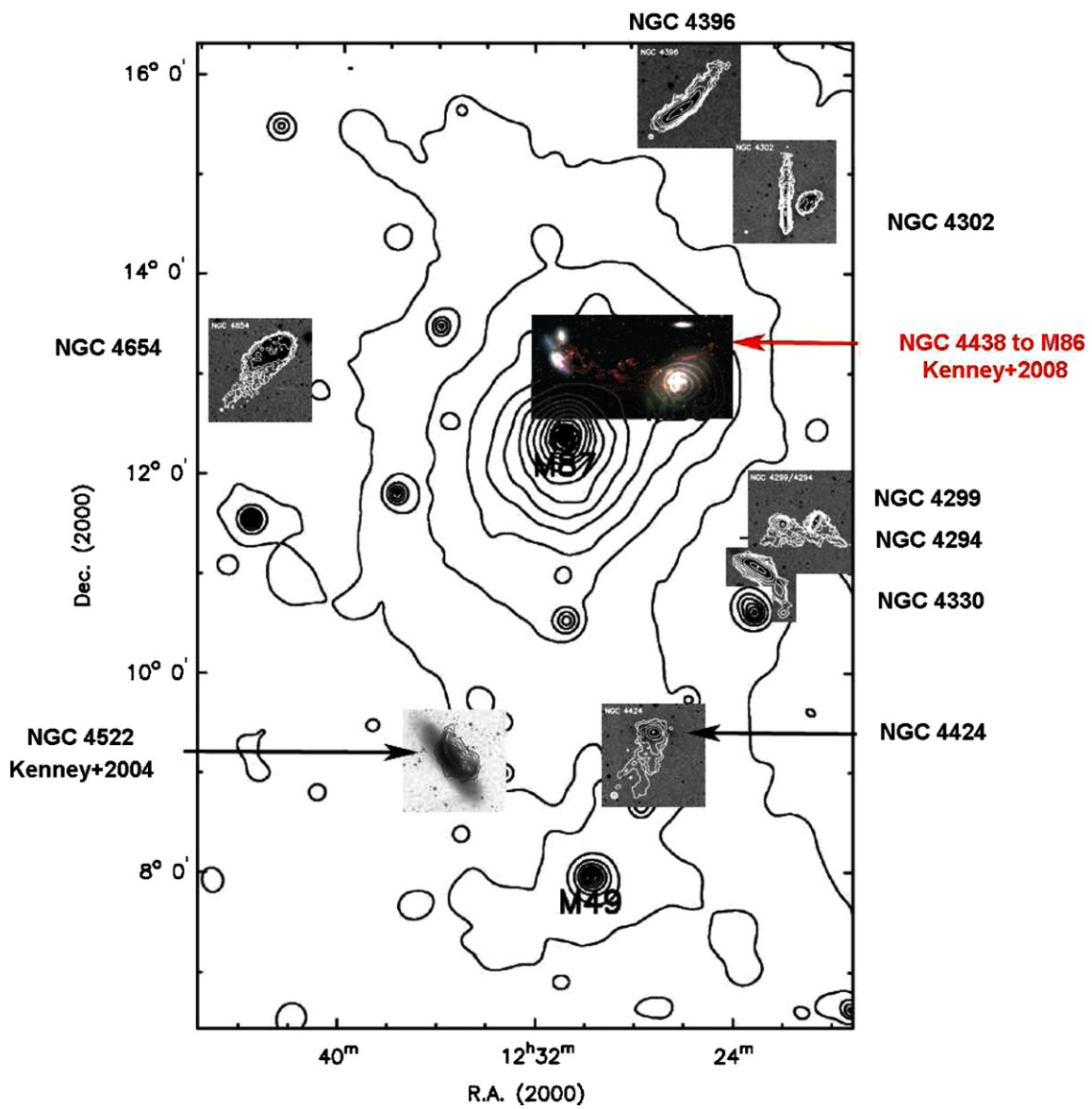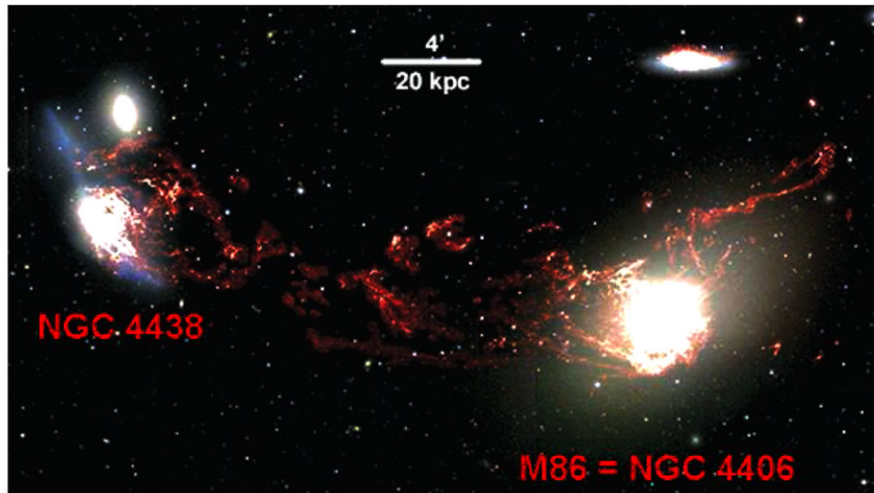
Figure 24. Large panel shows 0.5–2.0 keV X-ray brightness contours in the Virgo Cluster as measured with *ROSAT* by Böhringer et al. (1994). Superposed are gray-scale images of galaxies with H I tails indicative of ongoing ram-pressure gas stripping (white or black contours). The H I images are from Chung et al. (2007) and Kenney et al. (2004). The color inset image and larger-scale image at the top show the spectacular Hα emission filaments that extend from NGC 4438 to NGC 4406 (Kenney et al. 2008). Each small inset image shows the galaxy centered on its position in the cluster, but the panels are magnified. This is misleading only for NGC 4438 + NGC 4406: that inset image is positioned so that the center of NGC 4406 is correct, but then the enlargement makes it appear as though NGC 4438 is north of M 87, whereas in reality both NGC 4438 and NGC 4406 are north-west of M 87. This figure is adapted from Figure 4 in Chung et al. (2007).

"most of these galaxies in the [cluster] core also show gas displaced from the disk which is either currently being stripped or falling back after a stripping event." The three most depleted galaxies illustrated in Figure 8 of Chung et al. (2009) are NGC 4402, NGC 4405, and NGC 4064. They have a mean absolute magnitude $M_V = -19.4 \pm 0.2$. Virtually all Sphs are fainter than this (Figure 17). If even the deep gravitational potential wells of still-spiral galaxies suffer H I stripping, then the shallow potential wells of dS + Im galaxies are more likely to be stripped. Moreover, while NGC 4402 is close to NGC 4406 and NGC 4405 is only 20′ north of NGC 4396 (see Figure 24), NGC 4064 is almost 9° from M 87. Most galaxies in the cluster outskirts have relatively normal H I content, but a few are H I depleted even there.

Thus, finding observational evidence for ram-pressure stripping in action has become a substantial industry. An incomplete list of additional papers includes Kenney & Koopmann (1999, NGC 4522), Yoshida et al. (2004, NGC 4388), Oosterloo & van Gorkom (2005, NGC 4388), Vollmer et al. (2008, NGC 4501), and Abramson et al. (2011, NGC 4330). Such observations and theoretical developments both suggest that ram-pressure stripping is more effective than we have thought (Mori & Burkert 2000; Quilis et al. 2000; Grebel et al. 2003; Roediger & Hensler 2005; Tonnesen et al. 2007; Tonnesen & Bryan 2008, 2009, 2010; Boselli et al. 2008; van Gorkom & Kenney 2011).

This supports early suggestions that Sph galaxies are ram-pressure-stripped dS + Im galaxies (Faber & Lin 1983; Lin & Faber 1983; Kormendy 1987; van den Bergh 1994c).

Still, many authors argue that ram-pressure stripping is not the whole—or even the main—story, because it is difficult to strip dense central gas in giant galaxies (Farouki & Shapiro 1980; Abadi et al. 1999; Quilis et al. 2000; Tonnesen & Bryan 2009). Additional processes such as galaxy harassment (Section 8.3), starvation (Section 8.4), or tidal shaking (Section 8.5) may be important. Before we turn to these, we recall indirect evidence regarding stripping.

8.2. Ram-Pressure Stripping.
II. The Morphology–Density Relation

We find it impossible to think about ram-pressure stripping except in the context of the morphology–density relation. Dressler (1980) surveyed the relative numbers of E, S0, and S + Im galaxies as a function of local galaxy density in 55 clusters of galaxies; his results are reproduced here in Figure 25. He showed that field environments are dominated by S + Im galaxies, with only ∼10% contributions each from ellipticals and S0s. The E and S0 fractions then rise and the S + Im fractions fall with increasing galaxy density until there are almost no S + Im galaxies in the richest cluster environments.

Postman & Geller (1984) extended Dressler's results to lower-density environments, showing that the E, S0, and S fractions saturate at ∼0.1, 0.2, and 0.7, respectively, over a range of low densities. As Dressler emphasized, there are S0s in the field. If spirals get turned into S0s, the process cannot depend completely on high galaxy densities.

Gunn & Gott (1972) suggested that spirals would quickly get ram-pressure stripped when they fell into the Coma cluster. In Figure 25, Coma is included in the right panel. However, based on data in Figure 25, Dressler argued: *"The relationship between population and local density appears to hold without regard to the type of cluster involved.* This result contradicts the interpretation that spirals have been swept of their gas to form S0s in the high concentration clusters. If the idea of sweeping

is to be kept, it would have to be argued that the process is common even in regions where the space density of galaxies, and thus presumably of gas, is 10^2–10^3 times lower than in the rich cores of the regular clusters. This is improbable."

However, ram-pressure stripping is widespread in the Virgo Cluster. Virgo is not included, but its densities overlap with Figure 25. Moreover, Figure 25 shows that the ratio of S + Im to S0 galaxy numbers is larger than average at all densities in low-concentration clusters and smaller in X-ray-emitting clusters. Dressler noted this and suggested that stripping or gas evaporation could contribute a little. Given results of Section 8.1, it seems more likely that ram-pressure stripping happens more easily than we thought and that it helps to turn spirals into S0s even in clusters like Virgo. We expect that Im → Sph conversion is still easier, as implied by evidence in the Local Group below.

Observing the evolution of the morphology–density relation with cosmological lookback time should tell us more about how S0s evolved. This is a big subject, mostly beyond the scope of this paper. We focus on two results. Dressler et al. (1997) and Wilman et al. (2009) compare the $z = 0$ morphology–density relation to that for clusters at $z \simeq 0.5$ and groups at $z \simeq 0.4$, respectively. For clusters, Dressler et al. (1997) find that the differences shown here in Figure 25 are much larger at $z \simeq 0.5$: then, centrally concentrated, regular clusters show a relation similar to that at $z = 0$, but low-concentration, irregular clusters show almost no relation. Dressler concludes that "S0s are generated in large numbers only after cluster virialization." These results are consistent with ours. In contrast, Wilman et al. (2009) find that $z \simeq 0.4$ groups with ∼5–20 bright galaxies and velocity dispersions ∼200–500 km s^{-1} (Wilman et al. 2005) are indistinguishable from clusters in their galaxy populations. I.e., they already have larger S0 and smaller S fractions than does the field. Then, between $z \simeq 0.4$ and the present, the S0 fractions increase and the spiral fractions decrease in the same way in groups and clusters. "The S0 fraction in groups is at least as high as in $z \sim 0.4$ clusters and X-ray-selected groups, which have more luminous intragroup medium (IGM). Interactions with a bright X-ray-emitting IGM cannot be important for the formation of the majority of S0s in the universe" (Wilman et al. 2009). Instead, they conclude that "minor mergers, galaxy harassment, and tidal interactions are the most likely mechanisms [to make S0s]."

We partly agree and we partly disagree. The Wilman et al. (2009) results, like the Dressler (1980) results, may be explained if ram-pressure stripping happens more easily than we have thought. At the same time, we, like Wilman, suggest (Section 8.5) that other transformation processes happen, too. Also, we cannot exclude that some part of the difference between S + Im and S0 galaxies is set by proto-cluster environments in ways that do not involve galaxy transformation. This possibility was preferred by Dressler.

A compelling observation which suggests that hot cluster gas is not necessary for ram-pressure stripping of dwarf galaxies is shown in Figure 26. Close dwarf companions of Local Group giant galaxies are almost all spheroidals. Distant companions are irregulars. Sph/Im galaxies have intermediate morphologies and live at intermediate distances. There are a few exceptions—at least three Sphs are free-flyers, and the Magellanic Clouds survive at Galactocentric distances at which other companions are gas-free. They are the largest companions illustrated. This result has been known for a long time (Einasto et al. 1974; van den Bergh 1994b, 1994c; Mateo 1998) and is beautifully illustrated in Mateo's (2008) figure.
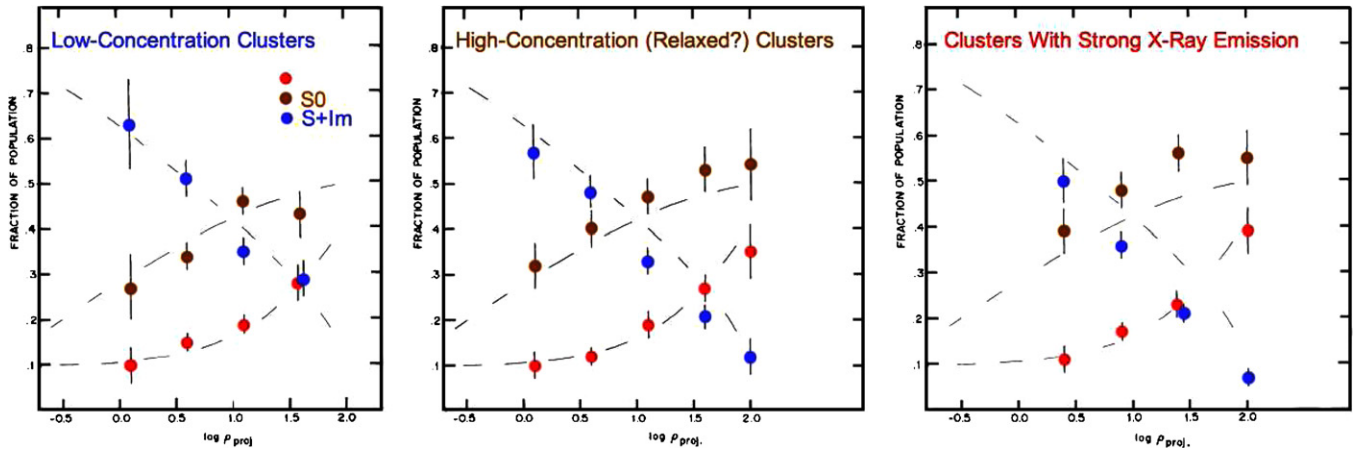
Figure 25. Morphology–density relation as a function of cluster richness, adapted from Figures 8–10 of Dressler ([1980](#)). Each panel shows the fraction of E, S0, and S + Im galaxies as a function of the log of the projected density in units of galaxies Mpc^{-2}. The galaxies were classified by Dressler based mostly on large-scale (10″.9 mm^{-1}), B-band photographic plates taken with the Las Campanas Observatory 2.5 m telescope. The dashed lines show the mean fractions for all 55 rich clusters in the sample, while the data points show the fractions for 9 low-concentration clusters (left), 10 high-concentration clusters (center), and 8 strongly X-ray-emitting clusters ($L_X \gtrsim 10^{44}$ erg s^{-1} for $H_0 = 50$ km s^{-1} Mpc^{-1}, right).
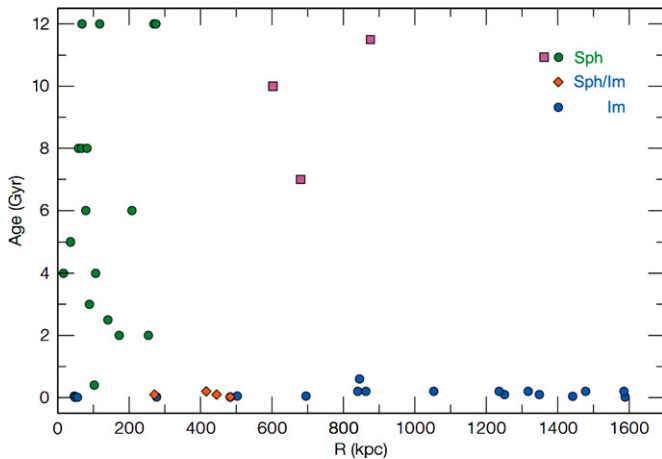
Figure 26. From Mateo ([2008](#)), the ages of the youngest stellar populations in dwarf galaxy companions vs. Galactocentric or M31centric distance R. Except for the Magellanic Clouds, all close companions of our Galaxy and of M 31 are spheroidals. Almost all distant companions are irregulars, with the exception of three free-flying Sphs, Cetus, Tucana, and And XVIII. The Sph/Im transition galaxies mostly lie at distances intermediate between those of spheroidals and irregulars. This figure is not up to date with all recent discoveries of dwarf galaxies, but the above generalizations are robust.

Living near a giant galaxy is dangerous for gas-rich dwarfs, but the reason is not established by Figure [26](#). Could the Im → Sph transformation process mainly be gravitational; e.g., tidal shaking that promotes star formation? But Local Group and M 81 Group spheroidals and irregulars overplot almost exactly in the Figure [20](#) parameter correlations. This requires fine-tuning of the star formation. It is not excluded. And it can happen concurrently with other effects. But Figure [26](#) may be an indication that ram-pressure stripping can happen even in environments that are gentler than cluster centers. It may be indirect evidence for a pervasive warm–hot intergalactic medium (WHIM; Davé et al. [2001](#)) that is difficult to detect directly but that may be enough to convert dwarf irregulars into spheroidals. Freeland & Wilcots ([2011](#)) present evidence based on bent radio jets for just such gas in galaxy groups. Still hotter hot gas can be retained in galaxies that have total masses $M \gtrsim M_{\rm crit} \sim 10^{12}\,M_\odot$ ("$M_{\rm crit}$ quenching" of star formation;

Dekel & Birnboim [2006](#); Cattaneo et al. [2006](#); Faber et al. [2007](#); KFCB). This corresponds to $M_V \lesssim -21.5$ (KFCB). Many of the first-ranked galaxies in these groups are massive enough (see Wilman et al. [2005](#), Table 2), and even when they are not, the potential well of a group is determined by more than one member.

Therefore, we suggest that ram-pressure stripping is one of the important processes that converts S + Im galaxies into S0 + Sph galaxies. Hierarchical clustering simulations are becoming powerful enough to follow ram-pressure stripping in a cosmological context (Tonnesen et al. [2007](#); Tonnesen & Bryan [2008](#), [2009](#), [2010](#)); they show that other processes discussed in the following subsections happen too. These other processes must be especially important for the small fraction of S0 galaxies that live in the field.

We emphasize that *it is not necessary to remove all central gas or even to prevent star formation in all S0s.* S0$_3$ galaxies with dust disks are illustrated in the *Hubble Atlas* (Sandage [1961](#)). Optical emission lines are seen in 75% of the SAURON galaxies, especially in S0s and even in the Virgo Cluster (Sarzi et al. [2006](#)). H I gas was discovered long ago (Balick et al. [1976](#); van Woerden et al. [1983](#); van Driel & van Woerden [1991](#)). Welch & Sage ([2003](#)) detected CO emission from molecular gas in 78% of the field S0 galaxies that they surveyed, usually near the center (see also Sage & Wrobel [1989](#); Thronson et al. [1989](#); Devereux & Young [1991](#); Young et al. [1995](#)). The ATLAS3D project shows these results in particular detail and again even in the Virgo Cluster (Davis et al. [2011](#); Young et al. [2011](#)). Also, 60% of S0s were detected by *IRAS* in 60 μm and 100 μm emission (Knapp et al. [1989](#)). Finally, Temi et al. ([2009](#)) observed E and S0 galaxies with the *Spitzer Space Telescope* and detected gas, dust, and small amounts of star formation. S0s have more star formation than ellipticals and show different correlations between 24 μm luminosity, molecular gas mass, and other star formation indicators. Temi et al. ([2009](#)) suggest that "rotationally supported cold gas in S0 galaxies may be a relic of their previous incarnation as late-type spirals." Some S0s are exceedingly gas-deficient, but many contain molecular gas, dust, and some star formation near the center, as predicted by theoretical studies of ram-pressure stripping. Similarly, H I deficient spirals in the Virgo Cluster often have normal molecular gas content (Kenney & Young [1986](#)).

Finally, it is important to remember that S0s occur in the field. For example, NGC 3115 is very isolated. The processes that clean field S0s of gas and convert them from "blue cloud" to "red sequence" galaxies in the SDSS color–magnitude relation remain an ongoing puzzle. NGC 3115 contains little X-ray gas (Li et al. 2011); "M_{crit} quenching" may help, but it is difficult to believe that it is the whole story. On the other hand, NGC 3115 contains an unusually massive black hole $M_\bullet \sim 10^9 M_\odot$ (Kormendy & Richstone 1992; Kormendy et al. 1996; Emsellem et al. 1999). It is possible that feedback from an AGN phase of accretion onto this black hole was instrumental in cleaning the galaxy of cold gas (van den Bergh 1993, 2009b).

8.3. Galaxy Harassment

Galaxy harassment is the cumulative effect of many, high-speed encounters with other galaxies in a cluster and with the overall cluster potential. Numerical simulations show that it strips outer mass, heats disks, and promotes gas inflow toward the center (Moore et al. 1996, 1998, 1999; Lake et al. 1998). A variant in the Local Group is tidal stirring of dwarfs on very elliptical orbits around the Galaxy or M 31 (Mayer et al. 2001a, 2001b, 2006). Harassment is suggested to convert flimsy, late-type disks into spheroidals and more robust, earlier-type spirals into hotter systems that resemble S0s in many ways. One success of this picture that comes "for free" is that inflowing gas feeds star formation; this helps to explain why spheroidals in which star formation stopped long ago do not have much lower surface brightnesses than current versions of spiral galaxy progenitors (Figure 20). The process is clean and inescapable. And it provides a natural explanation for many of the observations of Sph and S0c galaxies that we discussed in previous sections. We do not repeat them all, but the following are worth emphasizing.

1. Faint spheroidals are not flat, but some of the brightest contain edge-on disks (e.g., VCC 2048 in Section 4.1.3). NGC 4638 is similar (Section 4.1.4). Also similar but less extreme are the edge-on SB0s NGC 4762 (Section 4.1.1) and NGC 4452 (Section 4.1.2). They have very flat inner disks but very thick outer disks, as expected from dynamical heating processes. The fat outer disk of NGC 4762 is still warped and irregular; this is one example among many of an ongoing tidal encounter; i.e., of harassment in action.

2. Sph and Im galaxies have similar distributions of observed axial ratios; this is another sign that these two types of galaxies are closely related (Ferguson & Sandage 1989; Binggeli & Popescu 1995). Spheroidals are also similar in shape to ellipticals (above papers; Ichikawa 1989), but the flattest Sphs are flatter than any elliptical (e.g., Ryden & Terndrup 1994). It is difficult to turn this *consistency* with Im → Sph evolution into an argument *either for or against* such evolution (Binggeli & Popescu 1995). Progenitor Ims need not have the same shapes as descendent Sphs if harassment is one of the transformation processes.

3. Stars and gas that are liberated by gravitational stripping form a cluster intergalactic background. Remarkably deep imaging observations by Mihos (2011) and by Mihos et al. (2005, 2009) reveal this background light in the Virgo Cluster. It is also detected via planetary nebulae (e.g., Arnaboldi et al. 1996, 2002, 2004; Castro-Rodriguéz et al. 2009; see Arnaboldi & Gerhard 2010 and Arnaboldi 2011 for reviews). These can be used at surface brightnesses that are otherwise unreachable, and they provide velocity information. Intracluster globular clusters are also detected

in Virgo (Williams et al. 2007a), and metal abundance distributions have been measured in individual intracluster stars (Williams et al. 2007b). These observations show that the intracluster light in Virgo is irregular and riddled with tidal streams, indicating that it is in the early stages of formation.

Beginning with a photographic detection in Coma (Thuan & Kormendy 1977), intracluster light has been detected and studied in the Coma cluster (e.g., Adami et al. 2005; Okamura 2011) and in many other clusters (e.g., Krick & Bernstein 2007; Gonzalez et al. 2007, see Arnaboldi & Gerhard 2010 and Arnaboldi 2011 for reviews). In many cases, the intracluster light shows irregularities such as streams that are indicative of non-equilibrium, ongoing formation.

On the largest scales, cD halos (Morgan & Lesh 1965; Oemler 1976; Schombert 1988) belong gravitationally to their clusters more than to their central galaxies (Dressler 1979; Kelson et al. 2002) and also consist of tidally disrupted galaxies (Richstone 1976).

On the smallest scales, the halos of our Galaxy (Ibata et al. 1994, 1995, 2001b) and M 31 (Ibata et al. 2001a, 2007; Ferguson et al. 2002) contain stellar streams that are dwarf galaxies which are being torn apart by tides.

Gravity is not negotiable. The above are all results of galaxy harassment. If it can disrupt dwarf galaxies to produce giant galaxy halos and intracluster light, then it can heat individual galaxies short of disrupting them. This is a paraphrase for the production of spheroidal galaxies via harassment.

4. Harassment should also produce outcomes that are intermediate between disk thickening by dynamical heating and total galaxy disruption. Sandage & Binggeli (1984) discovered "a new class of dwarfs that are of huge size (10000 pc in diameter in the extreme) and of very low surface brightness of about 25 B mag arcsec^{-2} at the center." A Sph example is shown in Figure 27. We interpret these galaxies as spheroidals that have been harassed almost to death.

5. Harassment produces Sphs that are triaxial and slowly rotating. It is consistent with the observation that the brightest Sphs are often the most disky ones, whereas fainter spheroidals often rotate much less than isotropic systems of the observed flattening. Furthermore, Sph flattening distributions are best explained if these galaxies are modestly triaxial (Binggeli & Popescu 1995).

6. Harassment can make Sphs that have kinematically decoupled subsystems, including counter-rotation of the harassed outer parts with respect to the remnant inner galaxy (De Rijcke et al. 2004; González-García et al. 2005). Thomas et al. (2006) see counter-rotation in the spheroidal galaxy VCC 510.

8.4. Starvation

Larson et al. (1980) point out that continued star formation at current rates would exhaust the available gas in most spirals in much less than a Hubble time and suggest that their lifetimes are prolonged by late gas infall. A corollary is that starving star formation by cutting off the supply of cold gas forces the galaxy to evolve into an S0.

Starvation is often discussed in terms of gravitational stripping of a cold gas reservoir. A more likely scenario in clusters is that the only available gas is hot. Virgo qualifies. Starvation naturally accompanies and assists ram-pressure stripping
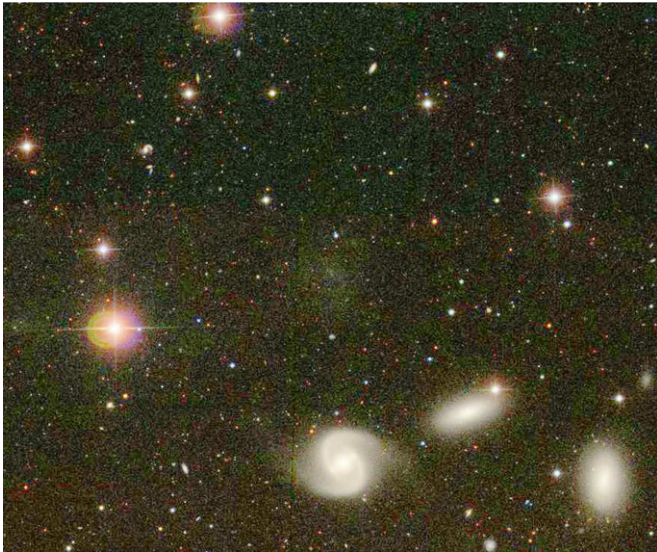
Figure 27. Ultra-low-surface-brightness dwarf galaxy VF18-71 = VCC 1052 discovered by Sandage & Binggeli (1984). This is an SDSS color image from WIKISKY. The contrast is set extremely high near the sky to show the low-surface-brightness dwarf, but it is set very low at higher surface brightnesses to show some of the internal structure in the trio of galaxies (left to right: NGC 4440, NGC 4436, and NGC 4431) to the south. VCC 1052 is 4′.5 north of NGC 4440. This field is in the heart of the Virgo Cluster: M 87 is almost due east (to the left) and NGC 4374 + NGC 4406 are to the northwest (toward the upper right).

in turning gas-rich galaxies into S0s. A drawback is that starvation decreases surface brightnesses; then Sph and S0 surface brightnesses are surprisingly high (Boselli et al. 2009). Nevertheless, it seems unavoidable. We do not discuss it further only because no observations that are within the scope of this paper constrain it very directly.

8.5. Everything That Is Not Forbidden Is Mandatory

Astronomers like clean explanations. They debate about which of many possible processes make spheroidals. We have not reviewed them all; additional examples include various tidal shaking variants of harassment (e.g., D'Onghia et al. 2009; Kazantzidis et al. 2011) and the failure to accrete sufficient baryons after reionization (e.g., Bullock et al. 2000; Cattaneo et al. 2011).

We suggest that the relevant question is not "Which of these mechanisms is correct?" It is "How can you stop any of them from happening?" It seems likely to us that all of the above processes matter.

9. THE REVISED PARALLEL-SEQUENCE CLASSIFICATION AND GALAXY BIMODALITY IN THE COLOR–MAGNITUDE RELATION

Figure 28 shows how spheroidal galaxies and more generally the revised parallel-sequence classification relate to the galaxy bimodality in the SDSS color–magnitude diagram. The bright part of the red sequence consists of ellipticals, S0s, and early-type spirals. However, the luminosity functions of all of these galaxy types are bounded (Binggeli et al. 1988; see also Figure 3 here); they drop rapidly fainter than $M_V \sim -18$ (log $M/M_\odot \sim 9.7$ in the bottom panel).

Figure 3 shows further that spheroidals with $M_V < -18$ or log $M/M_\odot > 9.5$ are rare but that the Sph luminosity function rises rapidly at lower luminosities and masses. At the left
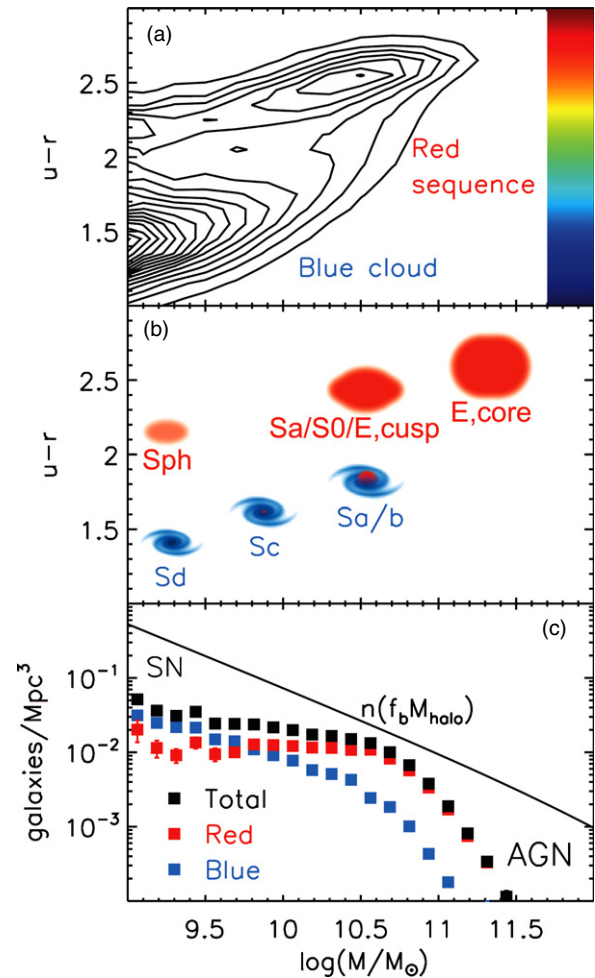
Figure 28. Correspondence between our parallel-sequence classification and color bimodality in the SDSS color–magnitude relation. This figure is adapted from a draft of Figure 1 in Cattaneo et al. (2009); we thank Andrea Cattaneo for permission to use it. Panel (a) shows contours of galaxy number density in the correlation between SDSS $u - r$ color and galaxy baryonic mass $M/M_\odot$ (Baldry et al. 2004). It shows the narrow "red sequence" of mostly non-star-forming galaxies and the broader "blue cloud" of actively star-forming galaxies. Panel (b) shows the morphological types from our Figure 1 that dominate in various parts of panel (a). The rapidly rising luminosity function of spheroidal galaxies at the low-mass limit of the diagram accounts for the contour around (9.0, 2.2) in panel (a). Panel (c) shows the baryonic mass functions of the red sequence, the blue cloud, and their sum (Bell et al. 2003). The faint-end upturn of the red-sequence mass function is a statistical fluctuation; it is not a detection of spheroidals. The diagonal line schematically shows the prediction from the ΛCDM density fluctuation spectrum. The baryonic mass is approximated by $f_b M_{halo}$, where f_b is the universal baryon fraction and M_{halo} is the halo mass. The well-known shortfall of observed galaxies with respect to this prediction is usually interpreted as the result of M_{crit} quenching aided by AGN feedback and continued infall at the high-mass end and supernova-driven ("SN-driven") baryon ejection at the low-mass end (see Cattaneo et al. 2009 for a review). We agree, but we suggest that other processes such as ram-pressure stripping also transform blue-cloud galaxies into red-sequence Sphs. The important "take-home point" is that the bright end of the red sequence consists of Es, S0s, and early-type spirals, but the faint end—beyond the magnitude limit of most SDSS studies—is dominated by spheroidal galaxies.

boundary of Figure 28, the red sequence is already dominated by spheroidals. The E–Sph dichotomy is visible in Figure 28 as two somewhat distinct high points in the red-sequence contours. This is not evident in most published color–magnitude correlations because the magnitude limits of most SDSS samples are too bright to reach the more numerous spheroidals.

Figure 28(c) illustrates the broader galaxy formation context within which our results are a small contribution. If all baryons in the universe were in galaxies, then the mass function of galaxies predicted by the cold dark matter fluctuation spectrum would be the almost-straight line (e.g., Somerville & Primack 1999). The total galaxy mass function (black squares) never quite reaches this line—no galaxies have quite the universal baryon fraction $f_b \simeq 0.17$ (Komatsu et al. 2009). This smallest shortfall is believed to be due to WHIM baryons (Davé et al. 2001).

The increasing shortfalls at higher galaxy masses are believed to be related to $M_{\rm crit}$ quenching (see Cattaneo et al. 2009 for a review). At these masses, galaxies and clusters of galaxies can hold onto hot, X-ray-emitting gas. Cooling is too slow to convert this gas into visible stars. Candidate processes to keep the hot gas hot are a combination of AGN feedback (e.g., Cattaneo et al. 2009) and heating from late cosmological infall (Dekel & Birnboim 2006, 2008). The universe is not old enough for galaxy formation to be as nearly completed at these masses as it is at lower masses. In particular, in rich clusters, more baryons are still in hot gas than in visible galaxies (e.g., Watt et al. 1992; David et al. 1995; Vikhlinin et al. 2006). These are hostile environments for gas-rich spirals, and we argue that ram-pressure stripping, galaxy harassment, and starvation can together convert blue-cloud spirals into red and dead S0s. In addition, processes that make S0s in the field; e.g., AGN feedback and perhaps others that we have not yet discovered, probably also work in clusters.

The increasing shortfall of baryonic galaxies at log $M/M_\odot <$ 10.5 is relevant to spheroidals. This shortfall is usually thought to be caused by supernova-driven mass ejection (Dekel & Silk 1986). We agree, but we present evidence in this paper and in KFCB that, in addition to baryonic blowout, other processes also help to convert blue irregulars into red spheroidals. Candidate processes again are ram-pressure stripping, galaxy harassment, and starvation, but in these dwarfs, probably not AGN feedback. If the color–magnitude plot were extended to very faint magnitudes, we expect a steep rise in the number of galaxies as spheroidals take over the red sequence.

In the smallest galaxies, the baryonic shortfall must continue to grow, as extreme dwarfs retain only a frosting of baryons in galaxies that are dominated by dark matter (Figure 19). Most of the smallest Sph galaxies may be too dark to be discovered (Kormendy & Freeman 2004, 2011).

are most sincerely grateful to Mr. and Mrs. Curtis T. Vaughan, Jr. for their continuing support of Texas astronomy.

Facilities: HST (WFPC2, ACS, NICMOS), Sloan (digital image archive)

APPENDIX

SURFACE PHOTOMETRY AND BULGE–DISK DECOMPOSITION OF VIRGO CLUSTER S0 GALAXIES

Section 4 discussed photometry results that illuminate our theme that parameter correlations are continuous from Sph galaxies through S0 disks. That is, we concentrated there on the "missing" S0c galaxies and on spheroidals that contain disks. The remarkably large range in B/T ratios in S0s is also central to our argument and is presented in Section 4.2. Table 1 contains parameters from the decompositions illustrated in Section 4.1 plus those derived in this Appendix. Parameters from bulge–disk decompositions of 19 additional Virgo Cluster S0s, 13 of which are ACS VCS galaxies, were taken from Gavazzi et al. (2000) and are plotted in Figures 17, 18, and 20, but these are not tabulated here. The details of our Section 4 photometry, together with similar photometry and bulge–disk decompositions for the remaining eight ACS VCS S0s, are the subjects of this Appendix.

A.1. Photometry Measurements

Our photometry measurement techniques were discussed in detail in KFCB. Here, we provide a short summary.

Except for NGC 4638 and VCC 2048, the profiles in the main paper were measured using program `profile` (Lauer 1985) in the image processing system `VISTA` (Stover 1988). The interpolation algorithm in `profile` is optimized for high spatial resolution, so it is best suited to the galaxies that contain edge-on, thin disks. NGC 4352 and NGC 4528 in this Appendix were also measured with `profile`.

The photometry of VCC 2048, NGC 4638, and the rest of the galaxies discussed in this Appendix was carried out by fitting isophotes using the algorithm of Bender (1987), Bender & Möllenhoff (1987), and Bender et al. (1987, 1988) as implemented in the ESO image processing system `MIDAS` (Banse et al. 1988). The software fits ellipses to the galaxy isophotes. It calculates the ellipse parameters and parameters describing departures of the isophotes from ellipses. The ellipse parameters are surface brightness, isophote center coordinates X_{cen} and Y_{cen}, major- and minor-axis radii, and hence ellipticity ϵ and position angle (P.A.) of the major axis. The radial deviations of the isophotes i from the fitted ellipses are expanded in a Fourier series of the form (θ = eccentric anomaly)

$$\Delta r_i = \sum_{k=3}^{N} \left[a_k \cos(k\theta_i) + b_k \sin(k\theta_i) \right]. \qquad (A1)$$

The most important parameter is a_4, expressed in the figures as a percent of the major-axis radius a. If $a_4 > 0$, the isophotes are disky-distorted; large a_4 at intermediate or large radii is the most reliable sign of an S0 disk in very bulge-dominated S0s (see KFCB for examples). If $a_4 < 0$, the isophotes are boxy. The importance of boxy and disky distortions is discussed in Bender (1987), Bender et al. (1987, 1988, 1989), Kormendy & Djorgovski (1989), Kormendy & Bender (1996), and Section 2.1 here.

We measured the ACS VCS g-band images of all the galaxies discussed here and SDSS g-band images for most of them. Both

profiles are illustrated in the figures. An average profile keeping only reliable data (ACS at small r, SDSS at the largest r, both data in between) is used for profile decompositions.

Photometric zero points are based on the ACS images and were calculated as discussed in KFCB. VEGAmag g magnitudes were converted to V using the calibration derived in KFCB for early-type galaxies:

$$V = g + 0.320 - 0.399(g - z). \qquad (A2)$$

VEGAmag $(g - z)$ is taken from the Ferrarese et al. (2006) tabulation of the AB mag galaxy color: $(g - z) = (g - z)_{AB} + 0.663$. SDSS g-band zero points agree very well with *HST* ACS zero points but were not used. Instead, the SDSS profiles were shifted in surface brightness to agree with the zero-pointed ACS profiles. Profile disagreements were pruned, and the cleaned profiles were averaged for use in photometric decompositions.

To tie our present photometry to that of KFCB, we remeasured the elliptical galaxy NGC 4551 = VCC 1630. The parameters are listed in Table 1. Here, we find a Sérsic index of $n = 1.968 \pm 0.056$; KFCB got $n = 1.98 \pm 0.06$. From our Sérsic fit here, we derive an effective radius in kpc of $\log r_e = 0.080 \pm 0.005$; KFCB got $\log r_e = 0.084 \pm 0.008$. We get an effective brightness $\mu_e \equiv \mu(r_e) = 20.715 \pm 0.032$ V mag arcsec^{-2}; KFCB measured $\mu_e = 20.75 \pm 0.04$ V mag arcsec^{-2}. The agreement with KFCB is satisfactory.

Profile decomposition into nuclei (when necessary), (pseudo)bulges, lenses (when necessary), and disks was carried out via χ^2 minimization using a combination of a grid-based technique (to explore wide parameter ranges) and the Levenberg–Marquardt algorithm as implemented by Press et al. (1986). Because S0 disks often turn out to have non-exponential surface brightness profiles, we always fitted the profiles with (at least) two Sérsic functions. Many S0s—especially barred ones—have $n < 1$; in fact, Gaussians ($n = 0.5$) or even profiles that cut off at large radii faster than a Gaussian ($n < 0.5$) are common for lens components and for the outer disks of barred galaxies. Our decompositions are based on major-axis surface brightness profiles, but we checked their reliability by decomposing mean-axis and minor-axis profiles as well as by visual inspection of the images. We provide a comparison of major- and mean-axis decompositions for two examples: NGC 4442 (Appendix A.7) and NGC 4483 (Appendix A.8).

Bulge and disk luminosities were calculated using major-axis Sérsic parameters and an ellipticity for each component that is consistent with the ellipticity profile of the galaxy. Total luminosity was used as a constraint for the calculated disk and bulge luminosities. Thus, the accuracy of the decompositions does not suffer because we used major-axis profiles rather than a two-dimensional decomposition technique. We actually benefit from the ease with which we can avoid complications due to bars.

The parameters for the galaxies' components are given in Table 1. Errors were derived from the covariance matrix at the minimum and mostly are marginalized 1σ errors. We explored a variety of fitting ranges and weighting schemes and, when the parameters varied more than the 1σ errors predicted, we increased the error estimates to be conservatively consistent with the parameter variation.

A.2. NGC 4762 = VCC 2095

The photometry of the (R)SB0bc galaxy NGC 4762 is presented in Section 4.1.1. We discuss the galaxy here only in

order to explain the counterintuitive result that the disk effective brightness μ_e looks almost the same as that of the whole galaxy, but the disk effective radius r_e is ~7 times larger than that of the whole galaxy. Since the disk by itself is fainter than the whole galaxy, this looks wrong.

This situation appears to be due to two problems with the Ferrarese et al. (2006) photometry.

Their g_{AB} parameters for the whole galaxy are taken from their Table 4 and plotted as the green point with the brown center in our Figure 7. Their parameters are converted to VEGAmag V as above and then converted to major-axis parameters by dividing their mean-profile r_e by $\sqrt{(1 - \epsilon)}$. As we do for all Ferrarese et al. (2006) galaxy parameters, we use the mean ellipticity for the whole galaxy from Table 4 of their paper. For NGC 4762 = VCC 2095, this is $\epsilon = 0.34$. But an axial ratio of $b/a = 0.66$ is clearly inconsistent both with the isophotes that they illustrate in their Figure 6 and with $b/a \simeq 0.15$ measured here (Figure 6). This accounts for a factor of 2.1 difference in their r_e versus any that we measure for the disk.

Second, their profile for NGC 4762 is azimuthally averaged. Ferrarese et al. (2006) remark that azimuthally averaged profiles of edge-on disks should be used with caution. We agree: we do not know how to interpret them. What is clear is this: the profile shown in their Figure 56 is much less sensitive to the disk. They reach a maximum mean radius of $100''$, which corresponds to major-axis $r^{1/4} = 3.3$, using their value of ϵ. Our Figure 6 shows the inner two shelves in the brightness profile at $r^{1/4} \leqslant 3.3$. There is no sign of them in Ferrarese et al. (2006, Figure 56). The B(lens) shelves are shown in a major-axis cut profile in their Figure 107, but the cut profile was not used to determine the galaxy parameters. So we see a higher major-axis disk μ_e than one would derive from their photometry. And since the bulge profile is removed before the disk r_e is calculated, the effective radius of the disk is substantially larger than that of the galaxy as a whole. These effects account for the rest of the difference between the green + brown point in our Figure 7 and the point that represents the disk.

A.3. NGC 4452 = VCC 1125

Similar comments apply to the total-galaxy and disk parameters of NGC 4452 = VCC 1125 in our Figure 9. Ferrarese et al. (2006) measure a mean ellipticity $\epsilon \simeq 0.68$ or $b/a = 0.32$ (their Table 4). We agree at large radii (our Figure 8). But the inner B(lens) structure that contributes much of the disk light is flatter ($\epsilon \simeq 0.9$). Our measurements of the major-axis profile show the B(lens) shelves, but their measurements of the azimuthally averaged profile (their Figure 72) do not. These are the reasons why we measure a higher effective surface brightness of the pseudobulge-subtracted disk than Ferrarese measures for the galaxy as a whole.

A.4. NGC 4352 = VCC 698

NGC 4352 is an unbarred and well-inclined S0 galaxy, so the photometry and decomposition are straightforward. Figure 29 (top) shows a color image of the galaxy made from the *HST* ACS images (blue = g; green = mean of g and z; red = z). The bulge-to-total luminosity ratio looks moderately small, but a contour plot of the SDSS g image (smoothed with a $2''$-FWHM Gaussian, middle panel) shows that the isophote ellipticity at $r \simeq 80''$ is $\epsilon \simeq 0.35$, similar to the value in the bulge. This suggests that the bulge dominates at both small and large radii.

Surface photometry of the ACS g image was carried out with VISTA profile, and the results are shown in the bottom two
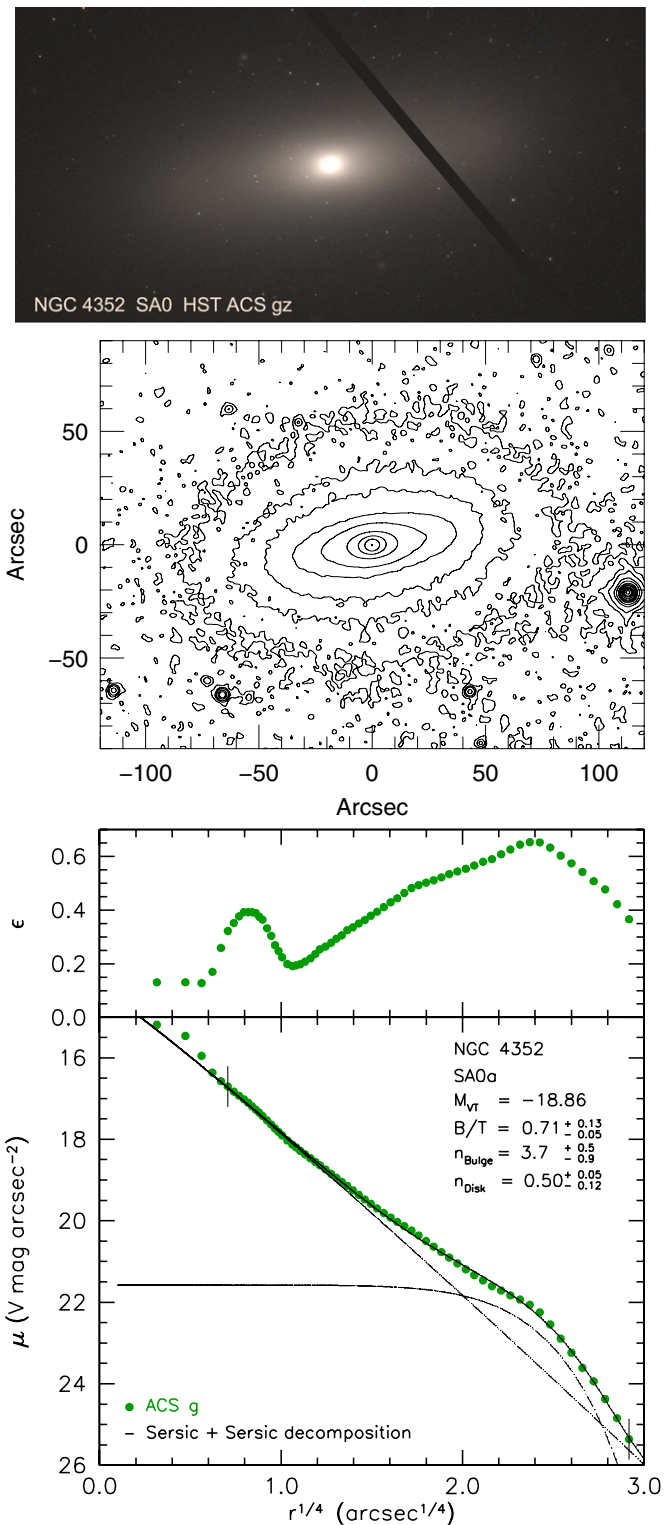
Figure 29. Top: color image of the SA0 galaxy NGC 4352. North is up and east is at the left as in all images illustrated. The field is $130''$ wide. Middle: brightness contours in the SDSS g image. Bottom: ellipticity and surface brightness along the major axis of NGC 4352. The dashed curves show the bulge–disk decomposition inside the fit range shown by vertical dashes. The sum of the components (solid curve) fits the data with rms = 0.049 mag arcsec^{-2}.

panels of Figure 29. The galaxy has a nucleus together with disky, central "extra light" (both seen by Ferrarese et al. 2006) like that in the extra light ellipticals in KFCB. We include this in our bulge–disk decomposition, but we take account of a fit that

omits the nuclear disk in the parameter error estimates. The disk is Gaussian. There is a small pseudobulge contribution from the nuclear disk, but the bulge is robustly classical whether the nuclear disk is included ($n = 3.7 \pm 0.2$) or not ($n = 2.9^{+0.3}_{-0.1}$). We adopt $n = 3.7^{+0.5}_{-0.9}$ as shown in the key. The bulge-to-total luminosity ratio is $B/T = 0.71^{+0.13}_{-0.05}$. The outer drop in ϵ is consistent with the decomposition result that the bulge dominates at large r. NGC 4352 is an S0a—a smaller, more face-on, less bulge-dominated version of NGC 3115.

The parameters from the above decomposition are listed in Table 1 and plotted in Figures 17, 18, and 20. However, there is an important caveat with the above discussion. It is possible that NGC 4352 resembles NGC 4638 (Figure 13); i.e., the rounder isophotes at large radii are not a sign that the bulge becomes comparable in brightness to the disk again at large radii. Rather, the rounder isophotes at large radii may belong to a heavily heated outer part of the disk. Then the disk would be more nearly exponential and we would derive $B/T \sim 0.25$. Our conclusions would not change, but the evidence for dynamical thickening of disks would get stronger. This caveat is discussed in Appendix A.12.

A.5. NGC 4528 = VCC 1537

NGC 4528 is shown in an ACS color image in Figure 30. *HST* resolution shows what was not clear at ground-based resolution: NGC 4528 is barred, and the bar lies almost along the minor axis (Ferrarese et al. 2006). There is a hint of an inner ring "(r)" around the end of the bar, but mainly, the ring outlines the rim of a lens component that shows up in our photometry (Figure 31) as a shelf in the light distribution interior to the outer disk. To put it differently, the major-axis disk brightness profile consists of two parts: a lens and an outer disk that form two distinct shelves in $\mu(r)$ in Figure 31. This is very common behavior in barred galaxies (Kormendy 1979b). In this case, the lens shelf is too abrupt to be well fitted by a Sérsic function; as a result, our best fits have rms $\simeq 0.1$ and $n \simeq 1.0 \pm 0.05$. The outer disk is well fitted by a Sérsic function with a very small index; our decomposition gives $n = 0.17$–0.3, but the outer disk photometry is very uncertain and the leverage is so small that its n is not well constrained. Note that the lens and disk have the same apparent ellipticity, i.e., the lens really is a part of the disk.

Taking $\epsilon(r)$ into account, our photometry implies that the lens-to-total luminosity ratio is lens$/T \simeq 0.54$ and the disk-to-total luminosity ratio is $D/T \sim 0.07$. The bar fraction is not accurately determined but is a few percent.

The bulge parameters are the ones that we need most. Despite the high surface brightness of the bulge above the lens, the bulge parameters are more uncertain than usual, in part because the photometry of the outer disk is very uncertain and in part because there is strong parameter coupling for three—not the usual two—components. The bulge Sérsic index is $n = 2.55^{+0.61}_{-0.20}$. Also, most of the bulge light is in an almost round distribution. We conclude that this is at least primarily a classical bulge. The bulge-to-total luminosity ratio is $B/T \simeq 0.38 \pm 0.13$. In comparison, the SAb galaxy M 31 has $B/T \simeq 0.25$, and the SAab galaxy M 81 has $B/T \simeq 0.34$ (Kormendy 2011b). We tentatively classify NGC 4528 as SB(r,lens)0ab. But we emphasize that the stage along the Hubble sequence is uncertain and that no conclusions of this paper are affected if it turns out, after further work, that a Hubble type of S0a or S0b is more appropriate.


Figure 30. Color image of the SB(r)0 galaxy NGC 4528 constructed from the *HST* ACS g image (blue), the mean of the g and z images (green), and the z image (red). The bar is located almost along the minor axis, so its effects on our major-axis bulge–disk decomposition are negligible.
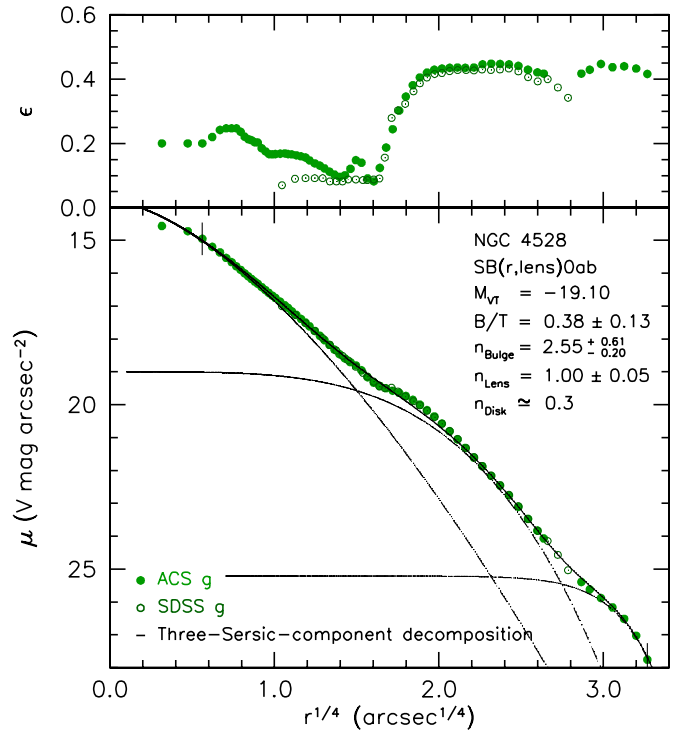
Figure 31. Ellipticity ϵ and surface brightness μ_V along the major axis of NGC 4528 measured by fitting ellipses to the isophotes in the ACS and SDSS g-band images. The dashed curves show a three-Sérsic-component, bulge–lens–disk decomposition inside the fit range (vertical dashes). The sum of the components (solid curve) fits the data with rms $= 0.105$ mag arcsec^{-2}.

Figure 32 shows, for both NGC 4352 and NGC 4528, the bulge and disk parameters derived in our photometric
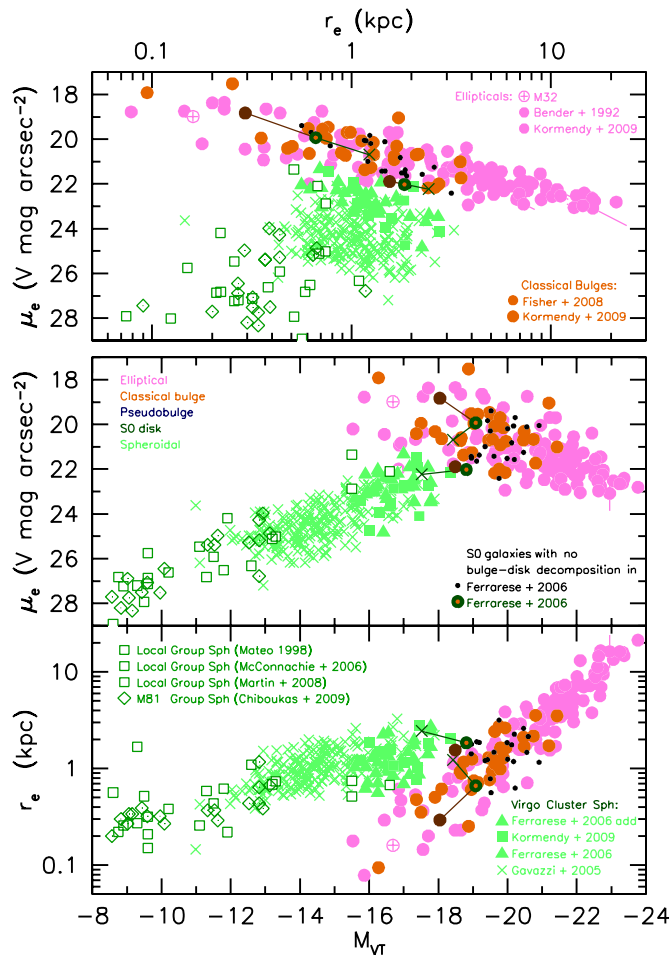
Figure 32. Parameter correlations from Figure 2 showing the results of the bulge–disk decompositions of the unbarred S0a galaxy NGC 4352 (lower points in the top panel) and the SB(lens)0ab galaxy NGC 4528 (upper points in the top panel). The dark green filled circles with the brown centers show the total parameters measured by F2006 for the bulge and disk together. These points are connected by straight lines to the bulge parameters (dark brown filled circles) and the disk parameters (dark green crosses).

decomposition compared with the F2006 parameters for the whole galaxy. Both galaxies are well behaved. The small bulge of NGC 4528 helps to define the extension of the E + bulge sequence to the left of (i.e., toward more compact bulges than) the spheroidals. Like other bulges, the explanation for the compactness of this classical bulge cannot be that it has been tidally stripped of its outer parts. In any case, its Sérsic index of $n = 2.55$ is normal.

A.6. NGC 4417 = VCC 944

NGC 4417 (Figure 33) is very similar to NGC 4352 (Appendix A.4): it is nearly edge-on; it has a prominent bulge at small r, and the flattened isophotes produced by the disk at intermediate radii gave way to rounder isophotes again at large radii. The usual interpretation is that the galaxy is bulge-dominated, and the photometry and decomposition (bottom panels of Figure 33) make this quantitative. The decomposition is straightforward and robust. Major- and mean-axis decompositions yield consistent results. They confirm that the bulge dominates the light at both small and large radii. The ellipticity maximum at $4''$ is due to a faint central disk, and the slightly boxy appearance of the bulge is due to a faint bar. However, the bulge is
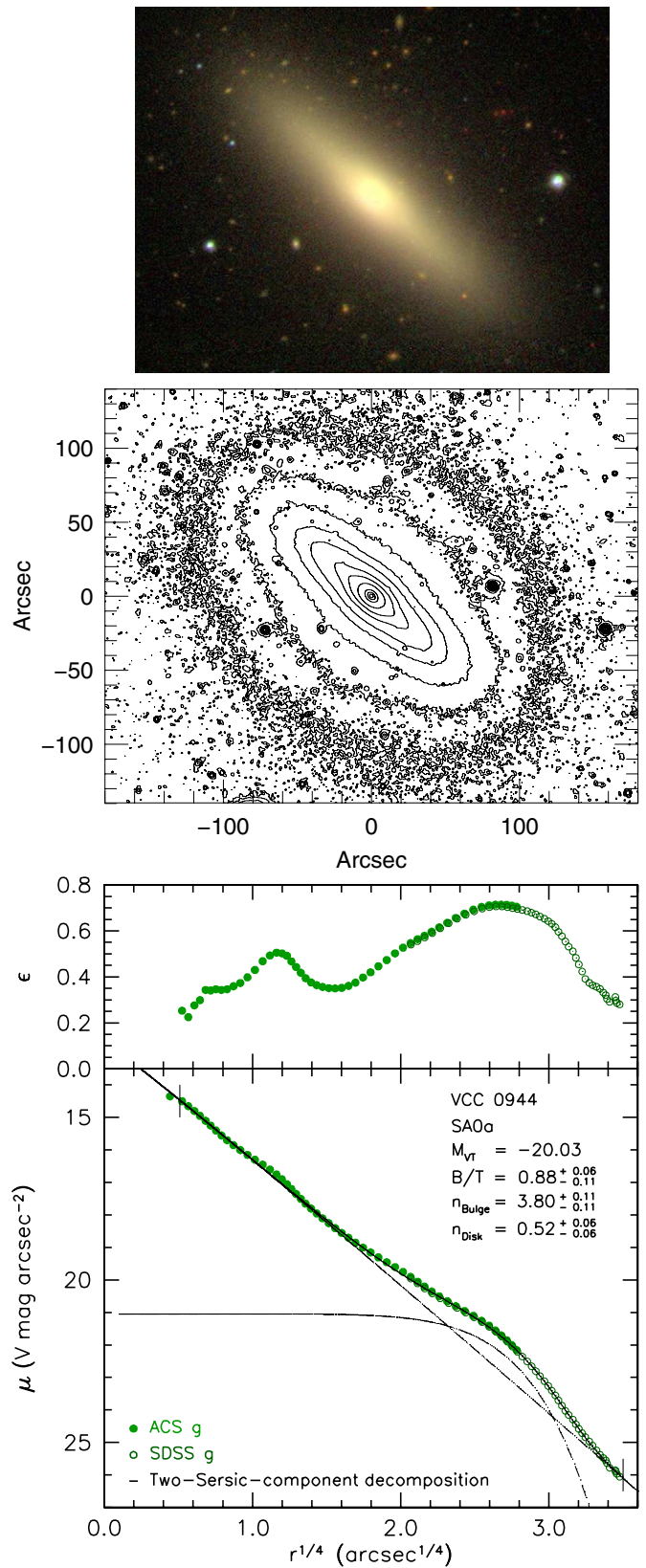
Figure 33. Top: WIKISKY image of NGC 4417 = VCC 944. Middle: brightness contours of the SDSS $g + r + i$ images smoothed with a $1''2$ -FWHM Gaussian. Bottom: major-axis brightness and ellipticity profiles. Dashed curves show the bulge–disk decomposition; the sum of the components (solid curve) fits the data with rms = 0.043 mag arcsec^{-2}.

classical ($n \approx 4$). The disk is essentially Gaussian. We measure $B/T = 0.88^{+0.06}_{-0.11}$ and classify the galaxy as SA0a.
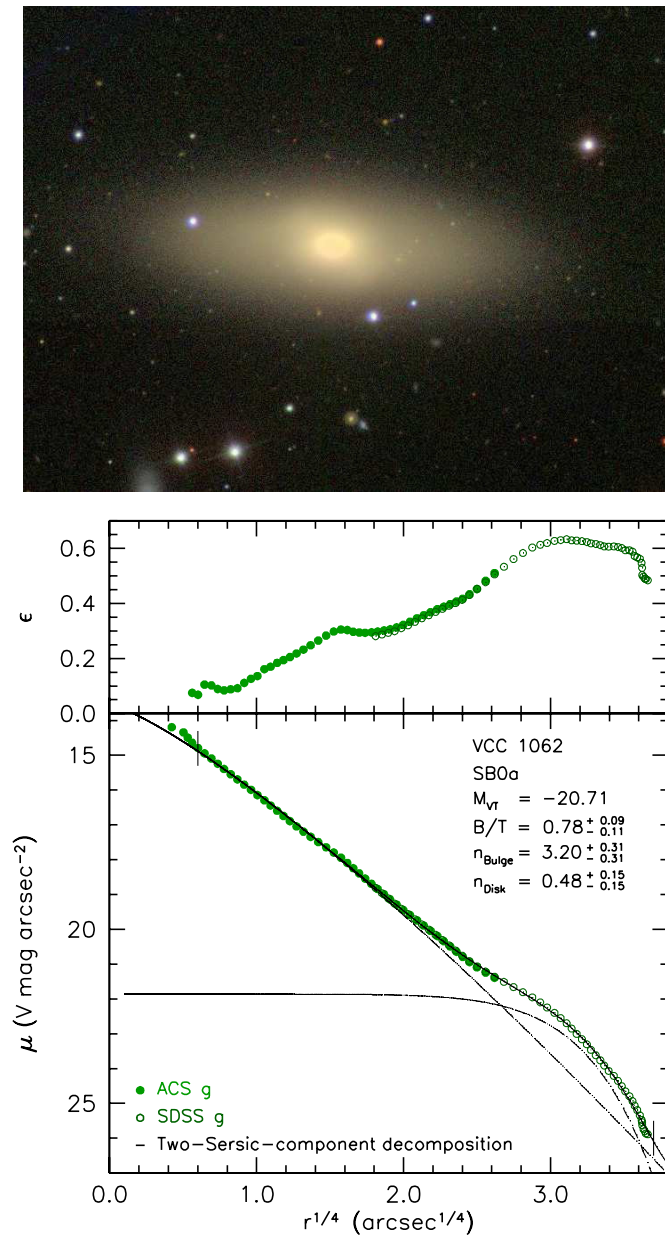
Figure 34. Top: color image of the barred S0 NGC 4442 = VCC 1062 from WIKISKY. Bottom: ellipticity ϵ and surface brightness μ_V along the major axis of NGC 4442. The dashed curves show the Sérsic–Sérsic, bulge–disk decomposition inside the fit range (vertical dashes). The sum of the components (solid curve) fits the data with rms = 0.060 mag arcsec^{-2}.

The same caveat that we discussed for NGC 4352 applies here. It is possible that the rounder, outer isophotes are a sign that the disk has been heated rather than that the bulge takes over again at large radii (Appendix A.12).

A.7. NGC 4442 = VCC 1062

NGC 4442 is a weakly barred S0. Decomposition is straightforward; our major- and mean-axis decompositions give fully consistent parameters for the bulge. The parameters of the disk are somewhat affected by the presence of the bar, as the comparison of major- and mean-axis profiles show (Figure 34 versus Figure 35). Nevertheless, the disk seems to be more nearly Gaussian than exponential. The bulge is classical and contributes significantly again at the largest radii. The bulge-to-total ratio is very robust and high, i.e., the galaxy is of type SB0a.
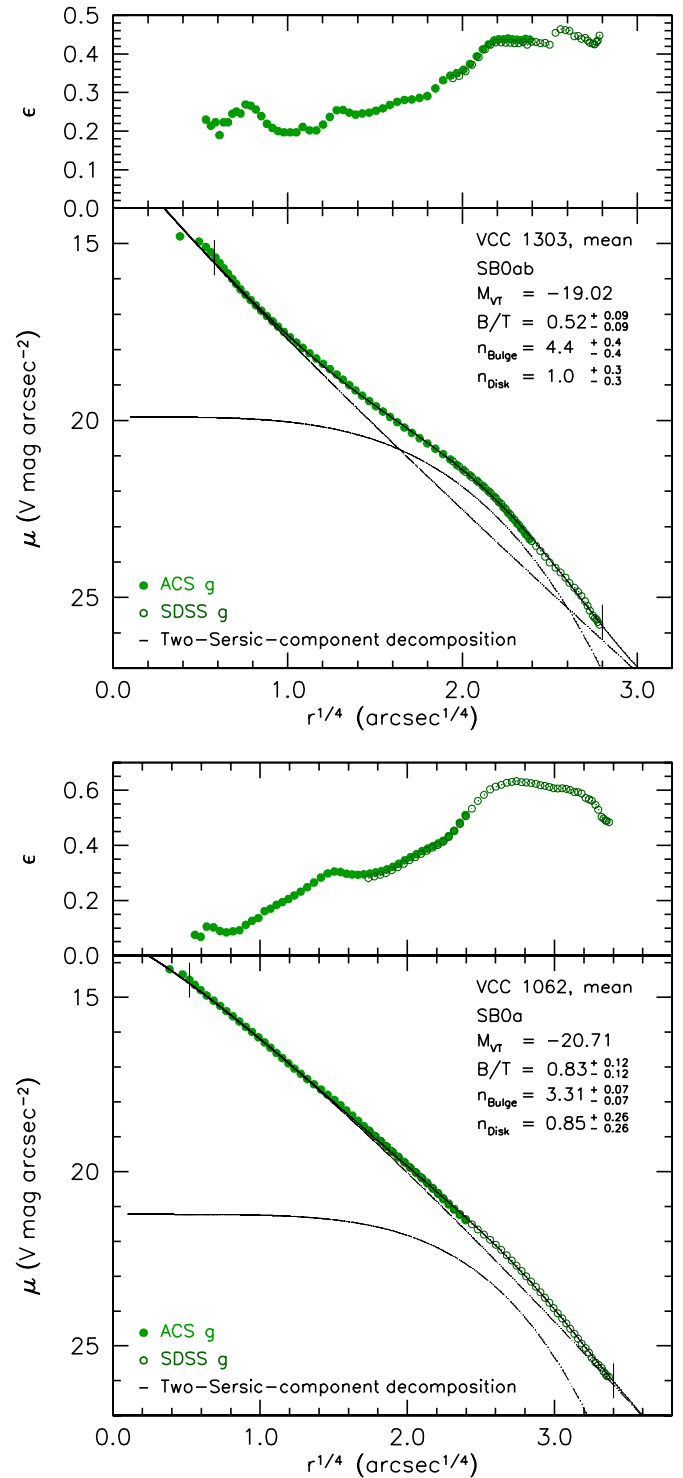

Figure 35. Mean-axis profiles of NGC 4442 = VCC 1062 (bottom) and NGC 4483 = VCC 1303 (top). The dashed curves show the decompositions; the component sums (solid curves) fit the data with rms = 0.033 mag arcsec^{-2} for NGC 4442 and rms = 0.048 mag arcsec^{-2} for NGC 4483. These decompositions can be compared with the major-axis decompositions of these galaxies in Figures 34 and 36. The bulge-to-total ratios are robust.

A.8. NGC 4483 = VCC 1303

NGC 4483 is a barred S0 galaxy in which the bulge and disk contribute equal amounts of light. There is evidence for a faint nucleus (F2006). The decompositions along the major and mean axes yield consistent results, both for the bulge and
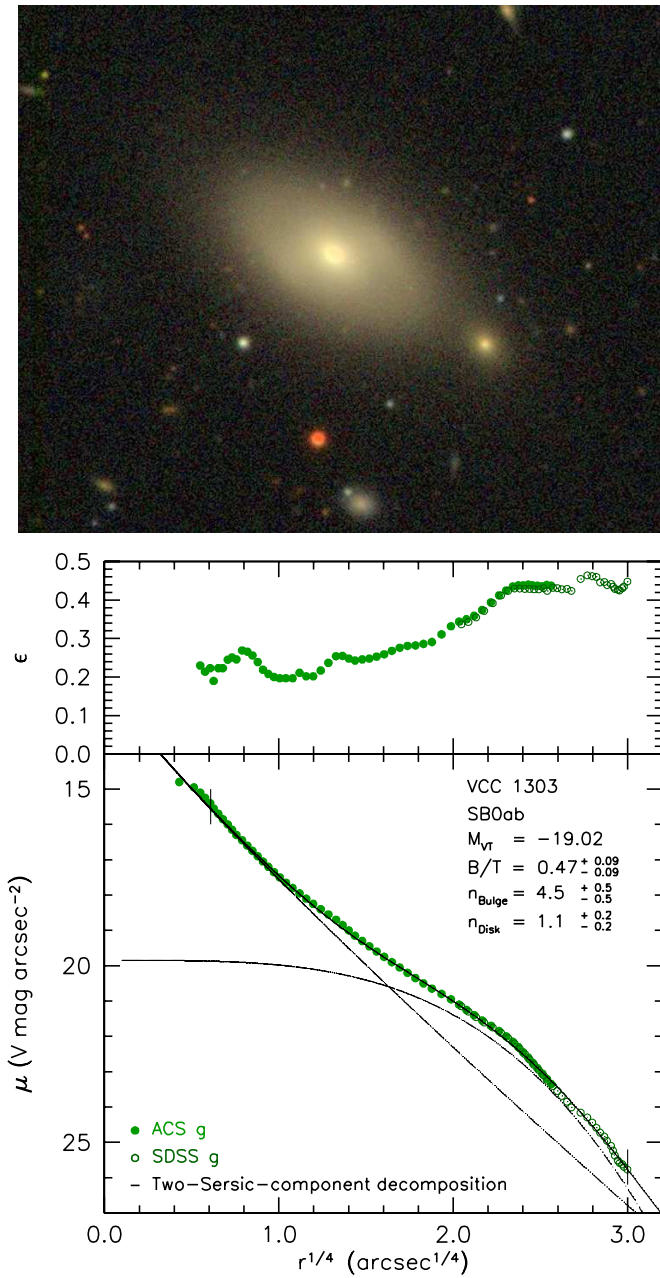
Figure 36. Top: color image of NGC 4483 = VCC 1303 from WIKISKY. Again, the bar is oriented well away from the major axis and has little effect on our decomposition. Bottom: ellipticity ϵ and surface brightness μ_V along the major axis of NGC 4483. The dashed curves show the decomposition; the sum of the components (solid curve) fits the data with rms = 0.058 mag arcsec^{-2}.

for the disk (cf. Figures 35 and 36). The bulge is classical with an almost-de-Vaucouleurs-law profile. The disk is exponential. The bulge-to-total ratio implies a type of SB0ab.

A.9. NGC 4550 = VCC 1619

NGC 4550 (Figure 37) is unusual: it consists of two counter-rotating disks (Rubin et al. 1992; Rix et al. 1992). They are coplanar and largely overlap in radius. In combination, they yield a brightness profile with a Sérsic index that is abnormally large for a single disk, i.e., $n = 1.69^{+0.13}_{-0.08}$ (Figure 37). The ACS image shows dust near the center, but the absorption is not strong enough to explain the large n. The disk surface brightness is high. We classify the tiny central component as a pseudobulge, based
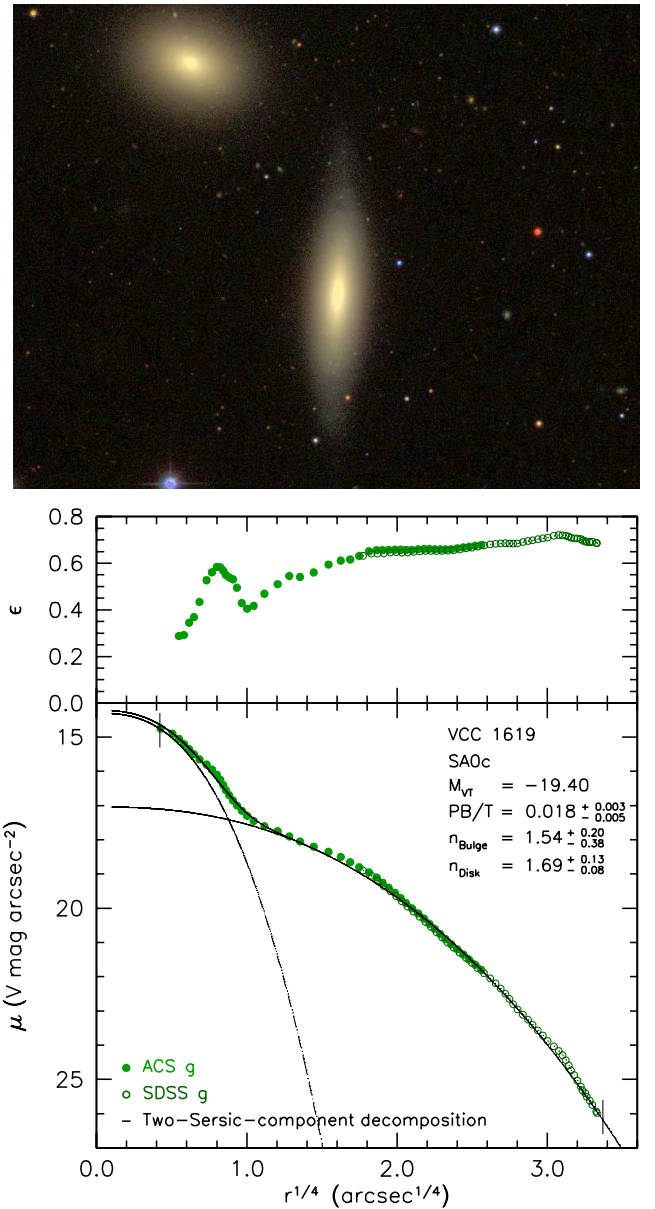
Figure 37. Top: color image of NGC 4550 = VCC 1619 from WIKISKY. Bottom: ellipticity ϵ and surface brightness μ_V along the major axis of NGC 4550. The dashed curves show the Sérsic–Sérsic, nucleus–disk decomposition inside the fit range (vertical dashes). The sum of the components (solid curve) fits the data with rms = 0.113 mag arcsec^{-2}.

on its high flattening. We classify NGC 4550 as an unbarred, peculiar SA0c.

A.10. NGC 4578 = VCC 1720

NGC 4578 is an almost-face-on, unbarred S0 galaxy with eas-ily separable bulge, disk and nucleus components (Figure 38). The bulge is classical and contains ∼56% of the galaxy light. We classify NGC 4578 as SA0ab. The disk is clearly inconsis-tent with an exponential profile; it requires a steeper cutoff; i.e., $n = 0.56 \pm 0.11$, consistent with a Gaussian. For the Virgo Clus-ter environment, the galaxy is relatively isolated (Figure 40).

A.11. NGC 4623 = VCC 1913

NGC 4623 is a disk-dominated S0 with a small bulge (Figure 39). The ellipticity profile reveals a nuclear disk, i.e.,
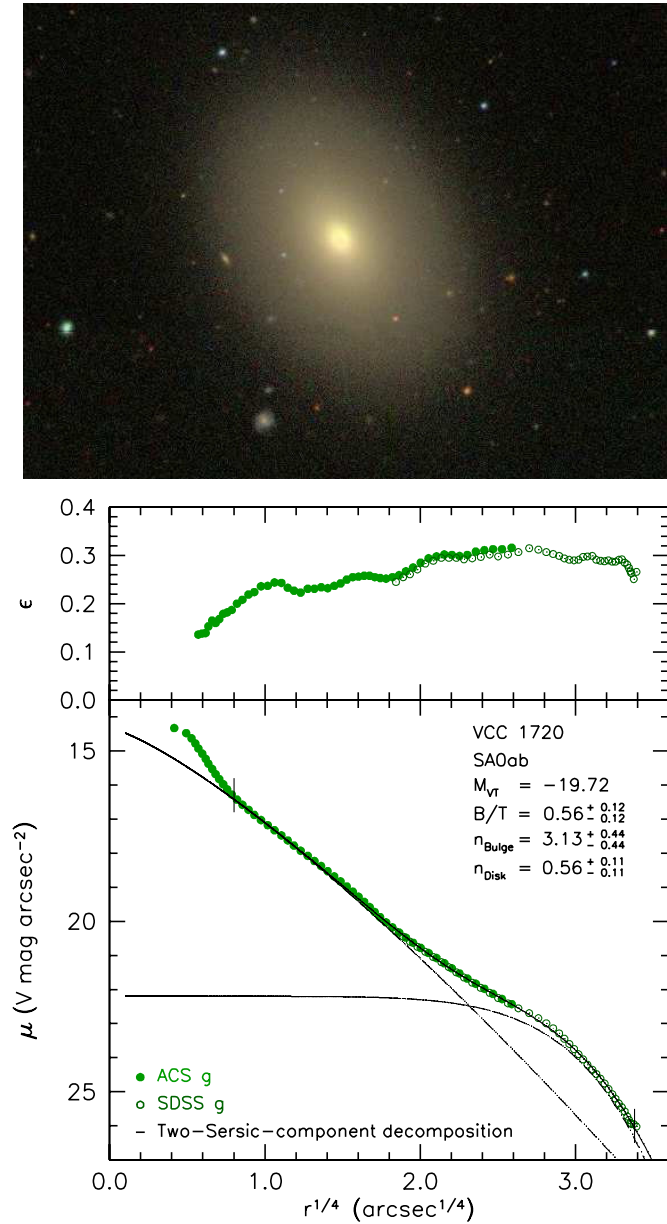
Figure 38. Top: color image of NGC 4578 = VCC 1720 from WIKISKY. The galaxy is unbarred and an easy case for bulge–disk decomposition. Bottom: ellipticity ϵ and surface brightness μ_V along the major axis of NGC 4578. The dashed curves show the bulge–disk decomposition; the sum of the components (solid curve) fits the data with rms = 0.038 mag arcsec^{-2}.

a pseudobulge contribution to bulge that also has a classical component (overall $n = 3.3 \pm 0.8$). The disky part covers almost the whole radius range of the bulge, so we classify it as pseudo. Its parameters are relatively uncertain, because it dominates over only a small brightness range. The disk profile is consistent with exponential. From PB/T, we classify the galaxy as SA0b.

A.12. Are the Disks of Many Virgo S0s Heated at Large Radii?

In Appendix A.4 on NGC 4352 and Appendix A.6 on NGC 4417, we noted a caveat with the assumption that a bulge dominates at both small and large radii when the outer ellipticity returns from high values that are characterstic of disks back down to values like those in the inner bulge. Such an ellipticity profile is observed in NGC 4638 (Figure 15), and
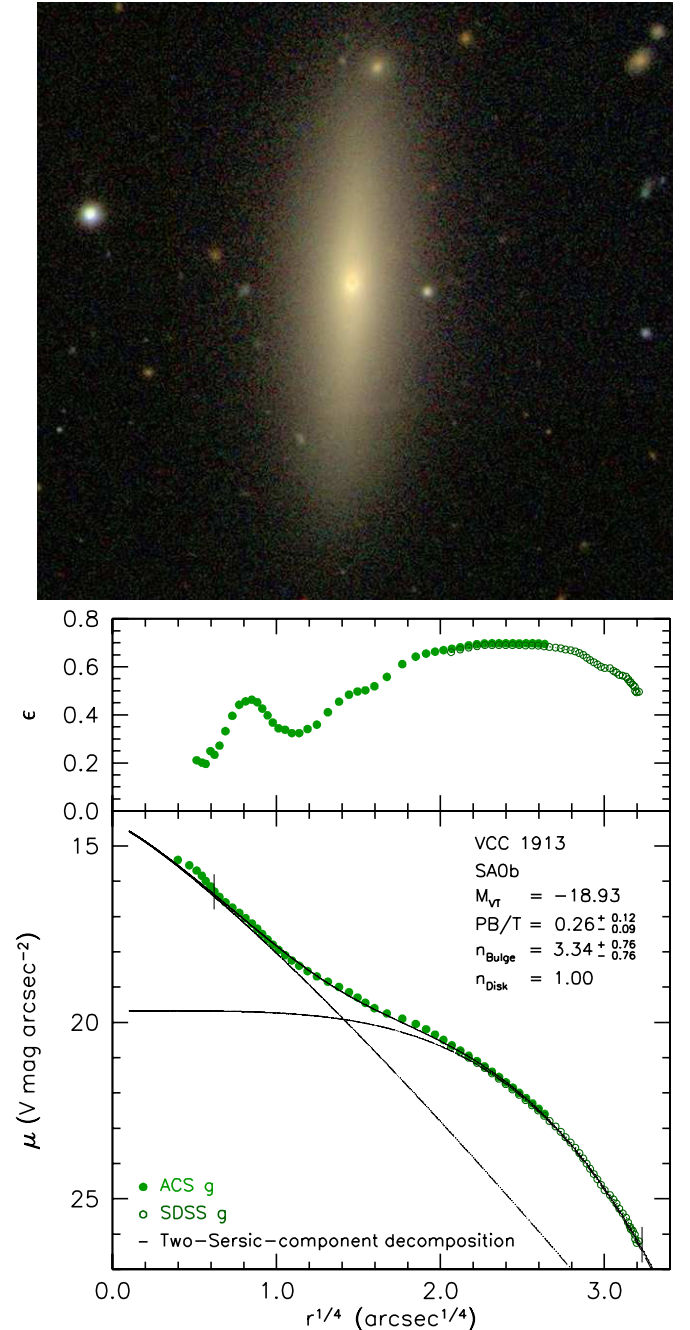

Figure 39. Top: color image of NGC 4623 = VCC 1913 from WIKISKY. Bottom: ellipticity ϵ and surface brightness μ_V along the major axis of NGC 4623. The dashed curves show the decomposition; the sum of the components (solid curve) fits the data with rms = 0.056 mag arcsec^{-2}.

there—because the galaxy is edge-on—we can tell that the outer isophotes belong to an Sph-like halo and not to the outward extrapolation of the bulge profile. We suggested that the halo was produced by dynamical heating of the outer disk. We used NGC 4638 as a "proof-of-concept" galaxy for the idea that Sph galaxies can be produced by the harassment of disks.

Similarly, the rounder outer isophotes of NGC 4352 and NGC 4417 may not be a sign that the bulge dominates there. If we assign this outer light to the disk, then revised decompositions give B/T values of ∼0.25–0.35 for both galaxies. Then we would classify them as S0ab–S0b. Our observations cannot test this possibility; we leave this for future
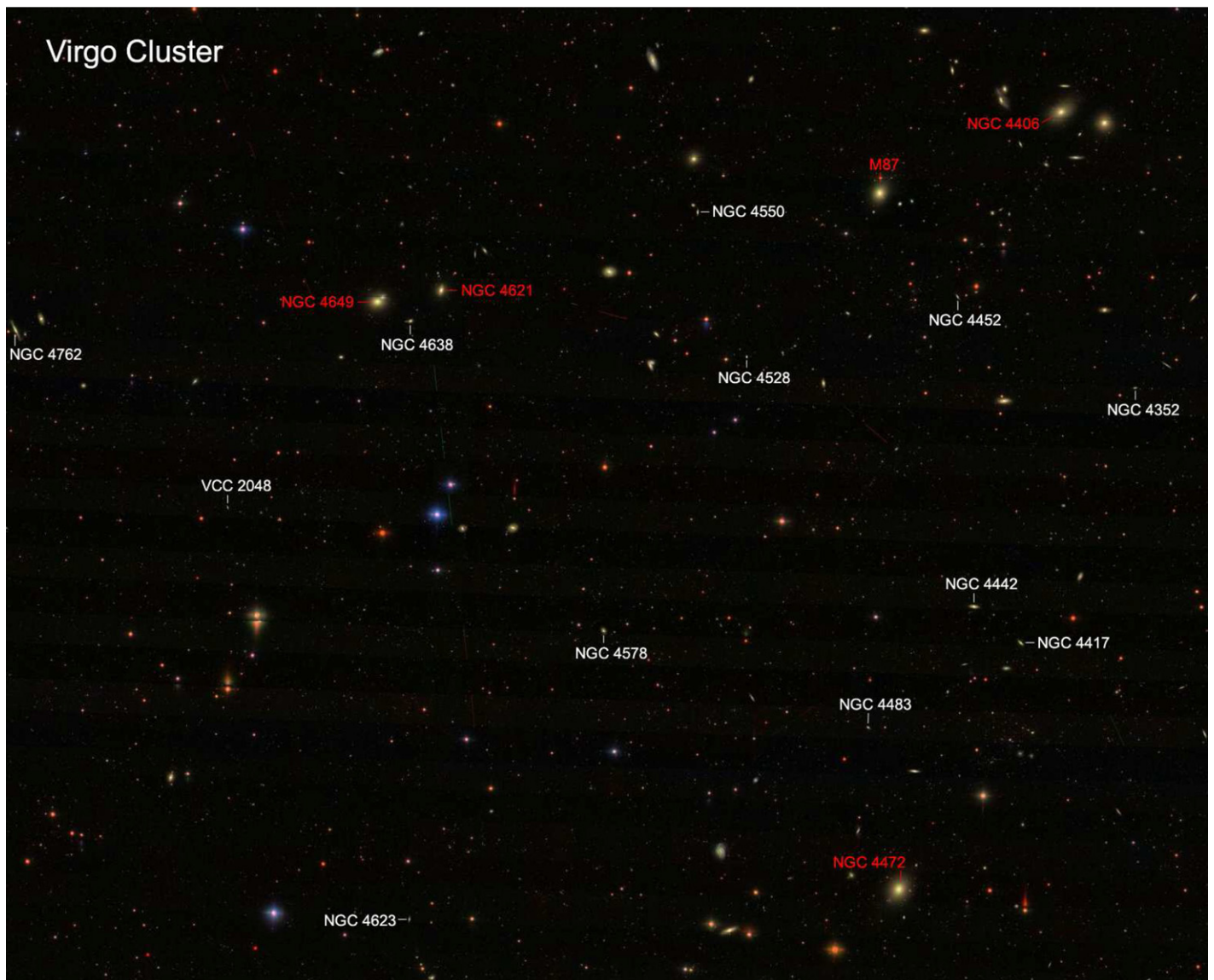
Figure 40. Central parts of the Virgo Cluster showing the positions of the S0 galaxies measured in this paper. Some of the brightest ellipticals in the cluster are labeled in red. The S0s are located near the cluster center, mostly in the region where Figure 24 shows ongoing ram-pressure stripping. NGC 4638, the remarkable S0 with a Sph halo (Section 4.1.4), is located almost between NGC 4649 and NGC 4621. This image is from www.wikisky.org.

work. Meanwhile, we adopt the conservative interpretation in Appendices A.4 and A.6. However, in this section, we note some hints that outer disk heating may indeed be more important than we suggested in the main text of this paper.

1. NGC 4638 is a powerful hint, as described above. It is located almost between two giant ellipticals in the Virgo Cluster (Figure 40), so it is not implausible that NGC 4638 has been dynamically harassed more than most galaxies.

2. Gaussian disks are surprisingly common in our analysis. It is no surprise to see outer cutoffs in the disk profiles of barred galaxies; they are characteristic of outer rings and of oval disks (Kormendy 1979b, 1982; Kormendy & Kennicutt 2004; Buta 1995, 2011; Buta et al. 2007). Thus the Gaussian components (lenses, outer disks, or both) in NGC 4762 (Section 4.1.1), NGC 4452 (Section 4.1.2), NGC 4528 (Appendix A.5), and NGC 4442 (Appendix A.7) are no surprise. But it is surprising that the unbarred galaxies NGC 4352 (Appendix A.4), NGC 4417 (Appendix A.6),

and NGC 4578 (Appendix A.10) have Gaussian disks, not exponential disks (Freeman 1970). However, a disk with a gradual outer cutoff may be the result if the disk is heated at large r and therefore—especially in edge-on galaxies such as NGC 4352 and NGC 4417—much reduced in surface brightness.

3. NGC 4442 and NGC 4483 have no visible outer disks. Each galaxy has a weak bar that fills a strong lens in one dimension. This is normal. But we see no sign of an outer disk around the B(lens) structure. We have not seen this behavior before; one additional example (NGC 4340, also in Virgo) is noted in the de Vaucouleurs Atlas (Buta et al. 2007). The observational remark is sufficient, but we note that we know no way to form a bar that completely fills its disk. This observed situation could result if the outer disk has been heated enough so that we do not detect it.

4. Exactly the sort of disk heating that we propose is in progress in NGC 4762. The B(lens) structure is thin and flat. But the outer disk is thicker, warped, and distorted

symmetrically into an $\int$ structure that is a signature of tidal responses. The culprit is presumably NGC 4754, a similar-luminosity SB0 located less than two diameters away along the minor axis of NGC 4762. The warped outer disk of NGC 4762 is expected to phase-wrap in azimuth at different rates at different radii. Eventually, its outer disk will just look thick. Many impulsive encounters such as the present one or the long-term result of more gradual dynamical harassment could plausible produce an S0 + Sph galaxy such as NGC 4638. The same observations and conclusions apply to NGC 4452; its minor-axis companion is the large Sph galaxy IC 3381 = VCC 1087.

These are hints that outer disk heating may be more important than the main text suggests. Figure 40 shows that the S0 galaxies discussed above lie in the central, "busy" parts of the Virgo Cluster, where galaxy harassment is most likely. The main conclusions of this paper would be strengthened by this result but do not depend on it. In Table 1, we make the more conservative assumption that NGC 4352 and NGC 4417 are bulge-dominated.

We are conscious of the apparent contradiction in claiming that tidal truncation of small ellipticals is minor, whereas dynamical heating of S0 disks may be important. But (1) the above evidence favors disk heating, whereas observations discussed in Section 3.2.2 disfavor serious tidal truncation of small Es. Also (2) the smallest ellipticals are a factor of ~10 smaller than the smallest S0 disks. Tidal forces are more effective in harassing larger objects. Most important (3) *there is a natural radius in S0 disks beyond which it is relatively easy to tilt orbits vertically and hence to thicken the disk after radius-dependent azimuthal phase wrapping. This is the radius outside which the disk is non-self-gravitating within the dark halo. At smaller radii, the structure is relatively stiff because of disk restoring forces. But where the dark matter dominates the potential, there are virtually no disk restoring forces.* The result—we suggest—can be seen in NGC 4762: the bright B(lens) structure is flat and thin, whereas the much fainter outer disk is strongly warped. Small ellipticals are already almost round; they have no "handle" at large radii, and scrambling their orbits further has little effect.

REFERENCES

Abadi, M. G., Moore, B., & Bower, R. G. 1999, MNRAS, 308, 947
Abramson, A., Kenney, J. D. P., Crowl, H. H., et al. 2011, AJ, 141, 164
Adami, C., Slezak, E., Durret, F., et al. 2005, A&A, 429, 39
Arnaboldi, M. 2011, Paper presented at the ESO Workshop on Fornax, Virgo, Coma et al.: Stellar Systems in High Density Environments, ed. M. Arnaboldi, http://www.eso.org/sci/meetings/2011/fornax_virgo2011/talks_pdf/Arnaboldi_Magda.pdf
Arnaboldi, M., Aguerri, J. A. L., Napolitano, N. R., et al. 2002, AJ, 123, 760
Arnaboldi, M., Freeman, K. C., Mendez, R. H., et al. 1996, ApJ, 472, 145
Arnaboldi, M., & Gerhard, O. 2010, Highlights Astron., 15, 97
Arnaboldi, M., Gerhard, O., Aguerri, J. A. L., et al. 2004, ApJ, 614, L33
Baggett, W. E., Baggett, S. M., & Anderson, K. S. J. 1998, AJ, 116, 1626
Bahcall, J. N., & Casertano, S. 1985, ApJ, 293, L7
Baldry, I. K., Glazebrook, K., Brinkmann, J., et al. 2004, ApJ, 600, 681
Balick, N., Faber, S. M., & Gallagher, J. S. 1976, ApJ, 209, 710
Banse, K., Ponz, D., Ounnas, C., Grosbøl, P., & Warmels, R. 1988, in Instrumentation for Ground-based Optical Astronomy: Present and Future, ed. L. B. Robinson (New York: Springer), 431
Barazza, F. D., Binggeli, B., & Jerjen, H. 2002, A&A, 391, 823
Bedregal, A. G., Aragón-Salamanca, A., & Merrifield, M. R. 2006, MNRAS, 373, 1125
Begelman, M. C., Blandford, R. D., & Rees, M. J. 1980, Nature, 287, 307
Bell, E. F., McIntosh, D. H., Katz, N., & Weinberg, M. D. 2003, ApJS, 149, 289
Bender, R. 1987, Mitt. Astron. Ges., 70, 226

Bender, R., Burstein, D., & Faber, S. M. 1992, ApJ, 399, 462
Bender, R., Burstein, D., & Faber, S. M. 1993, ApJ, 411, 153
Bender, R., Döbereiner, S., & Möllenhoff, C. 1987, A&A, 177, L53
Bender, R., Döbereiner, S., & Möllenhoff, C. 1988, A&AS, 74, 385
Bender, R., & Möllenhoff, C. 1987, A&A, 177, 71
Bender, R., & Nieto, J.-L. 1990, A&A, 239, 97
Bender, R., Paquet, A., & Nieto, J.-L. 1991, A&A, 246, 349
Bender, R., Surma, P., Döbereiner, S., Möllenhoff, C., & Madejsky, R. 1989, A&A, 217, 35
Bernardi, M., Sheth, R. K., Annis, J., et al. 2003, AJ, 125, 1882
Binggeli, B. 1994, in ESO/OHP Workshop on Dwarf Galaxies, ed. G. Meylan & P. Prugniel (Garching: ESO), 13
Binggeli, B., & Cameron, L. M. 1991, A&A, 252, 27
Binggeli, B., & Popescu, C. C. 1995, A&A, 298, 63
Binggeli, B., Sandage, A., & Tammann, G. A. 1985, AJ, 90, 1681
Binggeli, B., Sandage, A., & Tammann, G. A. 1988, ARA&A, 26, 509
Blanton, M. R., Eisenstein, D., Hogg, D. W., Schlegel, D. J., & Brinkmann, J. 2005, ApJ, 629, 143
Blanton, M. R., Hogg, D. W., Bahcall, N. A., et al. 2003, ApJ, 594, 186
Böhringer, H., Briel, U. G., Schwarz, R. A., et al. 1994, Nature, 368, 828
Böker, T., Laine, S., van der Marel, R. P., et al. 2002, AJ, 123, 1389
Böker, T., Sarzi, M., McLaughlin, D. E., et al. 2004, AJ, 127, 105
Boselli, A., Boissier, S., Cortese, L., & Gavazzi, G. 2008, ApJ, 674, 742
Boselli, A., Boissier, S., Cortese, L., & Gavazzi, G. 2009, Astron. Nachr., 330, 904
Bothun, G. D., & Thompson, I. B. 1988, AJ, 96, 877
Bullock, J. S., Kravtsov, A. V., & Weinberg, D. H. 2000, ApJ, 539, 517
Burstein, D. 1979, ApJ, 234, 435
Buta, R. 1995, ApJS, 96, 39
Buta, R. 2011, in Planets, Stars, and Stellar Systems, Vol. 6, ed. W. C. Keel (New York: Springer), in press (arXiv:1102.0550)
Buta, R., & Combes, F. 1996, Fundam. Cosm. Phys., 17, 95
Buta, R. J., Corwin, H. G., & Odewahn, S. C. 2007, The de Vaucouleurs Atlas of Galaxies (Cambridge: Cambridge Univ. Press)
Buta, R., & Crocker, D. A. 1991, AJ, 102, 1715
Buta, R., Laurikainen, E., Salo, H., & Knapen, J. H. 2010a, ApJ, 721, 259
Buta, R. J., Sheth, K., Regan, M., et al. 2010b, ApJS, 190, 147
Byun, Y.-I., & Freeman, K. C. 1995, ApJ, 448, 563
Cappellari, M., Emsellem, E., Bacon, R., et al. 2007, MNRAS, 379, 418
Cappellari, M., Emsellem, E., Krajnović, D., et al. 2011a, MNRAS, 413, 813
Cappellari, M., Emsellem, E., Krajnović, D., et al. 2011b, MNRAS, 416, 1680
Castro-Rodríguez, N., Arnaboldi, M., Aguerri, J. A. L., et al. 2009, A&A, 507, 621
Cattaneo, A., Dekel, A., Devriendt, J., Guiderdoni, B., & Blaizot, J. 2006, MNRAS, 370, 1651
Cattaneo, A., Faber, S. M., Binney, J., et al. 2009, Nature, 460, 213
Cattaneo, A., Mamon, G. A., Warnick, K., & Knebe, A. 2011, A&A, 553, 5
Cayette, V., Kotanyi, C., Balkowski, C., & van Gorkom, J. H. 1994, AJ, 107, 1003
Cayette, V., van Gorkom, J. H., Balkowski, C., & Kotanyi, C. 1990, AJ, 100, 604
Chen, C.-W., Côté, P., West, A., Peng, E. W., & Ferrarese, L. 2010, ApJS, 191, 1
Chiboukas, K., Karachentsev, I. D., & Tully, R. B. 2009, AJ, 137, 3009
Chung, A., van Gorkom, J. H., Kenney, J. D. P., Crowl, H., & Vollmer, B. 2009, AJ, 138, 1741
Chung, A., van Gorkom, J. H., Kenney, J. D. P., & Vollmer, B. 2007, ApJ, 659, L115
Combes, F., Dupraz, C., Casoli, F., & Pagani, L. 1988, A&A, 203, L9
Côté, P., Ferrarese, L., Jordán, A., et al. 2007, ApJ, 671, 1456
Courteau, S., Dutton, A. A., van den Bosch, F. C., et al. 2007, ApJ, 671, 203
Da Costa, G. S. 1994, in ESO/OHP Workshop on Dwarf Galaxies, ed. G. Meylan & P. Prugniel (Garching: ESO), 221
Davé, R., Cen, R., Ostriker, J. P., et al. 2001, ApJ, 552, 473
David, L. P., Jones, C., & Forman, W. 1995, ApJ, 445, 578
Davies, R. L., Efstathiou, G., Fall, S. M., Illingworth, G., & Schechter, P. L. 1983, ApJ, 266, 41
Davis, T. A., Bureau, M., Young, L. M., et al. 2011, MNRAS, 414, 968
Dekel, A., & Birnboim, Y. 2006, MNRAS, 368, 39
Dekel, A., & Birnboim, Y. 2008, MNRAS, 383, 119
Dekel, A., & Silk, J. 1986, ApJ, 303, 39
De Rijcke, S., Dejonghe, H., Zeilinger, W. W., & Hau, G. K. T. 2001, ApJ, 559, L21
De Rijcke, S., Dejonghe, H., Zeilinger, W. W., & Hau, G. K. T. 2003, A&A, 400, 119
De Rijcke, S., Dejonghe, H., Zeilinger, W. W., & Hau, G. K. T. 2004, A&A, 426, 53

De Rijcke, S., Prugniel, P., Simien, F., & Dejonghe, H. 2006, MNRAS, 39, 1321
de Souza, R. E., Gadotti, D. A., & dos Anjos, S. 2004, ApJS, 153, 411
de Vaucouleurs, G. 1959, in Handbuch der Physik, Vol. 53, ed. S. Flugge (Berlin: Springer), 275
Devereux, N. A., & Young, J. S. 1991, ApJ, 371, 515
de Zeeuw, P. T., Bureau, M., Emsellem, E., et al. 2002, MNRAS, 329, 513
Djorgovski, S., & Davis, M. 1987, ApJ, 313, 59
Djorgovski, S., de Carvalho, R., & Han, M.-S. 1988, in ASP 100th Anniversary Symp., The Extragalactic Distance Scale, ed. S. van den Bergh & C. J. Pritchet (San Francisco, CA: ASP), 329
Dolphin, A. E. 2002, MNRAS, 332, 91
D'Onghia, E., Besla, G., Cox, T. J., & Hernquist, L. 2009, Nature, 460, 605
Dressler, A. 1979, ApJ, 231, 659
Dressler, A. 1980, ApJ, 236, 351
Dressler, A., Oemler, A., Couch, W. J., et al. 1997, ApJ, 490, 577
Ebisuzaki, T., Makino, J., & Okamura, S. K. 1991, Nature, 354, 212
Einasto, J., Saar, E., Kaasik, A., & Chernin, A. D. 1974, Nature, 252, 111
Emsellem, E., Cappellari, M., Krajnović, D., et al. 2007, MNRAS, 379, 401
Emsellem, E., Cappellari, M., Krajnović, D., et al. 2011, MNRAS, 414, 888
Emsellem, E., Cappellari, M., Peletier, R. F., et al. 2004, MNRAS, 352, 721
Emsellem, E., Dejonghe, H., & Bacon, R. 1999, MNRAS, 303, 495
Faber, S. M. 1973, ApJ, 179, 423
Faber, S. M., Dressler, A., Davies, R. L., Burstein, D., & Lynden-Bell, D. 1987, in Nearly Normal Galaxies: From the Planck Time to the Present, ed. S. M. Faber (New York: Springer), 175
Faber, S. M., & Lin, D. N. C. 1983, ApJ, 266, L17
Faber, S. M., Tremaine, S., Ajhar, E. A., et al. 1997, AJ, 114, 1771
Faber, S. M., Willmer, C. N. A., Wolf, C., et al. 2007, ApJ, 665, 265
Farouki, R., & Shapiro, S. L. 1980, ApJ, 241, 928
Ferguson, A. M. N., Irwin, M. J., Ibata, R. A., Lewis, G. F., & Tanvir, N. R. 2002, AJ, 124, 1452
Ferguson, H. C., & Sandage, A. 1989, ApJ, 346, L53
Ferrarese, L., Côté, P., Jordán, A., et al. 2006, ApJS, 164, 334 (F2006)
Fisher, D. B., & Drory, N. 2008, AJ, 136, 773
Frebel, A. 2010, Astron. Nachr., 331, 474
Freeland, E., & Wilcots, E. 2011, ApJ, 738, 145
Freeman, K. C. 1970, ApJ, 160, 811
Gavazzi, G., Donati, A., Cucciati, O., et al. 2005, A&A, 430, 411
Gavazzi, G., Franzetti, P., Scodeggio, M., Boselli, A., & Pierini, D. 2000, A&A, 361, 863
Geha, M., Guhathakurta, P., Rich, R. M., & Cooper, M. C. 2006, AJ, 131, 332
Geha, M., Guhathakurta, P., & van der Marel, R. P. 2003, AJ, 126, 1794
Geisler, D., Smith, V. V., Wallerstein, G., Gonzalez, G., & Charbonnel, C. 2005, AJ, 129, 1428
Gerola, H., Carnevali, P., & Salpeter, E. E. 1983, ApJ, 268, L75
Gerola, H., Seiden, P. E., & Schulman, L. S. 1980, ApJ, 242, 517
Glass, L., Ferrarese, L., Côté, P., et al. 2011, ApJ, 726, 31
Gonzalez, A. H., Zaritsky, D., & Zabludoff, A. I. 2007, ApJ, 666, 147
González-García, A. C., Aguerri, J. A. L., & Balcells, M. 2005, A&A, 444, 803
Graham, A. W., Erwin, P., Trujillo, I., & Asensio Ramos, A. 2003, AJ, 125, 2951
Graham, A. W., & Guzmán, R. 2003, AJ, 125, 2936
Graham, A. W., & Guzmán, R. 2004, in Penetrating Bars Through Masks of Cosmic Dust: The Hubble Tuning Fork Strikes a New Note, ed. D. L. Block et al. (Dordrecht: Kluwer), 723
Grebel, E. K., Gallagher, J. S., & Harbeck, D. 2003, AJ, 125, 1926
Gunn, J. E., & Gott, J. R. 1972, ApJ, 176, 1
Gursky, H., Kellogg, E., Murray, S., et al. 1971, ApJ, 167, L81
Hamabe, M. 1982, PASJ, 34, 423
Hernandez, X., Gilmore, G., & Valls-Gabaud, D. 2000, MNRAS, 317, 831
Hinz, J. L., Rieke, G. H., & Caldwell, N. 2003, AJ, 126, 2622
Hogg, D. W., Blanton, M., Strateva, I., et al. 2002, AJ, 124, 646
Hogg, D. W., Blanton, M. R., Brinchmann, J., et al. 2004, ApJ, 601, L29
Hopkins, P. F., Bundy, K., Hernquist, L., Wuyts, S., & Cox, T. J. 2010, MNRAS, 401, 1099
Hopkins, P. F., Cox, T. J., Dutta, S. N., et al. 2009a, ApJS, 181, 135
Hopkins, P. F., Cox, T. J., & Hernquist, L. 2008, ApJ, 689, 17
Hopkins, P. F., Hernquist, L., Cox, T. J., Keres, D., & Wuyts, S. 2009b, ApJ, 691, 1424
Hubble, E. 1936, The Realm of the Nebulae (New Haven, CT: Yale Univ. Press)
Hurley-Keller, D., Mateo, M., & Nemec, J. 1998, AJ, 115, 1840
Ibata, R. A., Gilmore, G., & Irwin, M. J. 1994, Nature, 370, 194
Ibata, R. A., Gilmore, G., & Irwin, M. J. 1995, MNRAS, 277, 781
Ibata, R., Irwin, M., Lewis, G., Ferguson, A., & Tanvir, N. 2001a, Nature, 412, 49
Ibata, R., Lewis, G. F., Irwin, M., Totten, E., & Quinn, T. 2001b, ApJ, 551, 294
Ibata, R., Martin, N. F., Irwin, M., et al. 2007, ApJ, 671, 1591

Ichikawa, S.-I. 1989, AJ, 97, 1600
Irwin, M. J., Belokurov, V., Evans, N. W., et al. 2007, ApJ, 656, L13
Jerjen, H., & Binggeli, B. 1997, in ASP Conf. Ser. 116, The Second Stromlo Symposium: The Nature of Elliptical Galaxies, ed. M. Arnaboldi, G. S. Da Costa, & P. Saha (San Francisco, CA: ASP), 239
Jerjen, H., Kalnajs, A., & Binggeli, B. 2000, A&A, 358, 845
Jerjen, H., Kalnajs, A., & Binggeli, B. 2001, in ASP Conf. Ser. 230, Galaxy Disks and Disk Galaxies, ed. J. G. Funes & E. M. Corsini (San Francisco, CA: ASP), 239
Jørgensen, I., Franx, M., & Kjærgaard, P. 1996, MNRAS, 280, 167
Karachentsev, I., Aparicio, A., & Makarova, L. 1999, A&A, 352, 363
Kauffmann, G., Heckman, T. M., & Best, P. N. 2008, MNRAS, 384, 953
Kazantzidis, S., Łokas, E. L., Callegari, S., Mayer, L., & Moustakas, L. A. 2011, ApJ, 726, 98
Kelson, D. D., Zabludoff, A. I., Williams, K. A., et al. 2002, ApJ, 576, 720
Kenney, J. D., & Young, J. S. 1986, ApJ, 303, L13
Kenney, J. D. P., & Koopmann, R. A. 1999, AJ, 117, 181
Kenney, J. D. P., Tal, T., Crowl, H. H., Feldmeier, J., & Jacoby, G. H. 2008, ApJ, 687, L69
Kenney, J. D. P., van Gorkom, J. H., & Vollmer, B. 2004, AJ, 127, 3361
Kent, S. M. 1985, ApJS, 59, 115
King, I. R. 1966, AJ, 71, 64
Kirby, E. M., Jerjen, H., Ryder, S. D., & Driver, S. P. 2008, AJ, 136, 1866
Knapp, G. R., Guhathakurta, P., Kim, D.-W., & Jura, M. 1989, ApJS, 70, 329
Komatsu, E., Dunkley, J., Nolta, M. R., et al. 2009, ApJS, 180, 330
Kormendy, J. 1977a, ApJ, 217, 406
Kormendy, J. 1977b, ApJ, 218, 333
Kormendy, J. 1979a, in Photometry, Kinematics and Dynamics of Galaxies, ed. D. S. Evans (Austin, TX: Department of Astronomy, Univ. Texas at Austin), 341
Kormendy, J. 1979b, ApJ, 227, 714
Kormendy, J. 1981, in The Structure and Evolution of Normal Galaxies, ed. S. M. Fall & D. Lynden-Ball (Cambridge: Cambridge Univ. Press), 85
Kormendy, J. 1982, in Twelfth Advanced Course of the Swiss Society of Astronomy and Astrophysics, Morphology and Dynamics of Galaxies, ed. L. Martinet & M. Mayor (Sauverny: Geneva Obs.), 113
Kormendy, J. 1985, ApJ, 295, 73
Kormendy, J. 1987, in Nearly Normal Galaxies: From the Planck Time to the Present, ed. S. M. Faber (New York: Springer), 163
Kormendy, J. 1989, ApJ, 342, L63
Kormendy, J. 1999, in ASP Conf. Ser. 182, Galaxy Dynamics: A Rutgers Symposium, ed. D. Merritt, J. A. Sellwood, & M. Valluri (San Francisco, CA: ASP), 124
Kormendy, J. 2004, in Penetrating Bars Through Masks of Cosmic Dust: The Hubble Tuning Fork Strikes a New Note, ed. D. L. Block et al. (Dordrecht: Kluwer), 816
Kormendy, J. 2009, in ASP Conf. Ser. 419, Galaxy Evolution: Emerging Insights and Future Challenges, ed. S. Jogee, I. Marinova, L. Hao, & G. A. Blanc (San Francisco, CA: ASP), 87
Kormendy, J. 2011a, Paper presented at the ESO Workshop on Fornax, Virgo, Coma et al.: Stellar Systems in High Density Environments, ed. M. Arnaboldi, http://www.eso.org/sci/meetings/2011/fornax_virgo2011/talks_pdf/Kormendy_John.pdf
Kormendy, J. 2011b, ApJS, submitted
Kormendy, J., & Bender, R. 1994, in ESO/OHP Workshop on Dwarf Galaxies, ed. G. Meylan & P. Prugniel (Garching: ESO), 161
Kormendy, J., & Bender, R. 1996, ApJ, 464, L119
Kormendy, J., & Bender, R. 2009, ApJ, 691, L142
Kormendy, J., & Bender, R. 2011, Nature, 469, 377
Kormendy, J., Bender, R., Richstone, D., et al. 1996, ApJ, 459, L57
Kormendy, J., & Djorgovski, S. 1989, ARA&A, 27, 235
Kormendy, J., Drory, N., Bender, R., & Cornell, M. E. 2010, ApJ, 723, 54
Kormendy, J., & Fisher, D. B. 2008, in ASP Conf. Ser. 396, Formation and Evolution of Galaxy Disks, ed. J. G. Funes & E. M. Corsini (San Francisco, CA: ASP), 297
Kormendy, J., Fisher, D. B., Cornell, M. E., & Bender, R. 2009, ApJS, 182, 216 (KFCB)
Kormendy, J., & Freeman, K. C. 2004, in IAU Symp. 220, Dark Matter in Galaxies, ed. S. D. Ryder, D. J. Pisano, M. A. Walker, & K. C. Freeman (San Francisco, CA: ASP), 377
Kormendy, J., & Freeman, K. C. 2011, ApJ, in press
Kormendy, J., & Kennicutt, R. C. 2004, ARA&A, 42, 603
Kormendy, J., & Richstone, D. 1992, ApJ, 393, 559
Kotanyi, C., van Gorkom, J. H., & Ekers, R. D. 1983, ApJ, 273, L7

Krajnović, D. 2011, Paper presented at the ESO Workshop on Fornax, Virgo, Coma et al.: Stellar Systems in High Density Environments, ed. M. Arnaboldi, http://www.eso.org/sci/meetings/2011/fornax_virgo2011/talks_pdf/Krajnovic_Davor.pdf

Krajnović, D., Bacon, R., Cappellari, M., et al. 2008, MNRAS, 390, 93

Krajnović, D., Emsellem, E., Cappellari, M., et al. 2011, MNRAS, 414, 2923

Krick, J. E., & Bernstein, R. A. 2007, AJ, 134, 466

Lake, G., Katz, N., & Moore, B. 1998, ApJ, 495, 152

Larson, R. B. 1974, MNRAS, 169, 229

Larson, R. B., Tinsley, B. M., & Caldwell, C. N. 1980, ApJ, 237, 692

Lauer, T. R. 1985, ApJS, 57, 473

Laurikainen, E., Salo, H., & Buta, R. 2005, MNRAS, 362, 1319

Laurikainen, E., Salo, H., Buta, R., & Knapen, J. H. 2007, MNRAS, 381, 401

Laurikainen, E., Salo, H., Buta, R., & Knapen, J. H. 2011, MNRAS, 418, 1452

Laurikainen, E., Salo, H., Buta, R., Knapen, J. H., & Comerón, S. 2010, MNRAS, 405, 1089

Laurikainen, E., Salo, H., Buta, R., et al. 2006, AJ, 132, 2634

Li, J.-T., Wang, Q. D., Li, Z., & Chen, Y. 2011, ApJ, 737, 41

Lin, D. N. C., & Faber, S. M. 1983, ApJ, 266, L21

Lisker, T., Brunngräber, R., & Grebel, E. K. 2009, Astron. Nachr., 330, 966

Lisker, T., Grebel, E. K., & Binggeli, B. 2006, AJ, 132, 497

Lisker, T., Grebel, E. K., Binggeli, B., & Glatt, K. 2007, ApJ, 660, 1186

Makarova, L. 1999, A&AS, 139, 491

Makino, J., & Ebisuzaki, T. 1996, ApJ, 465, 527

Martin, N. F., de Jong, J. T. A., & Rix, H.-W. 2008, ApJ, 684, 1075

Mateo, M. 1998, ARA&A, 36, 435

Mateo, M. 2008, Messenger, 134, 3

Mayer, L., Governato, F., Colpi, M., et al. 2001a, ApJ, 547, L123

Mayer, L., Governato, F., Colpi, M., et al. 2001b, ApJ, 559, 754

Mayer, L., Mastropietro, C., Wadsley, J., Stadel, J., & Moore, B. 2006, MNRAS, 369, 1021

McConnachie, A. W., & Irwin, M. J. 2006, MNRAS, 365, 1263

McDermid, R. M., Emsellem, E., Shapiro, K. L., et al. 2006, MNRAS, 373, 906

Meekins, J. F., Fritz, G., Chubb, T. A., Friedman, H., & Henry, R. C. 1971, Nature, 231, 107

Mei, S., Blakeslee, J. P., Côté, P., et al. 2007, ApJ, 655, 144

Méndez-Abreu, J., Aguerri, J. A. L., Corsini, E. M., & Simonneau, E. 2008, A&A, 478, 353

Merritt, D. 2006, ApJ, 648, 976

Mihos, J. C. 2011, Paper presented at the ESO Workshop on Fornax, Virgo, Coma et al.: Stellar Systems in High Density Environments, ed. M. Arnaboldi, http://www.eso.org/sci/meetings/2011/fornax_virgo2011/talks_pdf/Mihos_Chris.pdf

Mihos, J. C., Harding, P., Feldmeier, J., & Morrison, H. 2005, ApJ, 631, L41

Mihos, J. C., & Hernquist, L. 1994, ApJ, 437, L47

Mihos, J. C., Janowiecki, S., Feldmeier, J. J., Harding, P., & Morrison, H. 2009, ApJ, 698, 1879

Milosavljević, M., & Merritt, D. 2001, ApJ, 563, 34

Milosavljević, M., Merritt, D., Rest, A., & van den Bosch, F. C. 2002, MNRAS, 331, L51

Moore, B., Ghigna, S., Governato, F., et al. 1999, ApJ, 524, L19

Moore, B., Katz, N., Lake, G., Dressler, A., & Oemler, A. 1996, Nature, 379, 613

Moore, B., Lake, G., & Katz, N. 1998, ApJ, 495, 139

Morgan, W. W. 1951, Publ. Obs. Univ. Michigan, 10, 33

Morgan, W. W., & Lesh, J. R. 1965, ApJ, 142, 1364

Mori, M., & Burkert, A. 2000, ApJ, 538, 559

Naab, T., Johansson, P. H., & Ostriker, J. P. 2009, ApJ, 699, L178

Neistein, E., Maoz, D., Rix, H.-W., & Tonry, J. L. 1999, AJ, 117, 2666

Oemler, A. 1976, ApJ, 209, 693

Okamura, S. 2011, Paper presented at the ESO Workshop on Fornax, Virgo, Coma et al.: Stellar Systems in High Density Environments, ed. M. Arnaboldi, http://www.eso.org/sci/meetings/2011/fornax_virgo2011/posters.html

Oosterloo, T., & van Gorkom, J. H. 2005, A&A, 437, L19

Oser, L., Naab, T., Ostriker, J. P., & Johansson, P. H. 2011, ApJ, in press (arXiv:1106.5490)

Oser, L., Ostriker, J. P., Naab, T., Johansson, P. H., & Burkert, A. 2010, ApJ, 725, 2312

Paturel, G., Petit, C., Prugniel, P., et al. 2003, A&A, 412, 45

Pedraz, S., Gorgas, J., Cardiel, N., Sánchez-Blázquez, P., & Guzmán, R. 2002, MNRAS, 332, L59

Peng, C. Y., Ho, L. C., Impey, C. D., & Rix, H.-W. 2002, AJ, 124, 266

Pildis, R. A., Schombert, J. M., & Eder, J. A. 1997, ApJ, 481, 157

Postman, M., & Geller, M. J. 1984, ApJ, 281, 95

Press, W. H., Flannery, B. P., Teukolsky, S. A., & Vetterling, W. T. 1986, Numerical Recipes: The Art of Scientific Computing (Cambridge: Cambridge Univ. Press)

Quilis, V., Moore, B., & Bower, R. 2000, Science, 288, 1617

Quinlan, G. D., & Hernquist, L. 1997, New Astron., 2, 533

Richstone, D. O. 1976, ApJ, 204, 642

Rix, H.-W., Franx, M., Fisher, D., & Illingworth, G. 1992, ApJ, 400, L5

Robertson, B., Cox, T. J., Hernquist, L., et al. 2006, ApJ, 641, 21

Roediger, E., & Hensler, G. 2005, A&A, 433, 875

Rubin, V. C., Graham, J. A., & Kenney, J. D. P. 1992, ApJ, 394, L9

Ryden, B. S., & Terndrup, D. M. 1994, ApJ, 425, 43

Sage, L. J., & Wrobel, J. M. 1989, ApJ, 344, 204

Saglia, R. P., Bender, R., & Dressler, A. 1993, A&A, 279, 75

Saito, M. 1979, PASJ, 31, 193

Sancisi, R., & van Albada, T. S. 1987, in IAU Symp. 117, Dark Matter in the Universe, ed. J. Kormendy & G. R. Knapp (Dordrecht: Reidel), 67

Sandage, A. 1961, The Hubble Atlas of Galaxies (Washington, DC: Carnegie Institution of Washington)

Sandage, A. 1975, in Galaxies and the Universe, ed. A. Sandage, M. Sandage, & J. Kristian (Chicago, IL: Univ. Chicago Press), 1

Sandage, A. 2004, in Penetrating Bars Through Masks of Cosmic Dust: The Hubble Tuning Fork Strikes a New Note, ed. D. L. Block et al. (Dordrecht: Kluwer), 39

Sandage, A., & Bedke, J. 1994, The Carnegie Atlas of Galaxies (Washington, DC: Carnegie Institution of Washington)

Sandage, A., & Binggeli, B. 1984, AJ, 89, 919

Sandage, A., Binggeli, B., & Tammann, G. A. 1985a, in ESO Workshop on the Virgo Cluster, ed. O.-G. Richter & B. Binggeli (Garching: ESO), 239

Sandage, A., Binggeli, B., & Tammann, G. A. 1985b, AJ, 90, 1759

Sarzi, M., Falcón-Barroso, J., Davies, R. L., et al. 2006, MNRAS, 366, 1151

Schombert, J. M. 1988, ApJ, 328, 475

Scorza, C., & Bender, R. 1995, A&A, 293, 20

Scorza, C., Bender, R., Winkelmann, C., Capaccioli, M., & Macchetto, D. F. 1998, A&AS, 131, 265

Sellwood, J. A., & Wilkinson, A. 1993, Rep. Prog. Phys., 56, 173

Sérsic, J. L. 1968, Atlas de Galaxias Australes (Córdoba: Observatorio Astronómico, Univ. Córdoba)

Shen, S., Mo, H. J., White, S. D. M., et al. 2003, MNRAS, 343, 978

Shetrone, M. D., Bolte, M., & Stetson, P. B. 1998, AJ, 115, 1888

Shetrone, M. D., Côté, P., & Sargent, W. L. W. 2001, ApJ, 548, 592

Shetrone, M. D., Siegel, M. H., Cook, D. O., & Bosler, T. 2009, AJ, 137, 62

Shetrone, M. D., Venn, K. A., Tolstoy, E., et al. 2003, AJ, 125, 684

Simard, L., Willmer, C. N. A., Vogt, N. P., et al. 2002, ApJS, 142, 1

Simien, F., & de Vaucouleurs, G. 1986, ApJ, 302, 564

Simien, F., & Prugniel, Ph. 2002, A&A, 384, 371

Somerville, R. S., & Primack, J. R. 1999, MNRAS, 310, 1087

Stover, R. J. 1988, in Instrumentation for Ground-based Optical Astronomy: Present and Future, ed. L. B. Robinson (New York: Springer), 443

Strateva, I., Ivezić, Ž., Knapp, G. R., et al. 2001, AJ, 122, 1861

Temi, P., Brighenti, F., & Matthews, W. G. 2009, ApJ, 695, 1

Thomas, D., Brimioulle, F., Bender, R., et al. 2006, A&A, 445, L19

Thronson, H. A., Tacconi, L., Kenney, J., et al. 1989, ApJ, 344, 747

Thuan, T. X., & Kormendy, J. 1977, PASP, 89, 466

Tolstoy, E., Hill, V., & Tosi, M. 2009, ARA&A, 47, 371

Tolstoy, E., Venn, K. A., Shetrone, M., et al. 2003, AJ, 125, 707

Tonnesen, S., & Bryan, G. L. 2008, ApJ, 684, L9

Tonnesen, S., & Bryan, G. L. 2009, ApJ, 694, 789

Tonnesen, S., & Bryan, G. L. 2010, ApJ, 709, 1203

Tonnesen, S., Bryan, G. L., & van Gorkom, J. H. 2007, ApJ, 671, 1434

Tremaine, S. 1981, in The Structure and Evolution of Normal Galaxies, ed. S. M. Fall & D. Lynden-Bell (Cambridge: Cambridge Univ. Press), 67

Tully, R. B., & Fisher, J. R. 1977, A&A, 54, 661

van Albada, T. S. 1982, MNRAS, 201, 939

van Albada, T. S., & Sancisi, R. 1986, Phil. Trans. R. Soc. Lond. A, 320, 447

van den Bergh, S. 1976, ApJ, 206, 883

van den Bergh, S. 1977, in Nearly Normal Galaxies: From the Planck Time to the Present, ed. S. M. Faber (New York: Springer), 19

van den Bergh, S. 1986, AJ, 91, 271

van den Bergh, S. 1993, ApJ, 411, 178

van den Bergh, S. 1994a, AJ, 107, 153

van den Bergh, S. 1994b, AJ, 107, 1328

van den Bergh, S. 1994c, ApJ, 428, 617

van den Bergh, S. 1995, AJ, 110, 613

van den Bergh, S. 2007, The Galaxies of the Local Group (Cambridge: Cambridge Univ. Press)

van den Bergh, S. 2009a, ApJ, 694, L120

van den Bergh, S. 2009b, ApJ, 702, 1502

van den Bosch, R. C. E., van de Ven, G., Verolme, E. K., Cappellari, M., & de Zeeuw, P. T. 2008, MNRAS, 385, 647
van der Kruit, P. C., & Freeman, K. C. 2011, ARA&A, 49, 301
van Dokkum, P. G., Whitaker, K. E., Brammer, G., et al. 2010, ApJ, 709, 1018
van Driel, W., & van Woerden, H. 1991, A&A, 243, 71
van Gorkom, J. H., & Kenney, J. D. P. 2011, ARA&A, in press
van Woerden, H., van Driel, W., & Schwarz, U. J. 1983, in IAU Symp. 100, Internal Kinematics and Dynamics of Galaxies, ed. E. Athanassoula (Dordrecht: Reidel), 99
van Zee, L., Skillman, E. D., & Haynes, M. P. 2004, AJ, 128, 121
Veilleux, S., Bland-Hawthorn, J., Cecil, G., Tully, R. B., & Miller, S. T. 1999, ApJ, 520, 111
Venn, K. A., & Hill, V. M. 2008, Messenger, 134, 23
Venn, K. A., Irwin, M., Shetrone, M. D., et al. 2004, AJ, 128, 1177
Vikhlinin, A., Kravtsov, A., Forman, W., et al. 2006, ApJ, 640, 691
Vollmer, B., Braine, J., Combes, F., & Sofue, Y. 2005, A&A, 441, 473

Vollmer, B., Soida, M., Chung, A., et al. 2008, A&A, 483, 89
Wakamatsu, K.-I., & Hamabe, M. 1984, ApJS, 56, 283
Watt, M. P., Ponman, T. J., Bertram, D., et al. 1992, MNRAS, 258, 738
Weinzirl, T., Jogee, S., Khochfar, S., Burkert, A., & Kormendy, J. 2009, ApJ, 696, 411
Weisz, D. R., Dalcanton, J. J., Williams, B. F., et al. 2011a, ApJ, 739, 5
Weisz, D. R., Dolphin, A. E., Dalcanton, J. J., et al. 2011b, ApJ, 743, 8
Welch, G. A., & Sage, L. J. 2003, ApJ, 584, 260
Williams, B. F., Ciardullo, R., Durrell, P. R., et al. 2007a, ApJ, 654, 835
Williams, B. F., Ciardullo, R., Durrell, P. R., et al. 2007b, ApJ, 656, 756
Williams, M. J., Bureau, M., & Cappellari, M. 2010, MNRAS, 409, 1330
Wilman, D. J., Balogh, M. L., Bower, R. G., et al. 2005, MNRAS, 358, 71
Wilman, D. J., Oemler, A., Mulchaey, J. S., et al. 2009, ApJ, 692, 298
Wirth, A., & Gallagher, J. S. 1984, ApJ, 282, 85
Yoshida, M., Ohyama, Y., Iye, M., et al. 2004, AJ, 127, 90
Young, J. S., Xie, S., Tacconi, L., et al. 1995, ApJS, 98, 219
Young, L. M., Bureau, M., Davis, T. A., et al. 2011, MNRAS, 414, 940